VTRC Virginia Transportation Research Council

We Bring Innovation to Transportation

Experimental and Analytical Evaluation of Repair Methods for Corrosion-Damaged Prestressed Concrete Bridge Beams

https://vtrc.virginia.gov/media/vtrc/vtrc-pdf/vtrc-pdf/27-R11.pdf

ALI ALFAILAKAWI, Graduate Research Assistant

MOJTABA ALIASGHAR-MAMAGHANI, Graduate Research Assistant

CARIN L. ROBERTS-WOLLMANN, PH.D., P.E., Professor

IOANNIS KOUTROMANOS, PH.D., Associate Professor
Charles E. Via, Jr. Dept. of Civil & Environmental Engineering

Virginia Polytechnic Institute and State University

MATTHEW HEBDON, PH.D., P.E., Associate Professor
The University of Texas at Austin

Final Report VTRC 27-R11

VIRGINIA TRANSPORTATION RESEARCH COUNCIL
530 Edgemont Road, Charlottesville, VA 22903-2454
vtrc.virginiadot.org

Standard Title Page—Report on State Project

Report No.: VTRC 27-R11	Report Date: October 2026	No. Pages: 73	Type Report: Final Contract	Project No.: 114590
			Period Covered: Nov. 2018 – Feb. 2023	Contract No.:

Title:
Experimental and Analytical Evaluation of Repair Methods for Corrosion-Damaged Prestressed Concrete Bridge Beams

Key Words: prestressed concrete, corrosion, repair, flexural, shear, post-tensioning, carbon fiber-reinforced polymer

Author(s): Ali Alfailakawi, Mojtaba Aliasghar-Mamaghani, Carin L. Roberts-Wollmann, Ioannis Koutromanos, and Matthew Hebdon

Performing Organization Name and Address:
Virginia Transportation Research Council
530 Edgemont Road
Charlottesville, VA 22903

Sponsoring Agencies' Name and Address:
Virginia Department of Transportation
1221 E. Broad Street
Richmond, VA 23219

Supplementary Notes:

Abstract:

A number of prestressed concrete bridges in Virginia are susceptible to chloride-induced corrosion. The fact that several bridges with many years of service exhibit damage in the form of corroded strands and cracking/spalling of the concrete necessitates the understanding of the impact of this damage on the safety of the bridge and the development of efficient repair methods. This project has addressed this need, through a synergy of experimental testing, computational simulation and design-oriented calculations.

The initial stage of the research investigated the ability to determine the in-situ strength of members that have visible corrosion-related damage. Two repair methods were then evaluated through large-scale experimental testing, aimed at restoring the strength of deteriorated prestressed concrete beams. The tests focused on beams with I- and box-sections retrieved from two bridges after decades of service. The investigated repairs included external post-tensioning for flexural strengthening, and carbon fiber reinforced polymer (CFRP) laminates applied to the bottom flange of beams for flexural strengthening and to the girder end regions for shear strengthening. A total of eleven full-scale bridge members were tested to failure throughout the research.

The experimental results were also used to evaluate the accuracy of current AASHTO guidelines for determining the capacity of prestressed beams with repairs. Building on the findings of this research, a set of recommendations and guidelines is established to enable designers to quantify the impact of corrosion on the flexural and shear capacity and determine the optimal repair method, for those beams that require repair.

FINAL REPORT

EXPERIMENTAL AND ANALYTICAL EVALUATION OF REPAIR METHODS FOR CORROSION-DAMAGED PRESTRESSED CONCRETE BRIDGE BEAMS

Ali Alfailakawi
Ph.D. Student

Mojtaba Aliasghar-Mamaghani
Ph.D. Student

Carin L. Roberts-Wollmann, Ph.D., P.E.
Professor

Ioannis Koutromanos, Ph.D.
Associate Professor

Charles E. Via, Jr. Department of Civil & Environmental Engineering
Virginia Tech

Matthew Hebdon, Ph.D., P.E.
Associate Professor
The University of Texas at Austin

Project Manager
Bernard L. Kassner, Ph.D., P.E.
Virginia Transportation Research Council

Virginia Transportation Research Council
(A partnership of the Virginia Department of Transportation
And the University of Virginia since 1948)

Charlottesville, Virginia

October 2026
VTRC 27-R11

DISCLAIMER

The project that is the subject of this report was done under contract for the Virginia Department of Transportation, Virginia Transportation Research Council. The contents of this report reflect the views of the authors, who are responsible for the facts and the accuracy of the data presented herein. The contents do not necessarily reflect the official views or policies of the Virginia Department of Transportation, the Commonwealth Transportation Board, or the Federal Highway Administration. This report does not constitute a standard, specification, or regulation. Any inclusion of manufacturer names, trade names, or trademarks is for identification purposes only and is not to be considered an endorsement.

Each contract report is peer reviewed and accepted for publication by staff of the Virginia Transportation Research Council with expertise in related technical areas. Final editing and proofreading of the report are performed by the contractor.

Copyright 2026 by the Commonwealth of Virginia.
All rights reserved.

ABSTRACT

A number of prestressed concrete bridges in Virginia are susceptible to chloride-induced corrosion. The fact that several bridges with many years of service exhibit damage in the form of corroded strands and cracking/spalling of the concrete necessitates the understanding of the impact of this damage on the safety of the bridge and the development of efficient repair methods. This project has addressed this need, through a synergy of experimental testing, computational simulation and design-oriented calculations.

The initial stage of the research investigated the ability to determine the in-situ strength of members that have visible corrosion-related damage. Two repair methods were then evaluated through large-scale experimental testing, aimed at restoring the strength of deteriorated prestressed concrete beams. The tests focused on beams with I- and box-sections retrieved from two bridges after decades of service. The investigated repairs included external post-tensioning for flexural strengthening, and carbon fiber reinforced polymer (CFRP) laminates applied to the bottom flange of beams for flexural strengthening and to the girder end regions for shear strengthening. A total of eleven full-scale bridge members were tested to failure throughout the research.

The experimental results were also used to evaluate the accuracy of current AASHTO guidelines for determining the capacity of prestressed beams with repairs. Building on the findings of this research, a set of recommendations and guidelines is established to enable designers to quantify the impact of corrosion on the flexural and shear capacity and determine the optimal repair method, for those beams that require repair.

FINAL REPORT
EXPERIMENTAL AND ANALYTICAL EVALUATION OF REPAIR METHODS FOR CORROSION-DAMAGED PRESTRESSED CONCRETE BRIDGE GIRDERS

Ali Afailakawi
Ph.D. Student

Mojtaba Aliasghar-Mamaghani
Ph.D. Student

Carin L. Roberts-Wollmann, Ph.D., P.E.
Professor

Ioannis Koutromanos, Ph.D.
Associate Professor

Charles E. Via, Jr. Department of Civil & Environmental Engineering
Virginia Tech

Matthew Hebdon, Ph.D., P.E.
Associate Professor
The University of Texas at Austin

INTRODUCTION

Background

The durability of infrastructure components such as bridges is significantly affected by long-term deterioration associated with corrosion. The transport of agents and the chemical processes associated with corrosion leads to cracking in the concrete, accelerating the corrosion process. Corrosion is a significant concern for prestressed concrete bridges in Virginia due to the frequent use of deicing salts during the winter and the number of structures in marine environments. Specifically, hydrogen embrittlement and stress corrosion cracking are concerns in exposed prestressing strands. Over time, the exposure of prestressing steel to corrosive agents can lead to complete loss of strands and, in extreme circumstances, complete failure of bridge beams (Harries, 2009).

The occurrence of extensive visible corrosion-induced damage in bridges located near seawater, such as the Hampton Roads Bridge-Tunnel (HRBT) approach spans, has given rise to serious concerns about the safety of such bridges. Research is necessary to assess the impact of corrosion on the local and global behavior of bridges and establish mitigation techniques to ensure long-term durability. There is a relatively limited amount of experimental research on bridge beams damaged by corrosion. Recent research at Virginia Tech provides guidance on methods to evaluate corrosion damage based on visible evidence and estimate residual flexural strength (Alfailakawi et al., 2020).

Methods to repair corrosion-damaged beams also has limited past research. Some repair techniques investigated for impact-damaged beams, such as strand splicing, are not appropriate for corrosion-damaged beams because of the difficulty in excavating an undamaged section of strand to splice. There is extensive research on using carbon fiber reinforced polymer (CFRP) layups for strengthening reinforced concrete beams (Rose et al., 2009; Duthinh and Starnes, 2004; Dong et al., 2013) and repairing impact-damaged beams (Klaiber et al., 2003; Soudki, 2006; Balasubramaniam et al., 2011). However, there is not as much attention paid to using CFRP to repair corrosion-damaged beams. External post-tensioning (PT), another repair technique, has been used for strengthening reinforced concrete beams (Bennitz et al., 2012; Zhang et al., 2020; Lee et al., 2018; Sayed-Ahmed et al., 2004), but not as frequently for repair.

To further study corrosion repair methods, Virginia Tech (VT) retrieved corrosion-damaged beams from two bridges during demolition for evaluation, repair, and testing. VT acquired three beams from the Aden Road Bridge, an adjacent prestressed concrete box beam bridge which carried Rt. 646 over Cedar Run near Quantico, Virginia. The beams on this bridge had severe deterioration due to leaking longitudinal joints, resulting in spalling of concrete on the beams' bottoms and exposed and fractured prestressing strands. Also, VT retrieved five beams with various corrosion damage levels from the Lesner Bridge, carrying U.S. Route 60 over the marine environment of Lynnhaven Inlet in Virginia Beach. Possession of these two beam types with various states of deterioration provided a unique opportunity to evaluate proposed methods for estimating residual capacity and repairing corrosion-damaged prestressed beams.

This report describes the evaluation, repair, and testing of beams from three bridges: the Aden Road and Lesner Bridges, as described above, and beams for the HRBT approach spans. The HRBT beams were never actually in service, but had been manufactured during the original construction of the westbound bridge. These beams were to serve as replacements in case of an emergency repair following a ship collision. While not exposed to deicing salts or direct contact with marine water, the bridge elements were stored in open air in the vicinity of the bridge, and thus were exposed to the same atmospheric chlorides as the in-service members. The HRBT beams did not have corroded strands, but did have some corrosion of the stirrups which extended from the top flange for the horizontal shear connection to the deck. Nevertheless, these beams were used as trials to evaluate two methods of strengthening implemented on the actual bridge. These methods included external PT and CFRP wraps, which were also used to repair the Aden Road and Lesner Bridge beams. In addition to testing beams repaired to return flexural strength, there was an investigation of methods to repair beams damaged near the beams' ends, which can reduce shear strength.

Problem Statement

The calculation of capacity of corrosion-damaged prestressed concrete beams, which have been subsequently repaired, requires additional study. This research evaluated damaged beams using Afailakawi et al.'s (2020) methods, developed repair schemes, repaired beams, and tested the repaired beams. Improvements in methods to estimate the residual capacity and the repaired capacity of corrosion-damaged beams will help mitigate catastrophic bridge structural failure in the future.

PURPOSE AND SCOPE

The overall purpose of this project was to develop improvements and provide recommendations for methods to evaluate residual strength and to evaluate the repaired strength of corrosion-damaged beams. The capacities of repaired corrosion-damaged prestressed beams were determined using large-scale experimental tests. Two repair methods, external PT and CFRP layups, were evaluated and compared to determine the resulting restoration of flexural capacity. In addition, methods to repair damage near the ends of beams to restore shear capacity were investigated. Beam testing included a total of three beams from the west bound HRBT approaches, five beams from the Lesner Bridge, and three beams from the Aden Road Bridge.

METHODS

Overview

The tasks undertaken to achieve the project objectives include:

1. **Perform a Literature Review** – The research team conducted a review of relevant literature concerning the repair of prestressed concrete beams.

2. **Test Strengthened Beams from Hampton Roads Bridge-Tunnel Approach Spans** – The testing included three beams from the HRBT approach spans . One beam had no damage and was used to establish the baseline strength. The second was strengthened with external PT and the third with CFRP layups. All three beams included a composite deck which was 48 in wide and 7 in thick. VDOT and a contractor designed and implemented the strength improvements.

3. **Inspect Deteriorated Beams** – Three Aden Road Bridge beams and five Lesner Bridge beams underwent visual inspection to identify all damage, such as cracks, spalls, delamination, patches, and exposed strands. In addition, half-cell potential measurements were taken on all beams.

4. **Implement Repair Techniques on Beams** – Two Lesner Bridge beams were repaired with external PT: one with grout in the tendon ducts and one with flexible filler. One Lesner Bridge beam and one Aden Road Bridge beam were repaired with CFRP to increase flexural strength. Finally, one Lesner Bridge beam and one Aden Road Bridge beam were repaired with CFRP to increase shear strength. The research team developed these repairs with the goal to return the beams to at least their original undamaged strength.

5. **Conduct Experimental Tests of Repaired Girders** – The six repaired beams from Aden Road and Lesner Bridges were tested to determine their actual repaired strength. The beams repaired for flexure were loaded in four-point bending, while the beams repaired for shear were tested at each end, with a single point load relatively close to the end of the beam. This allowed for two shear tests on each beam. In addition, one Lesner Bridge

beam and one Aden Road Bridge beam were tested in shear without repair to investigate the influence of corrosion damage near the ends of beams on shear strength.

6. **Conduct a Forensic Analysis** – After testing, various material samples were extracted from each beam to analyze. These samples included powdered concrete samples to determine chloride concentration, concrete cores to determine compressive strength, and strand samples to determine the stress-strain behavior of strands with various levels of corrosion damage.

7. **Execute an Analytical Evaluation** –Beam-based and truss-based finite element models were developed for the tested beams. The existing deterioration and the repairs were modeled to establish accurate methods for future evaluation of damaged and repaired beams.

8. **Develop Guidelines for Repair of Corrosion-Damaged Beams** – Based on the results of this research, guidelines for the evaluation and repair of corrosion-damaged beams were developed. These guidelines include methods for the repair of both flexural and shear damage.

Task 1: Perform a Literature Review

A literature review was undertaken to collect and synthesize information from previous research studies. Various specifications related to repair were reviewed, along with recommendations regarding nondestructive testing, evaluation of corrosion-damaged beams, and the effectiveness of repair techniques on deteriorated beams. The "Results" section provides a summary of the conducted literature review.

Task 2: Test Strengthened Beams from Hampton Roads Bridge-Tunnel Approach Spans

Hampton Roads Bridge-Tunnel

The HRBT connects the cities of Hampton and Norfolk by crossing the Chesapeake Bay. The structure is made up of two independent bridges, each with a tunnel in the middle. The two bridges are of different ages; the older one (westbound structure) dates from 1956, while the younger one (eastbound structure) dates from 1976. This report focuses on three beams that were cast to be used for rapid replacements for the westbound structure if it experienced damage, such as due to a ship impact. The beams were never needed, so they have been kept in a storage location near the bridge. As a result, the beams did not exhibit any corrosion damage. However, the findings of these tests can still be used to understand the behavior of damaged beams with similar repairs.

The beams had a design concrete strength of 5000 psi and were prestressed with 30, 3/8-in diameter, Grade 250, stress-relieved prestressing strands. The beams had a parabolically varying depth, from 46 in at the supports to 43 in at midspan. The thickness of the webs of the

beams also varied over the first 9 ft-7.5 in at each end. The webs were 7 in wide over the support and 5 in wide over the middle section of the beam. Prior to strengthening and testing, a 48-in wide by 7-in thick slab was cast on top of each beam. Figure 1 shows the cross-section of HRBT beams.

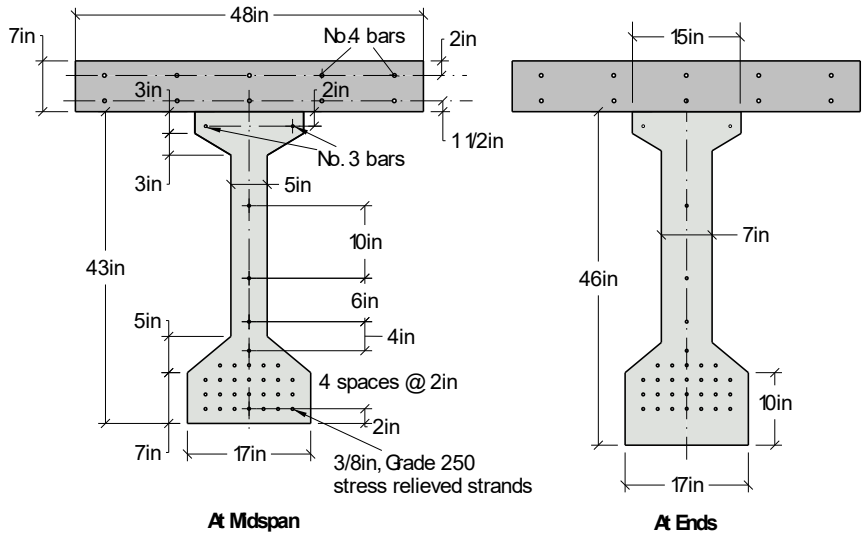

Figure 1. Cross-Section of Hampton Road Bridge-Tunnel Beams

Strengthening Methods

As mentioned previously, three beams were tested in this study. One beam had no strengthening, one was strengthened with external PT, and the third was strengthened with CFRP. The following sections describe the strengthening methods that were used for the HRBT beams.

Strengthening with External Post-Tensioning

One external tendon was added to each side of the beam to increase flexural strength. Four 0.6-in, seven-wire, uncoated, Grade 270, low-relaxation steel strands made up each tendon. Each external tendon was deviated twice within the length of the beam and was anchored in anchor blocks at the beam's ends (See Figure 2). Note that the anchor blocks were not in the same location on the live and dead ends. This was required because the live end needed to accommodate the length of the stressing ram between the anchor block and the end diaphragm in the actual bridge. The anchor at the dead end could be located closer to the support. Because of the differences in the location of the anchor blocks, the tendon inclination was different at each end. The live end had a 6° inclination, while the dead end had only a 4° inclination. The tendon deviation points correspond to the locations of the intermediate diaphragms in the actual bridge. The diaphragm walls and deviators were cast simultaneously with the anchor blocks and slab. Figure 2 presents an elevation view of the external PT strengthening and the support locations.

Each tendon was stressed with a multi-strand jack to 75% of the guaranteed ultimate tensile strength ($0.75f_{pu}$), for a total jacking force of 176 kips for each tendon. After friction and seating, the force in each tendon in the mid-span region of the beam was 153 kips. The beam was instrumented and monitored during the stressing operation, with particular attention paid to the

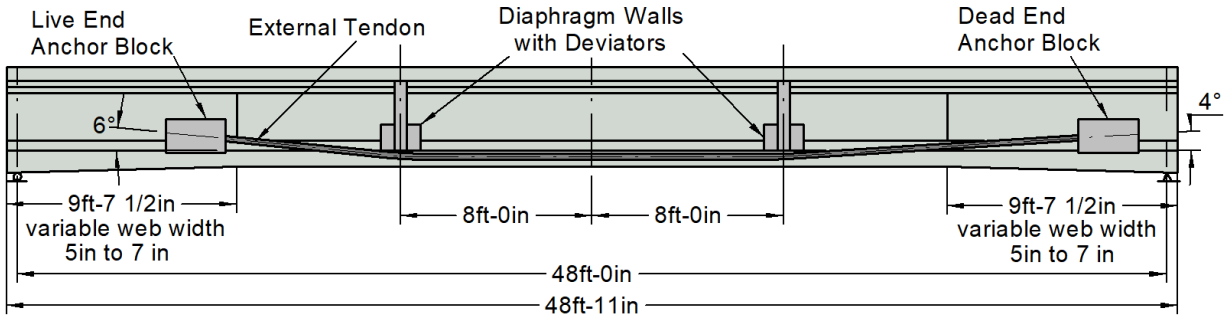

Figure 2. Elevation View of Hampton Roads Bridge-Tunnel Beam with External PT Strengthening

anchor blocks and the web of the beam close to the anchor blocks. No movement of the blocks relative to the beam was noted, no cracking was identified, and the strains were all relatively small. After stressing, the tendon ducts were filled with wax.

Strengthening with Carbon Fiber Reinforced Polymer

Figure 3 and Figure 4 show the details of the CFRP layups used to repair the beam. Three V-Wrap C400HM plies were attached to the soffit of the beam to increase the flexural strength. The breaking strength of the CFRP was 155 ksi. Each ply was 12 in wide and 0.08 in thick, so the total breaking strength of the three plies was 446 kips. However, failure could occur due to concrete crushing or debonding before the rupture of the CFRP. To enhance the bond of the longitudinal CFRP, one V-Wrap C200HM ply was wrapped around the bottom flange over 5 ft-6 in at the ends of the beam as an anchorage system. The plies wrapping the bottom flange were anchored with six CFRP anchors at each end, as shown in Figures 3 and 4.

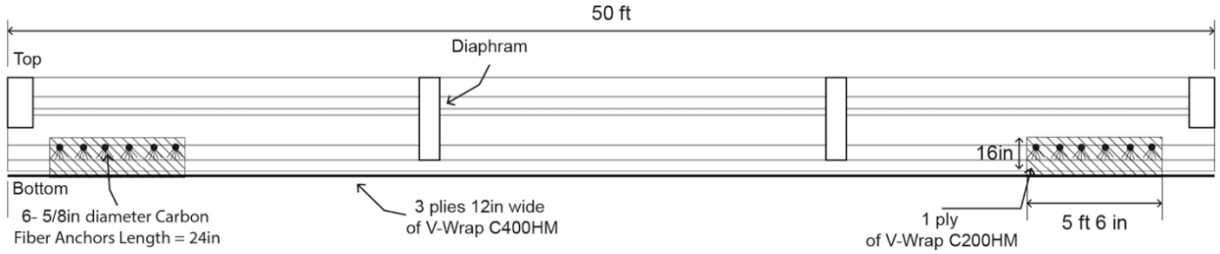

Figure 3. CFRP Layout for Hampton Roads Bridge-Tunnel Strengthening

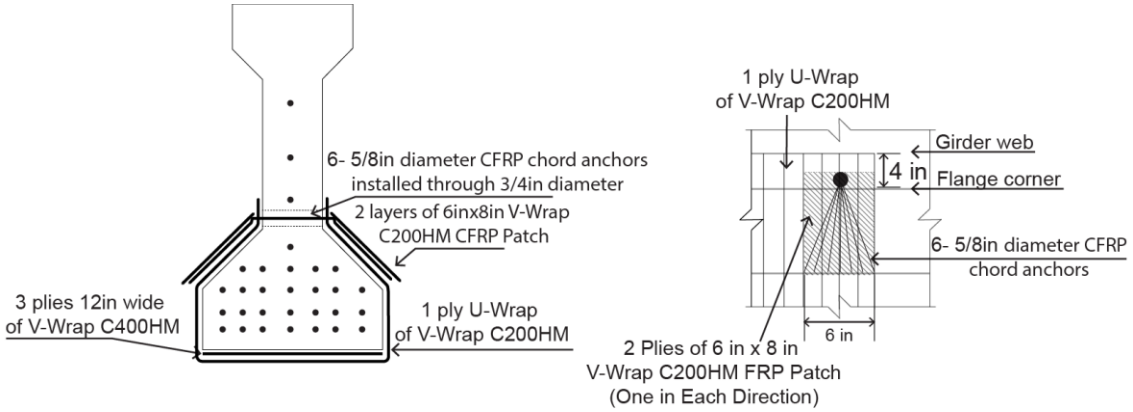

a) Beam – FRP detail **b) CFRP Patch Detail**

Figure 4. CFRP Strengthening Details for the Hampton Roads Bridge-Tunnel Beam

Preliminary Calculations of Flexural Strength

To gain an understanding of the expected loads, the flexural strength of each beam was calculated prior to testing. Of the three beams, the first beam was tested with no strengthening to provide a baseline for comparison to the other two strengthened beams. The second beam was strengthened with external PT and the third with CFRP.

For the unstrengthened beam, a strain compatibility approach was used to account for each layer of prestressing and the compression reinforcing in the deck. The simple method presented in the AASHTO LRFD Bridge Design Specifications (LRFD, 2020) in article 5.6.3.1.1, for components with bonded tendons, was also used for comparison.

For the beam with external PT, the approach described in AASHTO LRFD article 5.6.3.1.3b was employed. In lieu of a more rigorous analysis, this article allows the equation in 5.6.3.1.1 to be used to determine the stress in the bonded prestressing steel and the effective prestress to be used for the stress in the unbonded prestressing steel. The effective prestress in the unbonded tendon was assumed to be 153 ksi.

For the beam strengthened with CFRP, the methods presented in ACI 440R (ACI 440, 2017) and in the AASHTO Guide Specifications for Design of Bonded FRP Systems for Repair (AASHTO, 2012) were used. For the calculation of flexural strength, several modes of failure must be considered: concrete crushing, CFRP rupture, and CFRP debonding. The calculated strengths are presented in the Results section.

Test Set Up

All beams were tested in a simple span configuration, with one end supported by a roller and the other end supported by a pin. Loads were applied using a 400-kip actuator and a spreader beam, resulting in the application of two equal loads 8 ft apart, centered on the beam's midspan (see Figure 5). The span length for the HRBT beams was 48 ft.

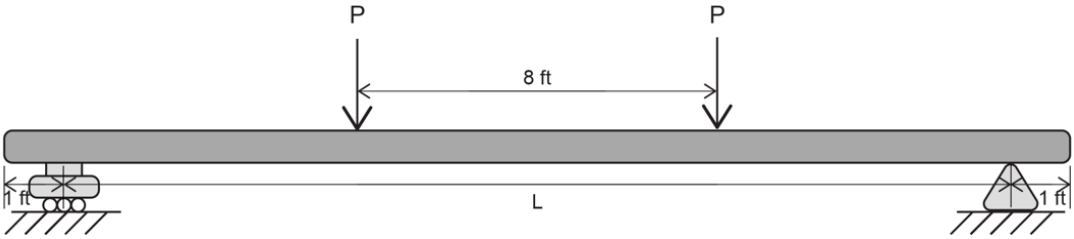

Figure 5. Flexural Test Set Up

For each of the three HRBT beams, a similar instrumentation plan was implemented. Deflections were measured at midspan and the quarter points, and an array of strain gages was placed over the height of the beams near midspan to investigate strain distribution and the location of the centroid. Other specialized instrumentation was added, depending on the strengthening method.

Task 3: Inspect Deteriorated Beams

In this project, eight corrosion-damaged beams were evaluated. Five were prestressed I-beams from the Lesner Bridge, and three were prestressed box beams from the Aden Road Bridge. This section provides basic information regarding the beams, creating damage maps, and the half-cell potential test.

Lesner Bridge Beams

The west bound lanes of the Lesner Bridge, also known as the Lynnhaven Inlet Bridge, were built in 1967. The approach spans were constructed using prestressed concrete beams, whereas the main spans were constructed with steel beams. The beams in the approach spans were 49 ft – 9 in long, 36-in deep AASHTO Type II prestressed I-beams. The beams were specified to have 5000 psi concrete strength and were prestressed with 22 - 7/16-in, Grade 270 stress-relieved prestressing strands. Each span included seven beams spaced 5 ft – 2.5 in, center-to-center.

The bridge was demolished and rebuilt in 2016 after almost 50 years of service. Nine beams were recovered during the demolition phase and sent to Virginia Tech for testing. The slab between the beams was saw-cut to enable the beams to be retrieved, together with a part of their cast-in-place composite deck. Figure 6 illustrates the level of degradation in typical beams. The Lesner Bridge was repaired several times over the years, so patching was evident in many locations. The cross-section of the Lesner Bridge I-beams is shown in Figure 7. Note that the sides of the beam were labeled as “bay side” and “inland side.” As this suggests, when the beams were in-situ, the “bay side” faced the Chesapeake Bay, and the “inland side” faced the Lynnhaven Inlet. The bay side of the beams always exhibited a higher level of corrosion damage.



Figure 6. Typical Deterioration on the Lesner Bridge

For simplification purposes, the Lesner Bridge beams in this report are referenced by I-Beam 1 through I-Beam 9. Table 1 presents the beam designations and their original locations in the bridge. Only I-Beams 1, 4, 5, 8, and 9 are presented in this study.

Aden Road Bridge Beams

The Aden Road Bridge was constructed in 1979 as a three-span bridge with nine prestressed box beams per span. The fascia beams were 3 ft – 0 in wide by 27 in deep, and the

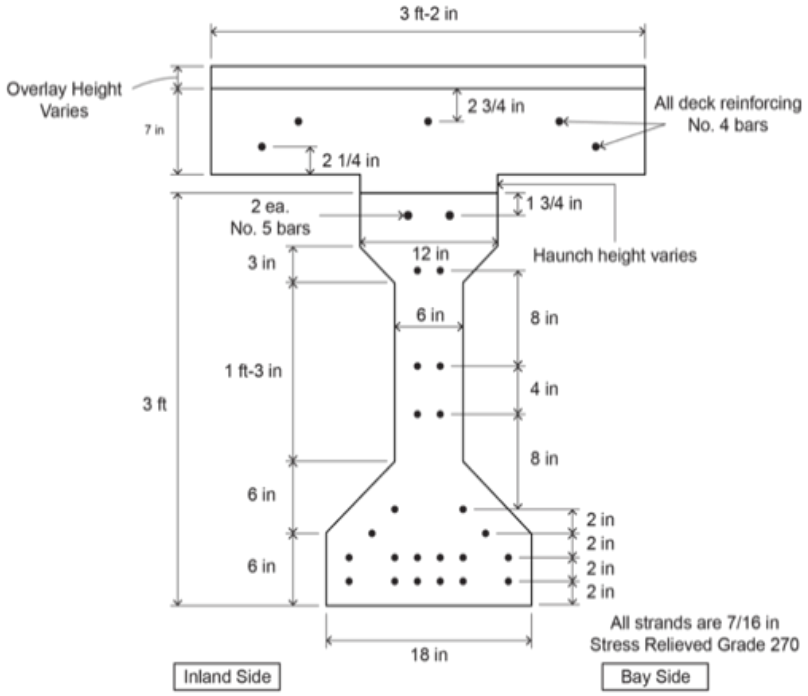

Figure 7. Cross-Section of Lesner Bridge I-Beams (All Straight Strands)

Table 1. Alternative Names of Lesner Bridge Beams

Beam #	Beam Designation on Bridge
I-Beam 1*	Span 22 Beam 5
I-Beam 2	Span 7 Beam 2
I-Beam 3	Span 19 Beam 4
I-Beam 4*	Span 22 Beam 2
I-Beam 5*	Span 19 Beam 2
I-Beam 6	Span 11 Beam 4
I-Beam 7	Span 13 Beam 5
I-Beam 8*	Span 7 Beam 4
I-Beam 9*	Span 5 Beam 2

* beam tested in this project

seven interior beams were 4 ft – 0 in wide by 27 in deep. Only interior beams were used in this project. The beams were 55 ft long and were prestressed with 33 - 7/16-in diameter, Grade 270 stress-relieved strands. The beams were connected transversely with grouted 12-in deep shear keys and ½-in diameter Grade 270 prestressing strands at each quarter point of each span. The bridge had an asphalt wearing surface applied directly to the top of the box beams, which was removed prior to the demolition of the bridge.

After slightly over 30 years of service, the joints had failed, and the bridge showed signs of severe deterioration, including exposed and fractured prestressing strands (see Figure 8). In 2013, the bridge was demolished and replaced. During demolition, six of the interior beams were transported to Virginia Tech for future testing. The Aden Road Bridge beams are referenced by the names Box Beam 1 through Box Beam 6, but their original positions in the bridge are unknown. Only three beams are presented in this study. The cross-section of the Aden Road Bridge box beams is shown in Figure 9.

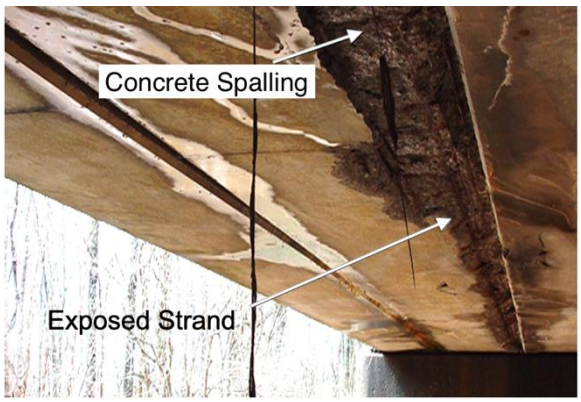

Figure 8. Typical Corrosion Damage on Aden Road Bridge

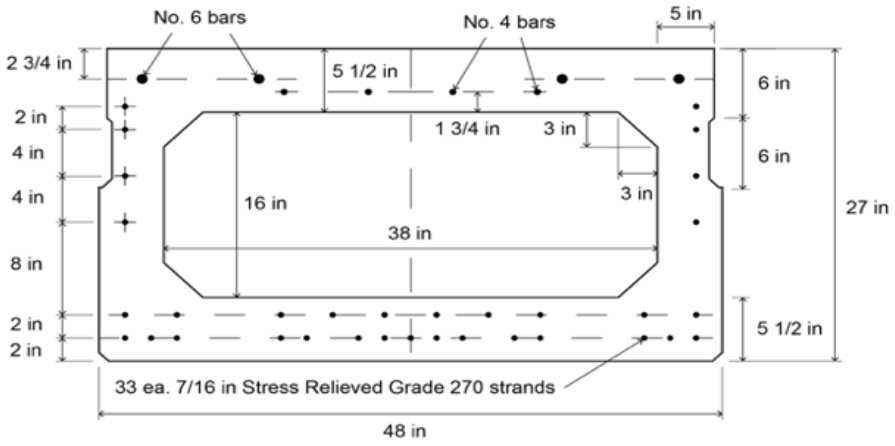

Figure 9. Cross-Section of Aden Road Bridge Box Beams

Visual Inspection and Damage Mapping

The beams were examined, and each beam's existing condition was thoroughly documented. The documentation included the location of damage such as cracks, delaminations, spalling, patching, and strand exposure. Delaminations were located by tapping the faces of the beams with a hammer and recording locations that had a hollow or dead sound. Detailed damage maps were created for each beam, indicating the size and location of each defect. Figure 10 presents an example of a damage map. In this figure, the top sketch is one side, oriented right-side-up, the middle sketch is the bottom of the beam, and the bottom sketch is the other side of the beam, oriented up-side-down. This allows the reader to see how side and bottom face damage are related spatially.

Half-Cell Potential

The half-cell potential method provides a fast, cost-effective, and non-destructive method to predict the corrosion in concrete by mapping the potential corrosion of the strands and mild reinforcement along the beam. The basic premise of the half-cell is to measure the potential difference between the steel and a standard copper sulfate electrode on the concrete surface. This measurement was made by placing the steel electrode on an exposed portion of the prestressing

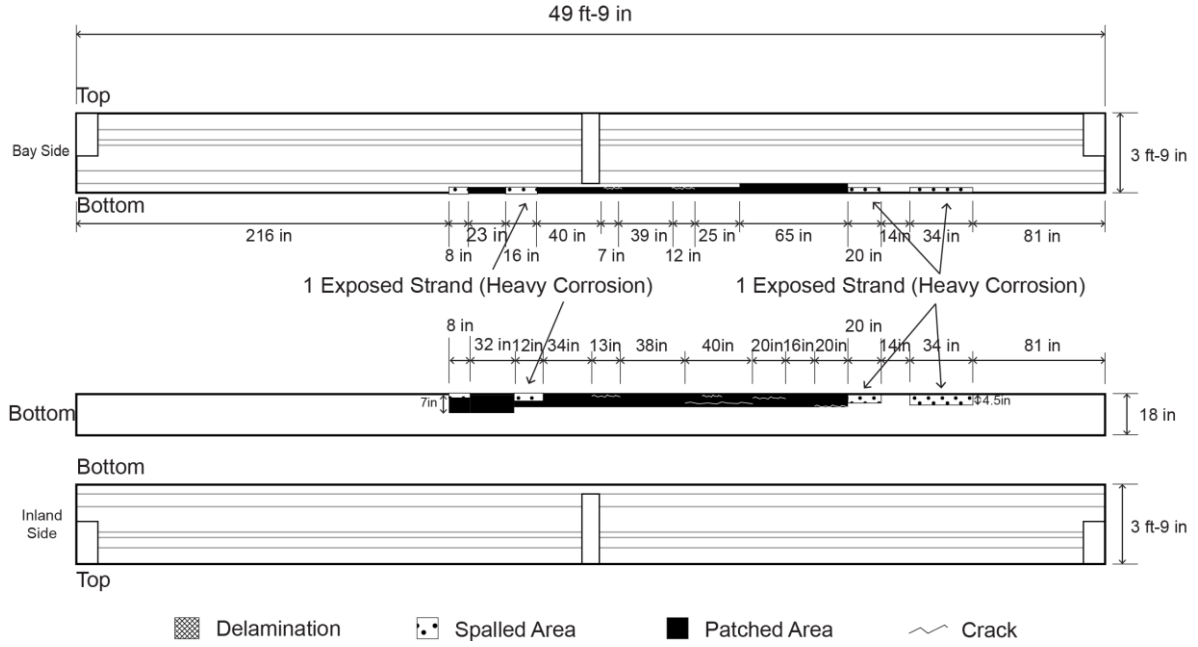

Figure 10. Damage Map for I-Beam 4

steel at the end of the beam, and the copper sulfate electrode on the concrete over the strand. The reading of the potential difference was displayed on a voltmeter. The more negative the voltage, the more likely corrosion was present at the measured location. The measurement and procedures were based on ASTM C876 (2015), which states that regions with half-cell potential values greater than -200 mV have a 90% probability of being free of corrosion in the reinforcing steel. Corrosion is possible in areas with values between -200 mV and -350 mV. Finally, locations with values less than -350 mV have a higher than 90% risk of corrosion. A map of potential readings was made for each beam and compared to the visible damage maps.

Task 4: Implement Repair Techniques on Beams

Evaluations of Strength Before and After Repairs

Evaluation of Residual Flexural Strength

In this study, two methods were used to assign a reduction in a given strand's cross-sectional area based upon its proximity to the damage observed on the surface of the concrete beam (see Table 2). The first method was presented in Naito et al. (2010) based on forensic investigations of box beams extracted from a decommissioned bridge. The second method is a slight modification to the Naito et al. method based on the results of the first phase of this study (Afailakawi et al., 2020). In both methods, the types of damage considered include longitudinal cracking, delamination, patching, exposed strands, and spalled sections. All damage that was within a distance of a strand's development length away from the section being evaluated was considered for strength calculation purposes. The AASHTO LRFD development length equation was used as a reference (AASHTO, 2020). The modified method was used to determine the residual capacity of I-beams, while box beams were evaluated using the recommendations provided by Naito et al. (2010).

Table 2. Damage Estimation for Strands to Calculate Flexural Capacity

Percentage of the original cross-sectional area of strands to be included in strength calculations		Strand condition
Naito et al. (2010)	Modified	
0%	0%	All exposed strands with a heavily corroded condition such as fracture or wire loss
0%	20%	All exposed strands, with a moderate condition such as heavy pitting
N.A.	10%	Strands in patched areas
75%	60%	Strand closest to a longitudinal crack and in the layer closest to the surface (see Figure 11)
75%	80%	Strands adjacent to a longitudinal crack, spalled area or patched area, in the layer closest to the surface, located no more than 3 in from the deterioration type (see Figure 11)
N.A.	80%	Strands, in the layer closest to the surface, within delaminated areas
95%	100%	All other strands in a longitudinally cracked beam

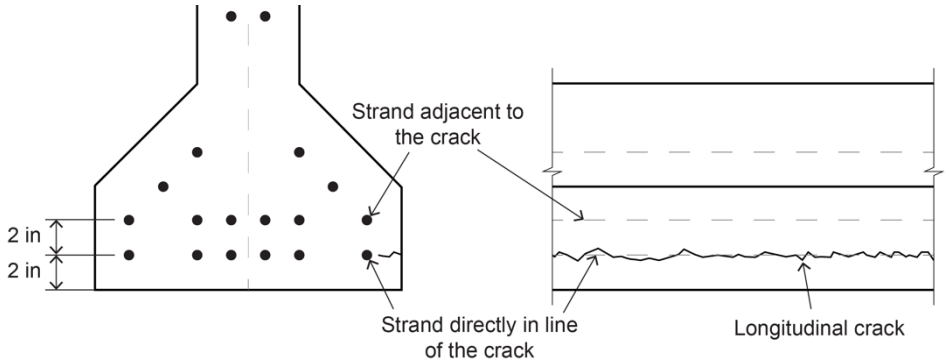

Figure 11. Cross-Section and Elevation View for I-Beam

The cross-section of I-beam 4 is illustrated in Figure 12. The flexural strength of the beam at mid-span is calculated and all of the damage within a region of one development length on each side of this section is included in the figure. Table 3 presents the area of strands assumed for each layer in the beam. Two methods were used to calculate the flexural strength. The first was a strain compatibility approach using an idealized stress-strain curve for the prestressing strand, which closely followed the behavior determined in tests of strand samples taken from the beams following testing (Alfailakawi et al., 2020). The second was the simplified method to calculate flexural strength presented in the AASHTO LRFD Bridge Design Specifications (AASHTO, 2020). Table 4 presents the calculated strength of I-beam 4 using the two methods. For comparison, Table 4 also presents the calculated strength assuming no damage. Note the flexural strength calculation includes a 3 ft - 2 in wide deck section, as shown in Figure 7.

Evaluation of Flexural Strength of Repaired Beams

The residual strength of the beams was calculated assuming that the repair would need to keep the beam in service for an additional 20 years. So, in addition to the currently observed damage, it was assumed that corrosion would continue to damage strands over an additional 20-year service life of the beam. If, at the time of a repair, only cosmetic repairs, such as patching,

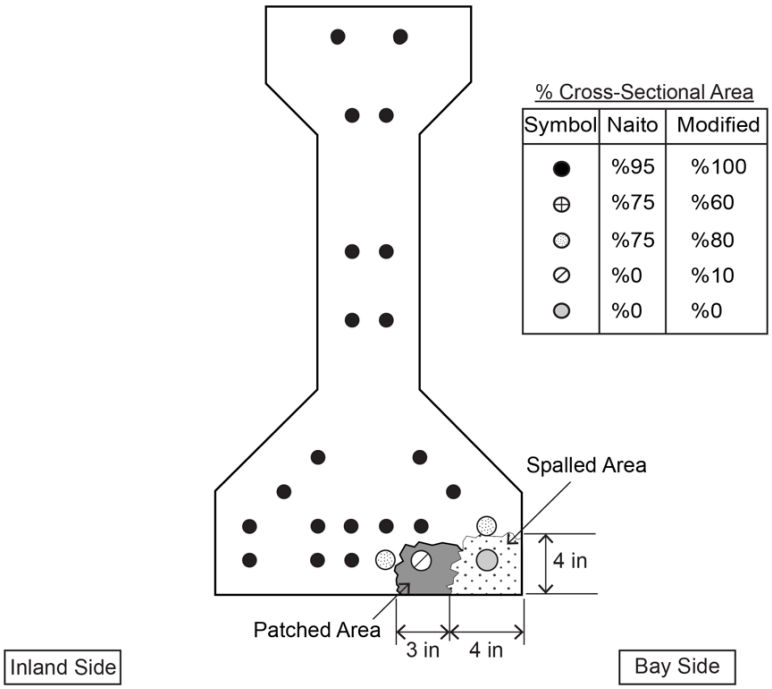

Figure 12. Visual Damage for I-Beam 4

Table 3. Strand's Cross-Area Reduction Based on Visual Damage

Level	Original Area	Distance from Bottom, in	Reduced Area for Strength Calculation
1	$A_1 = (6) * 0.117\ in^2 = 0.702\ in^2$	2	$A_1 = (1*0+3+1*0.1+1*0.8) * 0.117\ in^2 = 0.456\ in^2$
2	$A_2 = (6) * 0.117\ in^2 = 0.702\ in^2$	4	$A_2 = (5+1*0.8) * 0.117\ in^2 = 0.678\ in^2$
3	$A_3 = (2) * 0.117\ in^2 = 0.234\ in^2$	6	$A_3 = (2) * 0.117\ in^2 = 0.234\ in^2$
4	$A_4 = (2) * 0.117\ in^2 = 0.234\ in^2$	8	$A_4 = (2) * 0.117\ in^2 = 0.234\ in^2$
5	$A_5 = (2) * 0.117\ in^2 = 0.234\ in^2$	16	$A_5 = (2) * 0.117\ in^2 = 0.234\ in^2$
6	$A_6 = (2) * 0.117\ in^2 = 0.234\ in^2$	20	$A_6 = (2) * 0.117\ in^2 = 0.234\ in^2$
7	$A_7 = (2) * 0.117\ in^2 = 0.234\ in^2$	28	$A_7 = (2) * 0.117\ in^2 = 0.234\ in^2$

Table 4. Flexural Strength Calculations

Method	Beam with no damage		Beam with assumed damage	
	c	M_n	c	M_n
Strain Compatibility	5.35 in	1901 k-ft	4.32 in	1720 k-ft
AASHTO	5.38 in	1886 k-ft	4.35 in	1705 k-ft

c – neutral axis depth, M_n – flexural strength

were done to the beams, the corrosion would continue inside the beam. For example, Figure 12 shows the cross-section of I-beam 4, with the current level of damage determined by the visual inspection. It was assumed that after an additional 20 years of service, the four interior strands within 2 in of the existing spall or patch, would also become damaged by corrosion. This was a somewhat arbitrary assumption, because methods do not currently exist to attempt this type of extrapolation of future damage. It was only meant to give the researchers a basis for the design of the repairs.

To determine the residual strength of a beam with corrosion damage, the modified method presented in Table 2 was used to quantify damage based on visual inspection information. Based on this method, the estimated residual strengths of the beams repaired for flexure are presented in the Results section. These calculations were first made based on an estimate of damage 20 years from now, which was the basis for the design of the repair, and then repeated based on the current condition of the beams. Calculations were made for both time frames with and without repair.

As previously discussed for the unstrengthened HRBT beams, a strain compatibility approach was used to account for each layer of prestressing as well as the compression reinforcing in the deck. The simple method for components with bonded tendons, as presented in article 5.6.3.1.1 of the AASHTO LRFD Bridge Design Specifications (LRFD, 2020), was also used for comparison. The methods produced very similar results, so only the strain compatibility method–based strengths are presented in the Results section.

For the beams repaired with external PT, the approach described in AASHTO LRFD article 5.6.3.1.3b was employed. In lieu of a more rigorous analysis, this article allows the equation in 5.6.3.1.1 to be used to determine the stress in the bonded prestressing steel and the effective prestress to be used for the stress in the unbonded prestressing steel. The effective prestress in the unbonded tendon was assumed to be 152 ksi, based on the AASHTO refined method for estimation of prestress losses (AASHTO, 2020). The value was confirmed based on first cracking loads of unrepaired beams tested in a previous project (Alfailakawi et al., 2020). Also, a depth of 8.5 in was used for the deck along with 1.5 in for the haunch.

For the beams repaired with CFRP, the methods presented in ACI 440R (ACI 440, 2017) and in the AASHTO Guide Specifications for Design of Bonded FRP Systems for Repair (AASHTO 2012) were used. For the calculation of flexural strength, several modes of failure must be considered: concrete crushing, CFRP rupture, and CFRP debonding. For the I-beam, the height of the deck was 8 in, and the height of the haunch was 1.25 in.

Evaluation of Strength of Unrepaired Beams Tested in Shear

Several methods were used to evaluate the strength of the end regions of the beams that were tested in shear with no repair. The effect of the corrosion damage was estimated using the same methods as for the beams tested in flexure. However, the damage at the end of the beam was used, rather than at mid-span. The shear strength of the unrepaired beams was calculated using the sectional methods provided in the ACI and the AASHTO Codes. In calculating the concrete contribution to shear strength (V_c), the effective prestress stress and the area of prestress are inputs into the equations. Thus, if the longitudinal prestress is diminished due to corrosion damage, the V_c term is also smaller.

The shear strengths of the ends of the beams were also calculated using the strut-and-tie method. Figure 13 shows the type of strut-and-tie model that was used . Severe loss of cross-sectional area of the prestressing strands can adversely affect the strength by reducing the capacity of the bottom flange tie. Also, because the strength of the tie is calculated at the end of the nodal zone above the support, the capacity of the tie can be affected if the critical section is

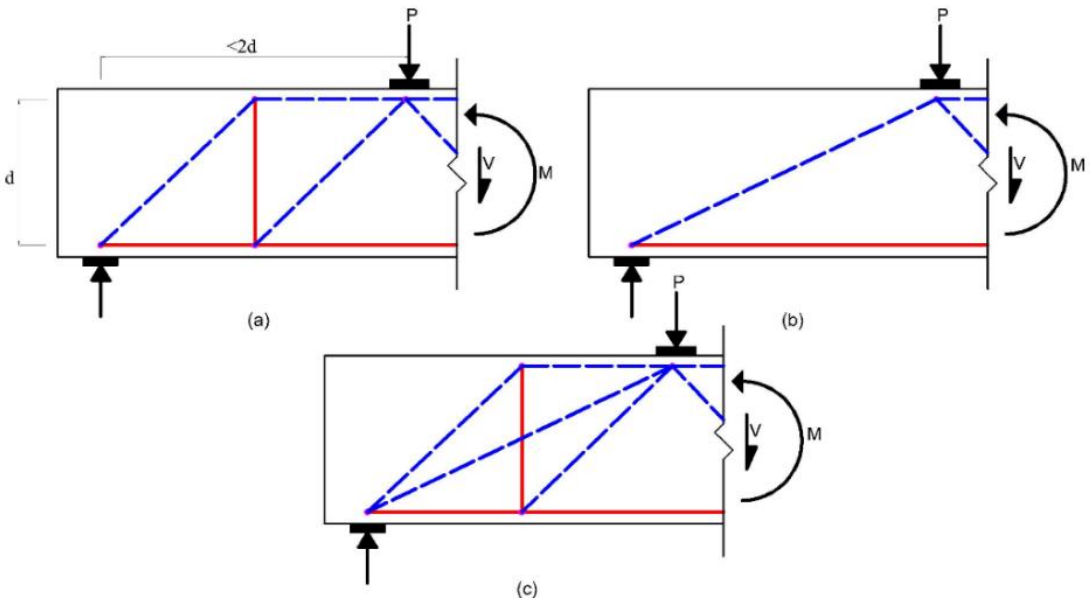

Figure 13. Three Different Strut-and-Tie Models Used to Evaluate Strength of Beams Tested in Shear (Al Rufaydah, 2020)

within the transfer length, as illustrated in Figure 14. The calculation of the shear strengths was performed considering the damaged cross-sectional areas of the strands following the recommendations mentioned in Table 2. However,the reduction in the strands' areas had an insignificant effect on the estimated strength using the strut-and-tie method.

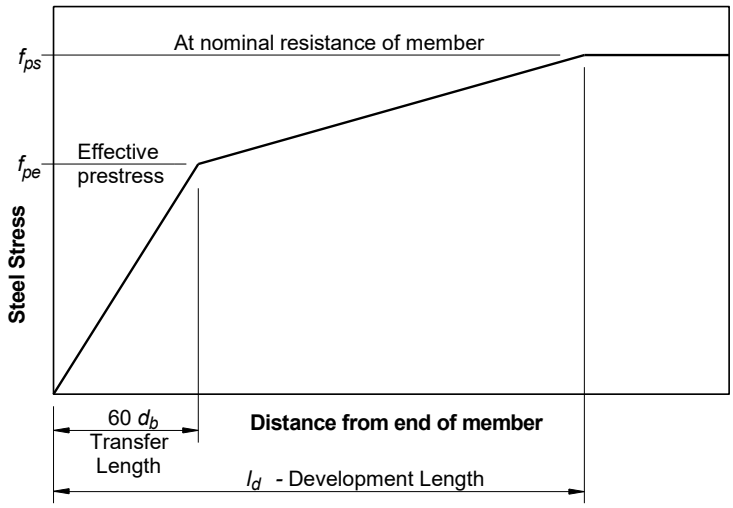

Figure 14. Stresses in Prestressing Strand in the Transfer and Development Length

Finally, according to AASHTO LRFD article 5.7.3.5, the capacity of the tension reinforcement at the location of a shear crack forming near the bearing of a simply supported beam must be checked. Figure 15 presents a free-body diagram of the forces assumed in the resistance model for this check. The equation to check this tensile capacity is as follows:

$$T = A_s f_y + A_{ps} f_{ps} \geq \left(\frac{V_u}{\varphi_v} - 0.5V_s - V_p\right) cot\,\theta$$

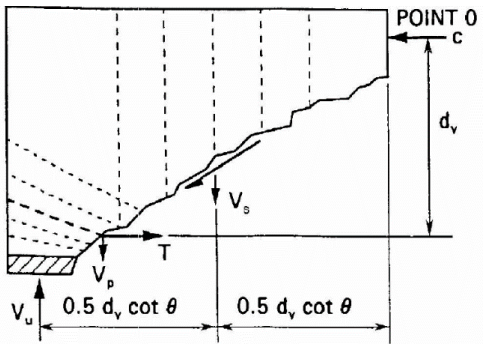

Figure 15. Free Body Diagram of the End of a Prestressed Beam (AASHTO, 2020)

where:

T = the capacity of the tension tie where it crosses the critical crack
A_s = cross-sectional area of reinforcing steel
f_y = yield strength of reinforcing steel
A_{ps} = cross-sectional area of prestressing steel
f_{ps} = stress in the prestressing steel, reduced as needed if the critical section is within the transfer length
V_u = *f*actored shear force
φ_v = strength reduction factor for shear
V_s = shear strength of stirrups
V_p = vertical component of prestressing force
θ = angle of crack

As with the strut-and-tie model, the check of the tensile capacity considered any assumed deterioration of the strands and the location of the crack relative to the transfer and development length of the strand. Again, this calculation did not govern the strength of any of the tested beams. The calculated strengths using these methods are presented in the Results section.

Evaluation of Strength of Repaired Beams Tested in Shear

The Lesner Bridge beam chosen for repair had significant visible corrosion on one end, but very little on the other. Thus, that end was subjected to accelerated corrosion efforts to induce more damage (Moraes, 2021). For the Aden Road Bridge, neither end had visible corrosion, so both ends were subjected to accelerated corrosion. The accelerated corrosion was achieved by placing the area of the beam, where more damage was desired, into a salt water bath, submerging the bottom 3 to 4 in of the bottom flange. Then a current generator was used to force electrical current from an electrode attached to an exposed strand at the end of the beam to a cathode plate which was submerged in the salt water bath. The forced current accelerated the corrosion process. The current was left in place until additional corrosion damage was evident in the form of new cracks, spalls and rust stains in the section of the beam within the salt bath.

The residual shear strengths of the end regions of the beams was calculated with the methods previously described. Then the repair was designed, using the methods presented in ACI 440R (ACI 440, 2017) and in the AASHTO Guide Specifications for Design of Bonded FRP Systems for Repair (AASHTO 2012), and the repaired strength was calculated. The results of these calculations are presented in the *Results* section.

Repair Methods

Two repair methods were investigated to recover the full undamaged flexural or shear strength of the corroded beams. CFRP repair was used for both Lesner Bridge and Aden Road Bridge beams, while external PT repair was used for the Lesner Bridge beams only. It is not feasible to repair box beams, such as the Aden Road Bridge beams, with external PT because in their in-situ, adjacent, configuration, the sides of the beams are not accessible to attach PT.

Repair with External Post-Tensioning

Two Lesner Bridge I-beams were repaired to restore flexural strength using external PT. One external tendon with four 0.6-in diameter strands was added to each side of the beam's web. The tendons were attached to each end of each beam by concrete anchor blocks. The anchor blocks were designed as corbels, and the required reinforcement was extended through holes, which were drilled through the webs, and anchored in the concrete in the block on the opposite side of the web. The blocks included PT anchorage devices for the tendons. Also, prior to placing the concrete for the anchor blocks, the surface of the beam's web was lightly chipped to create a roughened surface to improve the bond. In addition to casting the anchor blocks on the webs of the beams, additional concrete was cast at the bottom of the mid-span diaphragm wall to accommodate a deviation saddle so the tendon could have a single-point harping pattern. Figure 16 presents an elevation view of the repaired beam, while Figure 17 presents the details of the external PT repair.

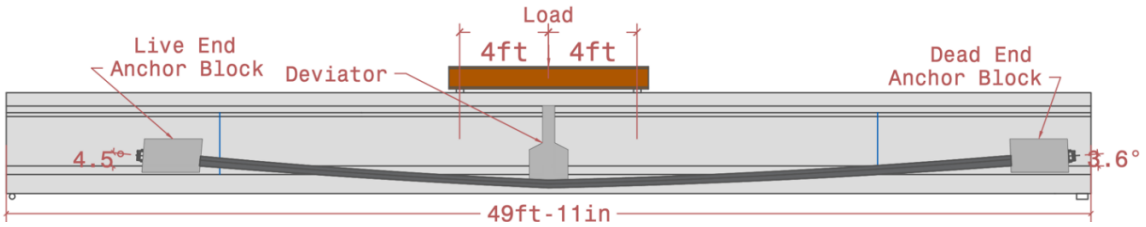

Figure 16. Elevation View of External PT Repair on Lesner Bridge Beam

After the new concrete components reached the desired strength of 5000 psi, high density polyethelene (HDPE) duct was installed between the anchor blocks, and the four 0.6-in diameter strands were placed in the ducts. The strands were anchored at the dead end anchor block and stressed at the live end to a jacking stress of 216 ksi. After friction and seating, calculations indicated that the live end stress was 180 ksi and the dead end stress 190 ksi.

After the completion of the stressing operations, the ducts were filled. One of the beams had conventional grout pumped into the ducts, while the other had hot wax, also called flexible filler, injected. Figure 18 presents photographs from the duct filling operations.

Repair with Carbon Fiber Reinforced Polymer

Two I-beams and two box beams were repaired using CFRP fabric using the wet layup method. One of each type was repaired to restore the original shear capacity, while the others were repaired to restore the original flexural strength, assuming a given level of damage. Figure 19 shows the details of the CFRP repair, which were used for flexural repair of one I-beam, and

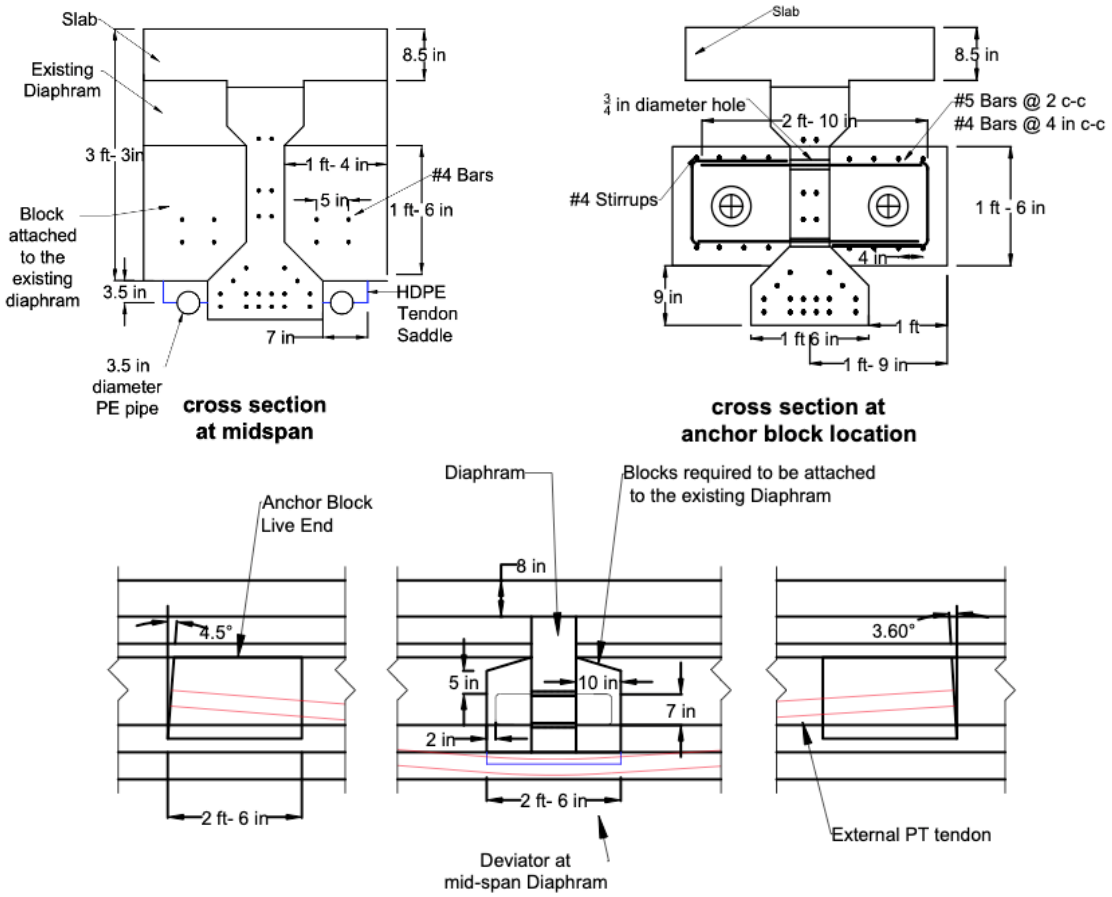

Figure 17. External PT Details for the Lesner Bridge Beams



Figure 18. External Post-Tensioning Repair

Figure 20 presents the shear repair for the other I-beam. For the beam repaired for shear the plies of CFRP that wrapped around the bottom bulb extended up to the top of the web on each side. On each wrap, one anchor was placed just above the web-bottom flange junction, and another was placed just below the web-top flange junction. Each repaired box beam had CFRP only on the bottom flange, as only this face of the beam would be accessible in-situ. The box beam repairs used no special anchoring system. Table 5 shows the details of all the repaired beams. The V-Wrap C400HM, which was also used for the flexural strengthening of one of the HRBT beams, had a breaking stress of 155 ksi and a thickness of 0.08 in. The V-Wrap C200HM had a breaking stress of 155 ksi and a thickness of 0.04 in.

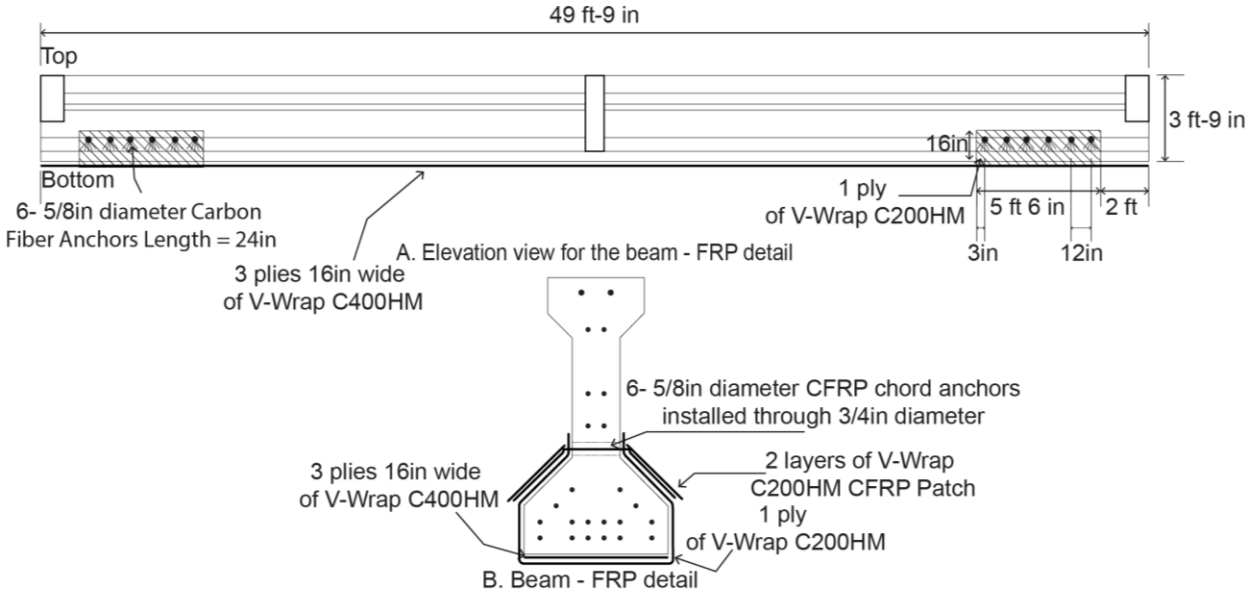

Figure 19. Details of CFRP Repair for I-Beam (Flexural) [Slab Not Shown]

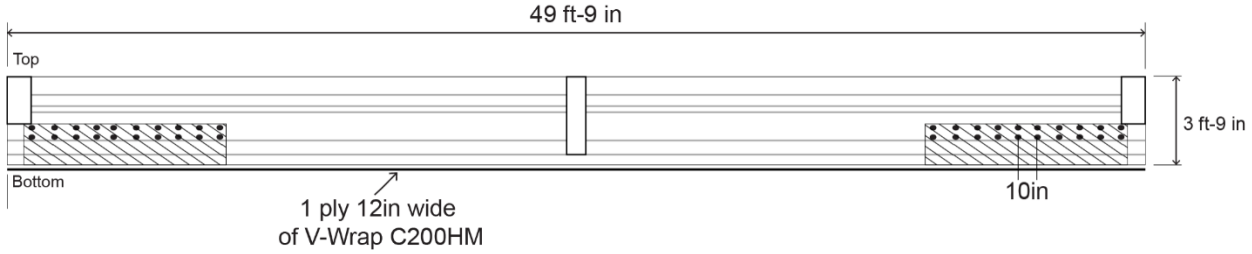

Figure 20. Details of CFRP Repair for I-Beam (Shear)

Table 5. CFRP Details for All Restored Beams

Beam #	Repair Type	CFRP Type	Number of Plies	Width of Ply
I-Beam 4	Flexural	C400HM	3	16 in
I-Beam 2	Shear	C200HM	1	12 in
Box Beam 5	Flexural	C200HM	1	36 in
Box Beam 6	Shear	C200HM	1	36 in

In order to get the maximum benefit from the CFRP repair, the weak surface of the concrete was removed using a chipping hammer, and then it was washed with water. Locations with spalls were patched with high-strength concrete. Holes for the CFRP anchors were drilled through the webs of the I-beams. Prior to drilling the holes in the web, a pachometer was used to locate the shear stirrups, so drilled holes would not hit the existing reinforcing. Finally, the CFRP sheets were applied using epoxy resin (see Figure 21).

Task 5: Conduct Experimental Tests of Repaired Girders

Test Setup

Four beams were tested to induce a flexural failure, while the other four were tested to induce a shear failure. The flexural test setup was similar to the one shown in Figure 5. The span



a) b) c)

Figure 21. CFRP Installation on Lesner Bridge Beams a) preparing layups, b) preparing anchors c) fibers of anchors splayed out on side of beam

length for the Lesner Bridge beams was 48 ft, and the span length for the Aden Road Bridge beams was 53 ft. A test was performed at each end of the four beams tested in shear. The end being tested was pin-supported, while the other end was roller-supported (see Figure 22). After testing the first end, the the roller was positioned beyond the cracks created by the first test, to ensure that the damage incurred in the first test did not adversely affect the results of the second test (see Figure 23). Table 6 presents the span lengths and shear span lengths for each test of each beam.

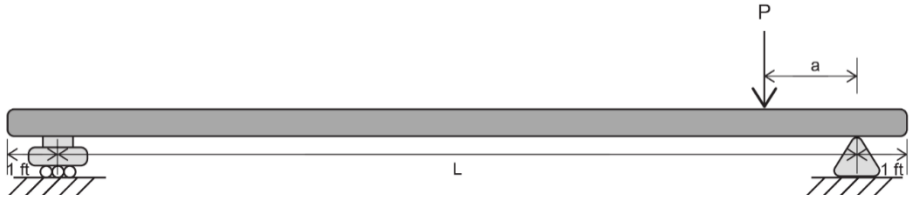

Figure 22. First End Shear Test Setup

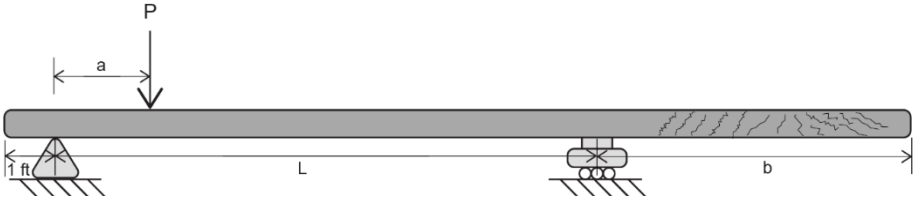

Figure 23. Second End Shear Test Setup

Table 6. Span Lengths and Shear Spans for Shear Tests

Beam	Test End No.	L Span Length, ft	a Shear Span, ft	d Depth to Prestressing, in	Span-to-Depth Ratio (a/d)
I-Beam 9 – Unrepaired	1	48.0	8.0	36.5	2.63
	2	32.5	6.0	36.5	1.97
I-Beam 2 – Repaired with CFRP	1	49.0	6.0	37.3	1.90
	2	38.0	6.0	37.3	1.90
Box Beam 3 – Unrepaired	1	53.3	4.0	21.6	2.22
	2	45.0	4.0	21.6	2.22
Box Beam 6 – Repaired with CFRP	1	53.0	4.0	21.6	2.22
	2	42.0	4.0	21.6	2.22

Hydraulic rams with a 400-kip capacity were used to load the beams during the tests. A transverse spreader beam was used for the box beams to prevent a punching shear failure of the top flange and ensure that the load was applied directly above the webs. Preliminary strength calculations on each end were performed based on the condition of the beam to select the loading location in an attempt to achieve a shear failure prior to flexural failure.

Instrumentation

Vertical deflections at the mid-span were determined using wire potentiometers. At many locations along the length of the beam, longitudinal strains were measured using surface strain gages. An array of strain gauges was mounted vertically through the depth of the beam at several locations to analyze strain distributions and identify the location of the centroid of the cross-section. Depending on the type of repair, different numbers of strain gauges were distributed along the beam. A load cell was placed between the hydraulic ram and the loading frame's cross-head.

Flexural test

Figure 24 through Figure 26 show the location of the strain gauges and linear variable displacement transformers used in the flexural tests for beams repaired with external PT and CFRP.

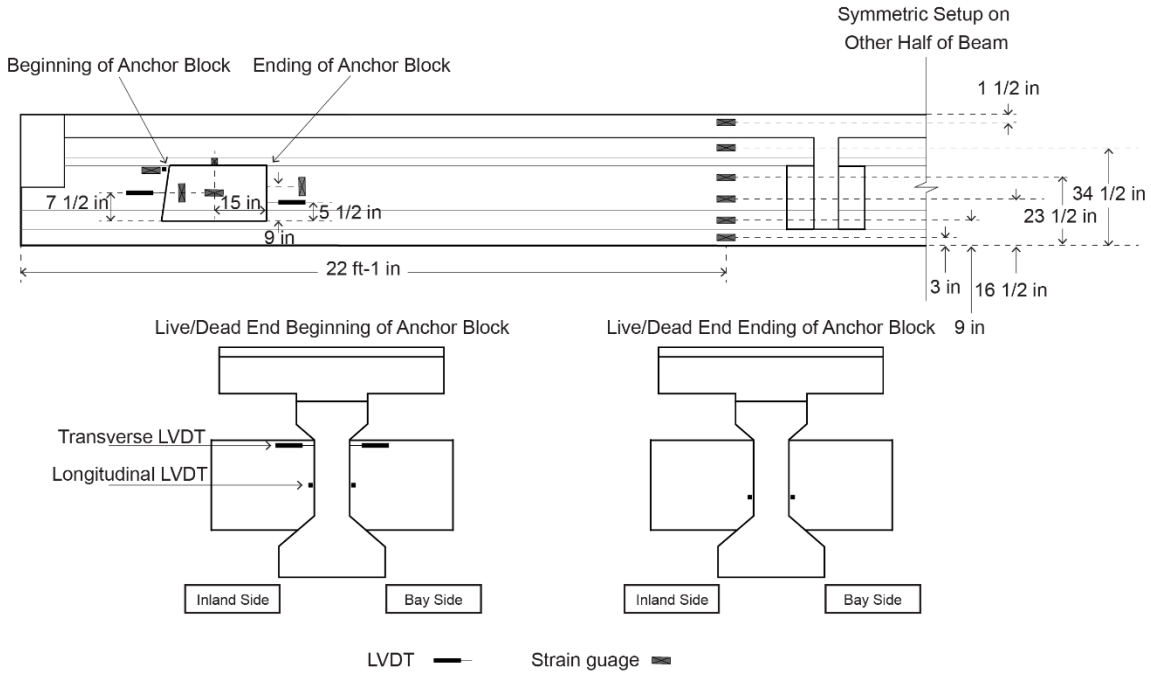

Figure 24. Instrumentation for I-Beams Repaired with External PT

Shear test

The locations of the strain gauges mounted for the shear tests are shown in Figures 27 and 28. The repaired and unrepaired beams had similar instrumentation layouts.

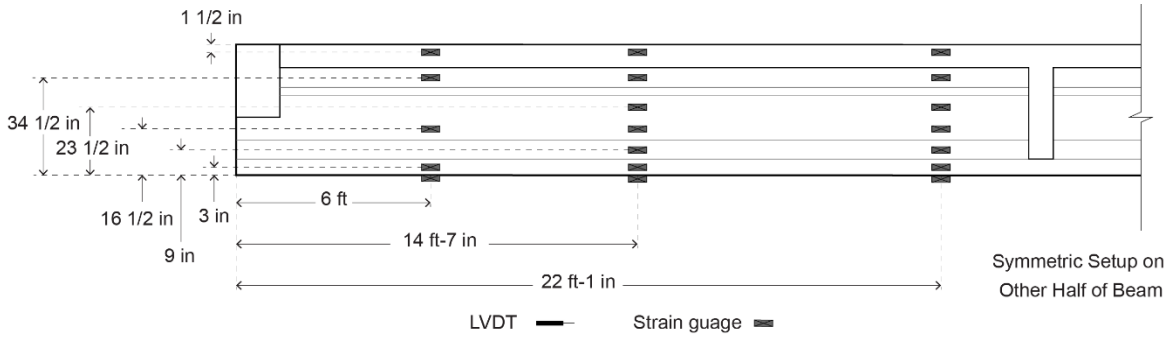

Figure 25. Instrumentation for I-Beam Repaired with CFRP

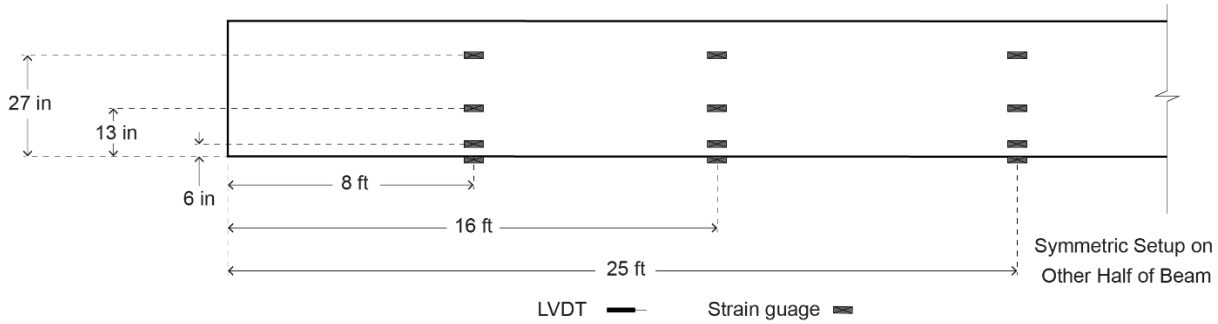

Figure 26. Instrumentation for Box Beam Repaired with CFRP

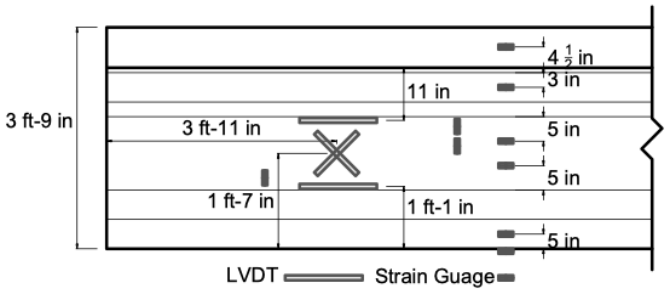

Figure 27. Instrumentation for I-Beams Tested in Shear

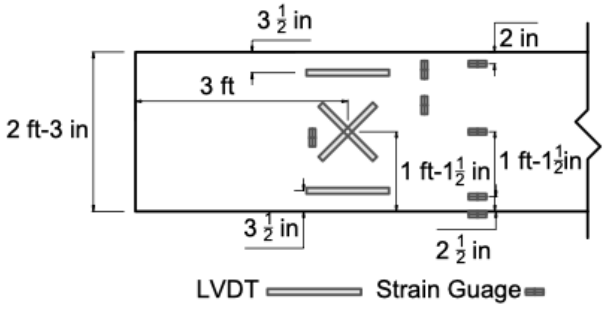

Figure 28. Instrumentation for Box Beams Tested in Shear

Test Procedure

In general, for all tests, the load was applied in 5- or 10-kip increments throughout testing until significant non-linear behavior initiated. All cracks were noted, and images were taken with

each consecutive load increase. After the beam began to exhibit signs that the prestressing was yielding and the load was not increasing significantly, the loading protocol was changed to a manual deflection control. An increment of deflection was chosen, and after each increment, loading was paused to make observations. Once it appeared that failure was imminent, the researchers no longer approached the beam. In the case of flexural tests, loading was continued until failure occurred either due to top flange crushing or the beam continuing to deform without resisting any additional load. For the shear tests, loading was continued until a shear failure in the web occurred.

After testing to failure, the load was removed and the beam was carefully inspected to identify the number of prestressing strands or stirrups, depending on the type of test, that had been broken prior to or during testing due to corrosion.

Task 6: Conduct a Forensic Analysis

Post-Test Visual Inspections

Following each test, after chipping the concrete, the condition of the strands was assessed and compared to the pre-test visual inspection findings.

Tension Tests of Retrieved Strands

Following the completion of flexural testing, samples of each beam's strands were extracted. The strands were retrieved from areas of the beams that were not damaged during testing. Samples were taken from locations on the beams that exhibited different signs of corrosion damage. Some strands were taken from beneath longitudinal cracks, or adjacent to spalling and patching. For each strand, the condition of the beam's surface was carefully recorded, and the condition of the extracted strand was also recorded.

The samples were tested in tension in accordance with ASTM A1061 procedure (2009). To ensure that the strands failed away from the gripping region, extra care was taken to cushion the gripping sections on both ends of the samples to avoid stress concentrations and premature failure. Thus, 8-in-long thin-walled aluminum pipes were cut in half in the long direction and each half was coated in a paste made of equal parts high-strength epoxy and grit. The two halves were then pressed into the strand ends to create a cushion for the grips.

The samples were tested in a Satec Universal Test Machine (UTM) with a capacity of 300 kips. A clip-on extensometer with an 8-in gage length was mounted to the strand. The tension force was applied at a rate of 0.025 in per second until the strand ruptured.

Concrete Compression Strength Testing

Core sample testing was conducted in accordance with ASTM C39 (2005) to measure the compressive strength of both bridges' beams and sections of the cast-in-place composite deck of the Lesner Bridge's I-beams. Core samples for each beam were taken in accordance with ASTM C42 (2016).

From each of the three Lesner Bridge beams, two cores were obtained from the beams and two from the decks. Two cores were extracted from each box beam. After removing each core, the researchers measured the specimen's length and diameter. If the length to diameter ratio was equal to or less than 1.75, a compressive strength correction factor (given in Table 7) was used to modify the compressive strength of the core sample as per the ASTM C39.

Table 7. Strength Correction Factor

Ratio of Length to Diameter (L/D)	Strength Correction Factor
1.75	0.98
1.50	0.96
1.25	0.93
1.00	0.87

Total Chloride Evaluation

The acid-soluble chloride profiles were determined using the method described by ASTM C1152 (2012). This method allows potentiometric titration to determine the chloride content in a given sample. Samples of concrete powders were collected from many locations on each side of each beam. A 10-g sample of pulverized concrete should pass through a fine sieve to be used.

For the Lesner Bridge I-beams, samples were taken from both sides, the bay side, which was the side of the beam facing the Chesapeake Bay in-situ, and the inland side. Also, two samples were taken from each side of the bottom flange, one from the vertical face and the other from the inclined face (see Figure 29). Usually, the bay side exhibited greater damage than the inland side.

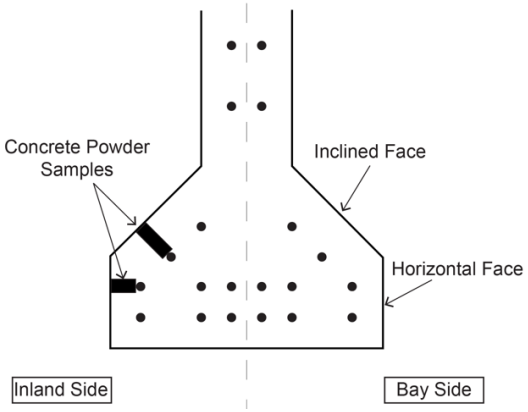

Figure 29. Locations of Concrete Powder Samples

A total of two hundred powder samples were taken from the eight beams. The samples were collected using a drill with a 1-in diameter bit at several locations along the length of each beam. The locations were chosen because they were in sound concrete, were not damaged during testing, and were not next to reinforcing bars, as assessed using a handheld GPR. Powdered samples were taken in increments of 0.5 in for a minimum depth of 2 in to the level of the strands at each location.

Task 7: Execute an Analytical Evaluation

The analyses of corrosion-damaged beams primarily relied on two modeling approaches, namely, beam model and nonlinear truss model (Aliasghar-Mamaghani et al., 2022). The former was created to capture the flexural capacity, while the latter was necessary to determine the shear strength. The computational simulation primarily focused on the analysis of six flexure-dominated and two shear-dominated cases. The visually observed corrosion damage discussed in the preceding section was supplemented in the analyses to elucidate the impact of corrosion damage on the load-carrying capacity of beams. A third modeling approach considered in this study relied on three-dimensional finite element models and was employed for the simulation of the external PT beam from the HRBT. The methods and results for this analysis can be found in Leicht et al. (2022), and are not presented herein.

Beam Model

The flexural capacity of the beams is captured using the beam model scheme. The analytical model relies on a beam (line) member discretized into multiple two-node elements. The kinematics of the beam model is governed by the Euler-Bernoulli beam theory, where the finite element approximation uses first- and third-order polynomials for axial and transverse displacement, respectively (Koutromanos, 2018). The internal force of each element is computed using a fiber section model, where the cross-section of each element is divided into multiple segments through the sectional depth. Each fiber has a constant axial strain from the reference axis and curvature. In addition, each individual strand is modeled with a separate fiber. The schematic of the beam model approach is provided in Figure 30. Each element had uniform section properties along the length of the beam.

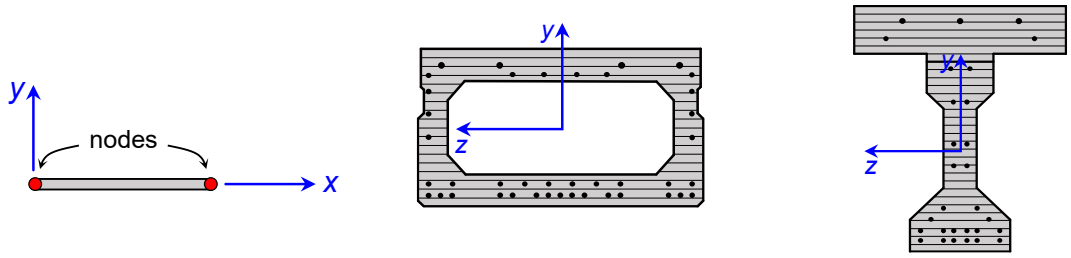

(a) 2-node element **(b) Fiber cross-sectional law**

Figure 30. Schematic of Nonlinear Beam Model

Truss Model

The nonlinear truss modeling approach is created to capture the shear strength of the beams because a beam-based model is unable to accurately predict the shear failure. The analytical model relies on a two-dimensional member discretized by quadrilateral elements, shown in Figure 31a. A truss panel representing an element of the truss model consists of two horizontal, two vertical, and two diagonal (inclined) truss (line) elements assembled in a four-node quadrilateral cell. The area of each component is defined as the product of element in-plane effective width b_{eff} (see Figure 31c), and the out-of-plane thickness (or cross-sectional width). The horizontal and vertical elements contain concrete and steel material, while the diagonal elements are composed only of concrete. The latter is meant to describe the compression field developed in cracked members. The materials used in the truss model are uniaxial.

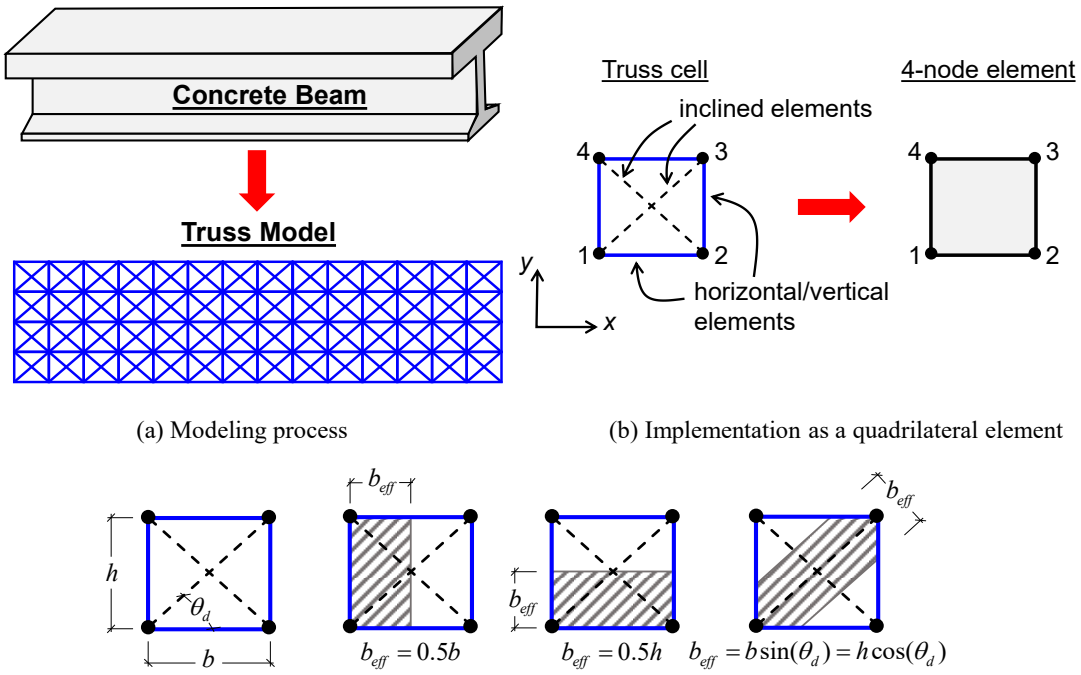

Figure 31. Nonlinear Truss Modeling Approach

Task 8: Develop Guidelines for Repair of Corrosion-Damaged Beams

Based on the beam tests and analytical investigation results, guidelines for evaluation and repair of corrosion-damaged prestressed bridge beams were developed. The guidelines include:

- Refinement of the recommended methods to evaluate shear and flexural strength of corrosion damaged beams based on new test results combined with a previous project (Alfailakawi et al., 2020) and other information from the literature.
- Recommendations on the selection of the better repair technique, external PT or CFRP layups, based upon the level of damage in a beam to be repaired.
- Recommendations on the details of CFRP repairs for returning flexural or shear strength
- Recommendations on the details of designing the external PT repair, including best placement of the anchor blocks and deviators, design of the anchor blocks and deviators, and determination of the required size and number of strands for the repair.

RESULTS AND DISCUSSION

Task 1: Perform a Literature Review

Non-Destructive Tests

Non-destructive testing (NDT) procedures have been developed to assess beam degradation without causing structural damage. NDT assessments are typically based on various

techniques such as visual inspection and half-cell potentials. Naito et al. (2011) and Alfailakawi et al. (2020) both concluded that there was a correlation between half-cell results and strand corrosion, but the coefficient of variance was high across tests and the half-cell results did not offer any additional quantitative information for the strength computation. Both documents also indicate that visual inspection should be the primary approach for evaluating damaged beams due to its excellent results.

Evaluation of Corrosion-Damaged Beams

Naito et al. (2011) conducted a study on seven corroded segments of adjacent box beam to assess the condition of their prestressing strands. These beams were recovered from three different Pennsylvania bridges that had been in use for more than 50 years. Five damaged indices were proposed based on the condition of the strands. A method to calculate the residual capacity of damaged beams based on a reduction in the strand's cross-section was proposed, and this method is used in this report.

The Effectiveness of Repair Techniques on Deteriorated Beams

External PT can be used as a repair method to restore the capacity of any structural element. By choosing the best fit path and anchorage system, the strength of damaged beams can be increased by 17%, 20%, or 40%, as per research conducted by Bennitz et al. (2012), Sayed-Ahmed et al. (2004), and Lee et al. (2018), respectively.

CFRP can be used as an alternative method to strengthen damaged beams and prevent corrosion. Similar to the external PT repair method, a good anchorage system must be chosen along with the right CFRP design. Studies show that using CFRP repair technique can increase the capacity up to 40% (Lee et al., 1997; Balasubramaniam et al., 2011). In addition, Klaiber et al. (2003) stated that flexural strengthening is feasible if 15% or less of the strands are damaged.

Task 2: Test Strengthened Beams from Hampton Roads Bridge-Tunnel Approach Spans

Flexural Tests

Preliminary Calculations of Flexural Strength

Three beams from HRBT were tested in flexure. The first was tested with no strengthening for a baseline comparison to the other two strengthened beams. One was strengthened with external PT and the other with CFRP. The flexural strength of each beam was calculated prior to testing.

The actual values of concrete compression strength, which are presented in the Material Tests Results section, were used to obtain the strength calculations for the three beams. The yield strength for the reinforcing steel in the decks was assumed to be 60 ksi.

Table 8 presents the strengths calculated prior to testing the beams. The anticipated load to cause flexural failure was based on the loading pattern shown in Figure 5, with each beam having a 48-ft span length, and the two point loads applied 4 ft each side of midspan.

Table 8. Predicted Flexural Strength for Hampton Roads Bridge-Tunnel Beams

Beam	Flexural Strength	Failure Mode	Self-Weight and Slab Weight Moment	Anticipated Applied Moment to Fail in Flexure	Anticipated Applied Load to Fail in Flexure
Unstrengthened Beam	1993 k-ft	Concrete Crushing at the top	215 k-ft	1778 k-ft	178 kips
Beam Strengthened with External Post-Tensioning	3150 k-ft	Concrete Crushing at the top	215 k-ft	2935 k-ft	294 kips
Beam Strengthened with Carbon Fiber	ACI: 2537 k-ft AASHTO: 2783 k-ft	Debonding between CFRP and Soffit of the Beam	215 k-ft	ACI: 2322 k-ft AASHTO: 2568 k-ft	ACI: 233 kips AASHTO: 257 kips

Unstrengthened Beam

This beam was used as a baseline beam to compare its strength to the subsequent strengthened beams. The first flexural crack was noticed at 80 kips. At 160 kips, a horizontal shear crack formed at the beam's end, resulting in delamination between the slab and the beam. The beam failed at a load of 178 kips, with a horizontal shear failure at the end of the beam that propagated to mid-span, followed by a large flexural shear crack at the span's third point (see Figure 32). Note that some FRP can be seen in the left photograph in Figure 32. This was applied as a test by the repair contractor, but did not add any strength to the beam. Although the beam did not fail in flexure as expected, the test results were consistent with the estimated flexural load shown in Table 8. Also, flexural failure was imminent based on the flattening of the load versus deflection plot presented later in this section.



Figure 32. Unstrengthened Hampton Roads Bridge-Tunnel Beam at Failure

Beam Strengthened with External Post-Tensioning

Loading steps of 10 kips were chosen at the beginning of the test. After first cracking at a load of about 180 kips, the load steps were reduced to 5 kips. Cracks in the anchor block region initiated in the web at an applied load of about 180 kips (see Figure 33).

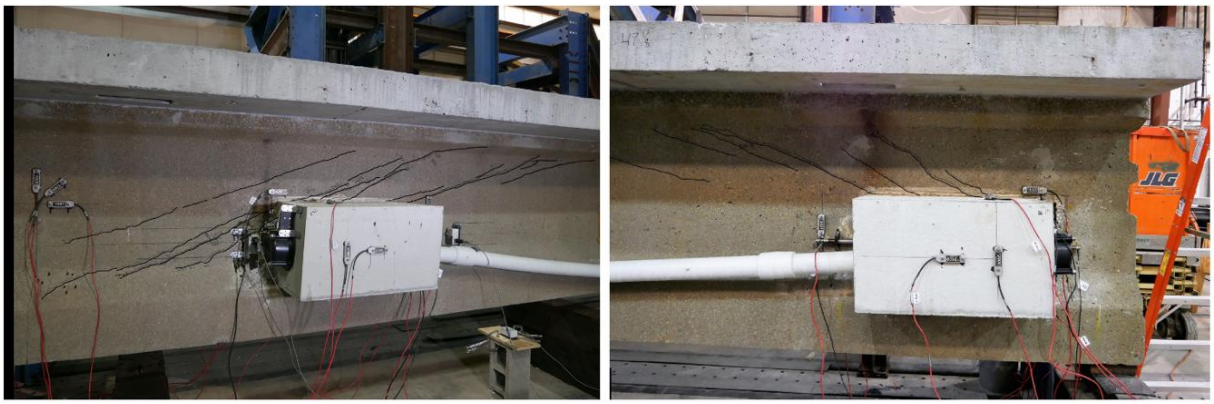

Figure 33. Cracks on Live and Dead Ends of the Hampton Roads Bridge-Tunnel Beam

The cracks in the anchor block region propagated and widened quickly compared to the flexural cracks. The final failure occurred at a load of 287 kips, due to crushing of the web concrete ahead of the anchor block on the live end and was quite explosive (see Figure 34). The failure load was slightly less than that shown in Table 8, which was based on an expected flexural failure. Instead, the failure mode was shear-compression. This highlights the need to check other modes of failure with this type of repair.



Figure 34. Failure at Live End of the Hampton Roads Bridge-Tunnel Beam

Beam Strengthened with Carbon Fiber Reinforced Polymer

At a load of 80 kips, the slope of the load versus deflection plot changed indicating that cracks had begun to develop. Visible cracking was not evident until a load of 100 kips. When the load reached 215 kips, the CFRP began delaminating and debonding from the beam (see Figure 35). The beam continued to be loaded until it failed at 245 kips with a very wide, long flexural shear crack, as seen in Figure 36.



Figure 35. CFRP Debonded from the Soffit of the Hampton Roads Bridge-Tunnel Beam



Figure 36. Flexural Shear Failure of the Hampton Roads Bridge-Tunnel Beam Strengthened with CFRP

The ultimate load of 245 kips was in between the predicted failure loads of 232.5 kips (ACI method) and 257 kips (AAASHTO method). The assumed failure mode, debonding, was consistent with the observed mode. The premature loss of bond could have been due to poor preparation of the bottom surface of the beam, but it could also be related to the parabolic curve of the bottom slab. Because of the curve, when the CFRP develops tensile stresses, the epoxy experiences both shear stresses and tensile stresses. No guidance could be found in the available literature regarding the reduction in epoxy shear strength when tensile stresses also exist.

A comparison of the load vs deflection behavior of the three HRBT beams is presented in Figure 37. As can be seen, the strengthening did not significantly alter the initial stiffness of the beams, but did change the ultimate load and deflection considerably.

Material Test Results

Concrete Compressive Tests

As described in the Methods section, cores were taken from the slab and beams and tested in compression after testing. Table 9 presents the results.

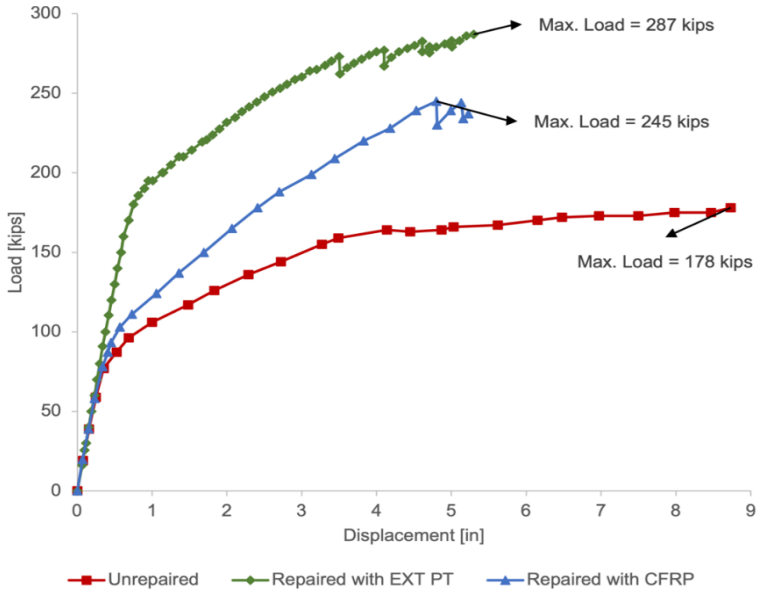

Figure 37. Load Versus Deflection - Hampton Roads Bridge-Tunnel Beams

Table 9. Results of Compression Tests of Cores from Hampton Roads Bridge-Tunnel Beams

Beam	Compressive Strength	
	Beam	Slab
Unstrengthened	7250 psi	4480 psi
External PT	5650 psi	5450 psi
CFRP	5800 psi	3630 psi

Tension Tests

Six strands were extracted from the beams after the flexural tests. These strands were tested in uniaxial tension to determine the stress-strain behavior. The plans indicated that the strands were Grade 250 stress relieved strands. Table 10 presents the tested properties, and Figure 38 presents examples of the tested stress-strain behavior.

Table 10. Key Properties of Prestressing Strands from Hampton Roads Bridge-Tunnel Beams

Strand Sample	Modulus of Elasticity, ksi	Yield Stress, ksi	Ultimate Strength, ksi	Ultimate Strain
Unstrengthened	30,000	237	258.5	0.068
Strengthened with EXT PT	30,000	234	256	0.038
Strengthened with CFRP	30,000	233	257.5	0.063

Summary and Discussion of HRBT Beams

The load-deflection plots for the three beams are shown in Figure 38. The external PT and CFRP strengthening increased the flexural capacity by 60% and 37%, respectively, compared to the unstrengthened beam. However, some ductility was sacrificed, and neither of the strengthened beams had an extended yield plateau. The failures of the two strengthened beams were not flexural failures but more sudden shear failures. This highlights the need to check all possible failure modes of a repaired beam. Figure 39 and Figure 40 illustrate the computed shear capacity versus the applied shear along the length of the beams strengthened

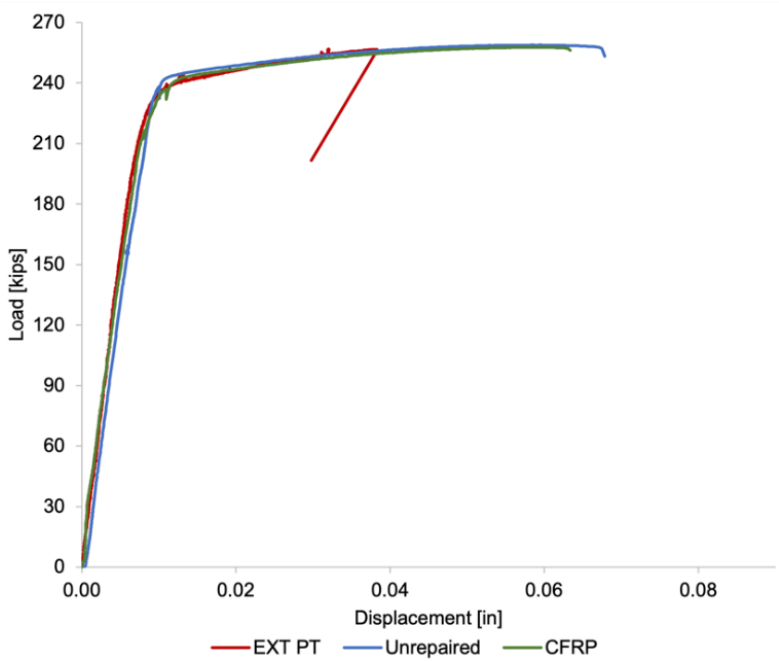

Figure 38. Stress-Strain Behavior of Prestressing Strands from the Hampton Roads Bridge-Tunnel Beams

using external PT and CFRP, respectively. For the beam strengthened with CFRP, the shear failure occurred within the shaded section in Figure 40. The failure of the beam strengthened with external PT, was a shear compression failure ahead of the anchor block, and this failure mode cannot be predicted with a sectional shear strength calculation method.

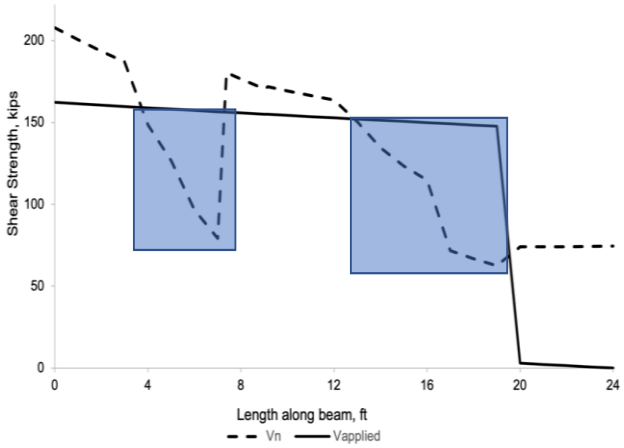

Figure 39. Shear Capacities along the Beam Strengthened with External PT (shaded area indicates where calculated strength is less than required strength from applied load)

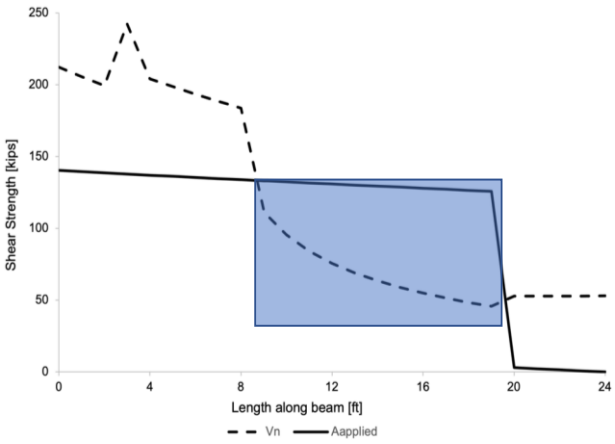

Figure 40. Shear Capacities along the Beam Strengthened with CFRP (shaded area indicates where calculated strength is less than required strength from applied load)

The capacities computed for various strengthening methods are compared to the test results in Table 11. These capacities are calculated using tested material properties of the concrete and steel. Note that the strengths presented in Table 11 are flexural strengths, although both the beam strengthened with CFRP and the beam strengthened with external PT failed in shear.

Table 11. Comparison of Strengthening Methods Flexural Strength Calculations

Beam	Tested Strength, k-ft	Estimated Strength, k-ft	$M_{test}/M_{estimated}$
Unstrengthened	1993	1993	1.0
External PT	3085	3150	0.98
CFRP	2663	ACI: 2537	1.05
		AASHTO: 2783	0.96

These tests highlight the need to check all possible modes of failure when developing repairs to increase flexural strength. However, it is also important to note that these strengthening methods were somewhat unrealistic because the beams had no corrosion damage. In an actual repair scenario, if a beam is repaired to return it to its original strength, the shear strength should be adequate, assuming the original shear design was correct and there has been no shear-related damage.

Task 3: Inspect Deteriorated Beams

Visual Inspection – Damage Maps

I-Beam 1: Repaired with External PT – Flexible Filler – Tested in Flexure

Figure 41 shows that the inland side had no signs of deterioration, while the bay side contained two spalled areas, one patched area, and four small longitudinal cracks.

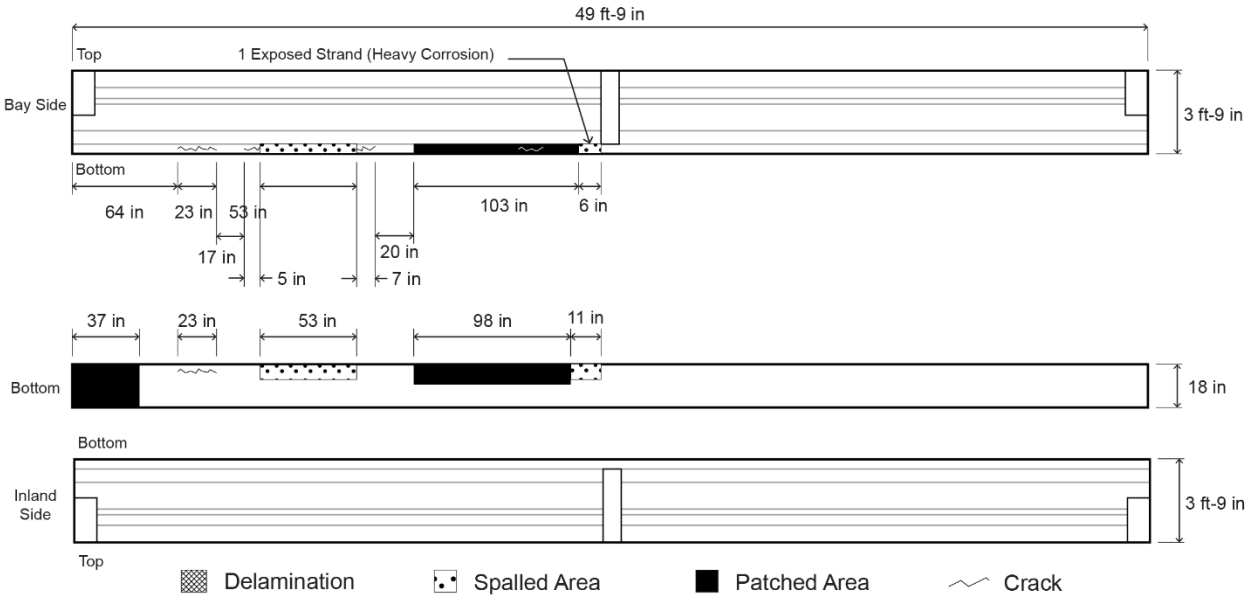

Figure 41. Damage Map for I-Beam 1

I-Beam 5: Repaired with External PT – Grout – Tested in Flexure

The inland side had no signs of deterioration (see Figure 42), while the bay side contained three spalled areas and three patched areas. One major corner spall was present near the midspan of the beam and contained an exposed strand.

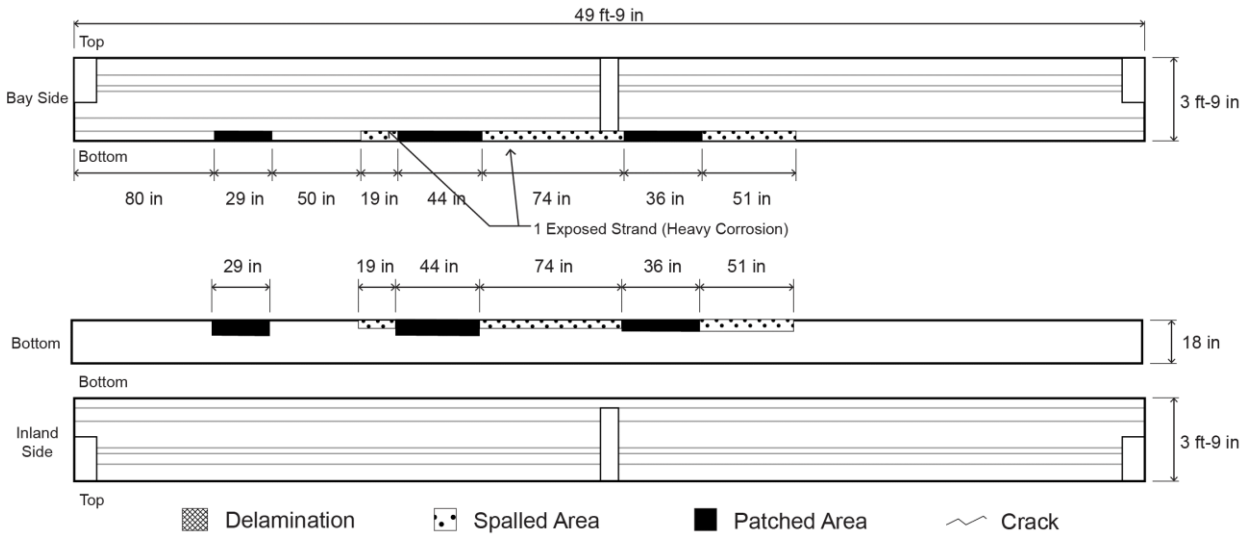

Figure 42. Damage Map for I-Beam 5

I-Beam 4: Repaired with Carbon Fiber Reinforced Polymer – Tested in Flexure

Figure 10 (presented in the "Methods" section) shows that the inland side had no signs of deterioration. The bay side had four spalled areas, two patched areas, and two small longitudinal cracks along its length. One exposed strand was observed in the spall located near the midspan. The bottom of the beam exhibited damaged areas that were extensions from the bay side spalls.

I-Beam 9: Unrepaired – Tested in Shear

The inland side had only a minor spall, while the bay side contained four spalled areas, one delamination, and four longitudinal cracks along its length (see Figure 43). The bottom of the beam contained three corner spalls that were extensions from the bay side spalls and ten longitudinal cracks.

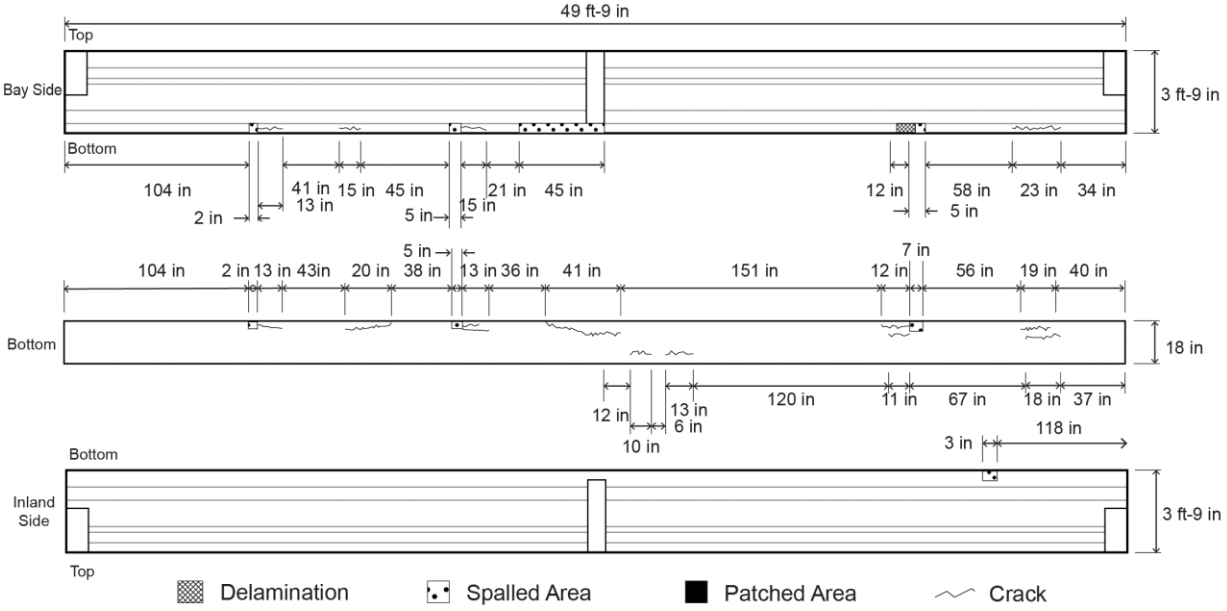

Figure 43. Damage Map for I-Beam 9

I-Beam 2: Repaired with Carbon Fiber Reinforced Polymer – Tested in Shear

Figure 44 shows that the inland side had no signs of deterioration. The bay side contained three large, patched areas. The bottom of the beam exhibited damaged areas that were extensions from the bay side patches.

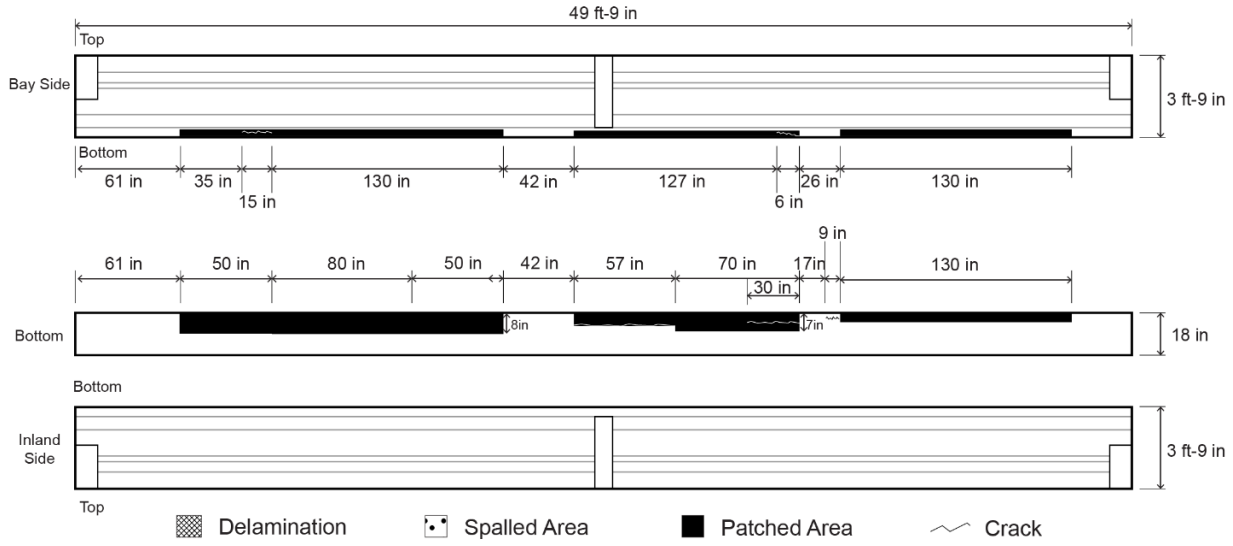

Figure 44. Damage Map for I-Beam 2

Box Beam 3: Unrepaired – Tested in Shear

Figure 45 shows that the east side contained a relatively major longitudinal crack extending about 208 inches near the girder's midspan. The west side of the Aden Road Bridge beam contained two longitudinal cracks and a significant continuous corner spall, with two exposed fractured strands from the bottommost two layers. The bottom of the beam contained several outer longitudinal cracks along with two major spalls with exposed strands. The first one was a corner spall that ran through about one-fifth of the beam's width and contained three exposed strands. The other is at the middle of the bottom of the box beam and had four exposed strands.

Box Beam 5: Repaired with Carbon Fiber Reinforced Polymer – Tested in Flexure

The east side contained longitudinal cracks along the beam varying in length from 40 in to 60 in (see Figure 46). Also, a large corner spall was located near the midspan of the beam and exposed two strands. The west side of the beam contained one 50-in longitudinal crack located at the end of the beam. The bottom of the beam exhibited several cracks and two major spalls.

Box Beam 6: Repaired with Carbon Fiber Reinforced Polymer – Tested in Shear

Figure 47 shows that the east side contained relatively minor cracks. The west side of the beam contained many small longitudinal cracks. The bottom of the beam contained several outer cracks and one small delamination area at the middle of the beam.

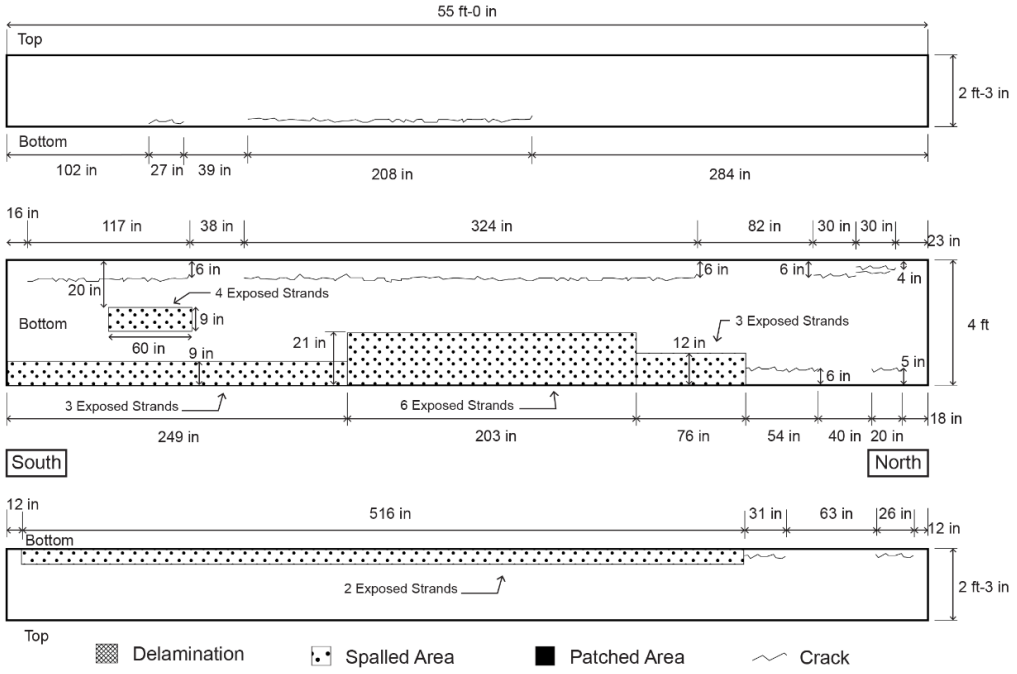

Figure 45. Damage Map for Box Beam 3

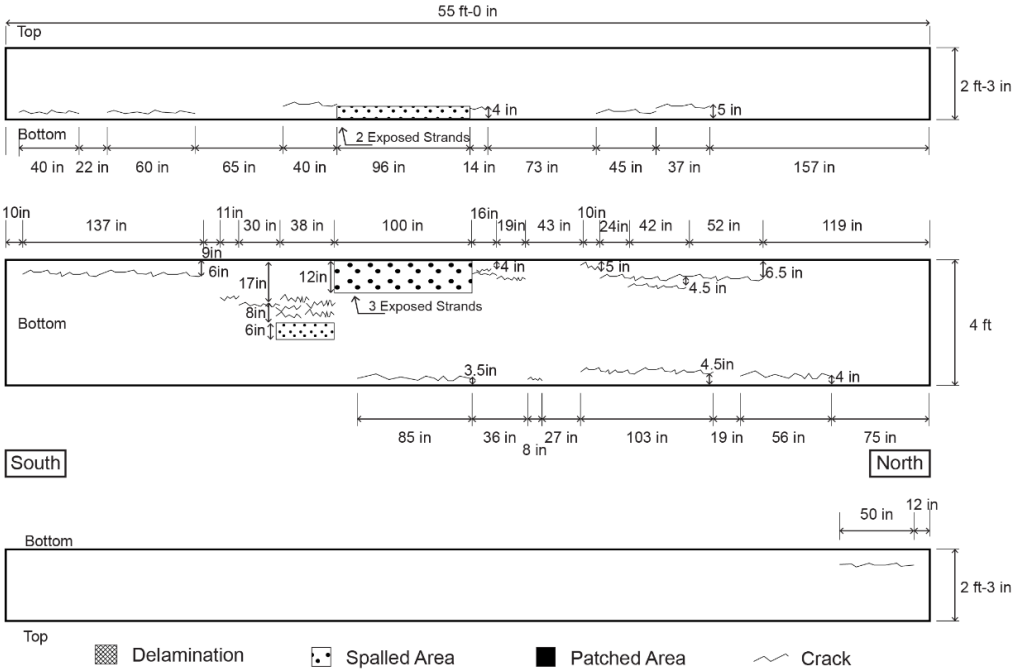

Figure 46. Damage Map for Box Beam 5

Half-Cell Potential Tests

Half-cell readings were taken on all the sides of the eight beams. Figure 48 shows a contour plot of the half-cell potential for Box Beam 3. All sides of the beam had a strong likelihood of corrosion everywhere a longitudinal crack or a concrete spall existed. In addition, the test showed that corrosion had propagated away from the expected location of corrosion, i.e.,

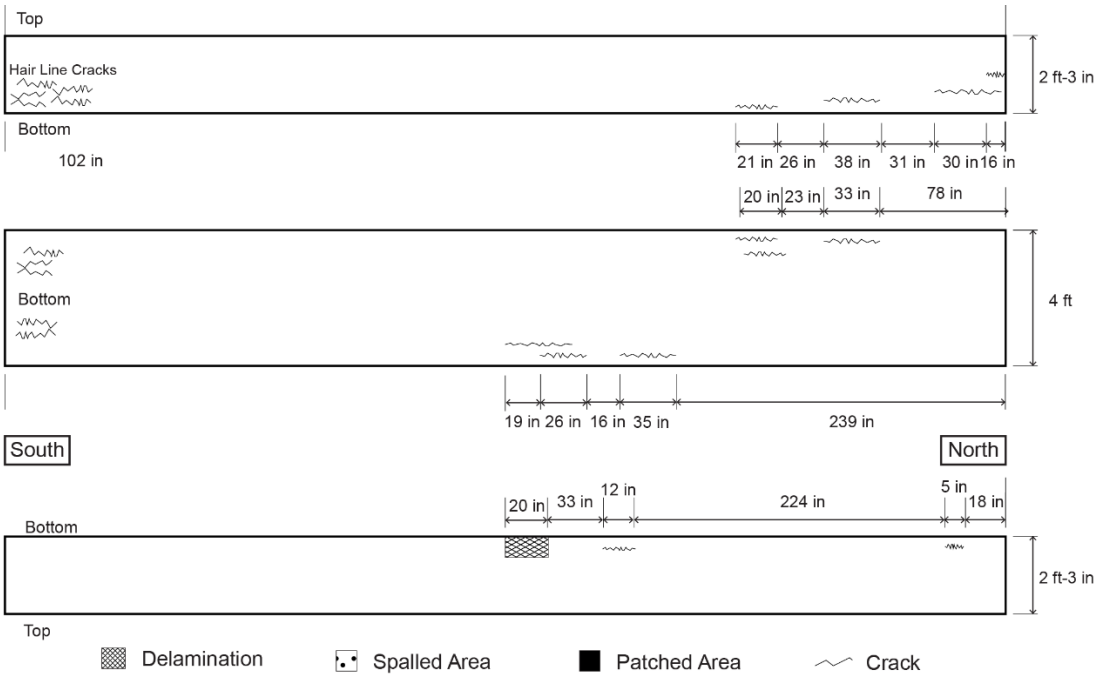

Figure 47. Damage Map for Box Beam 6

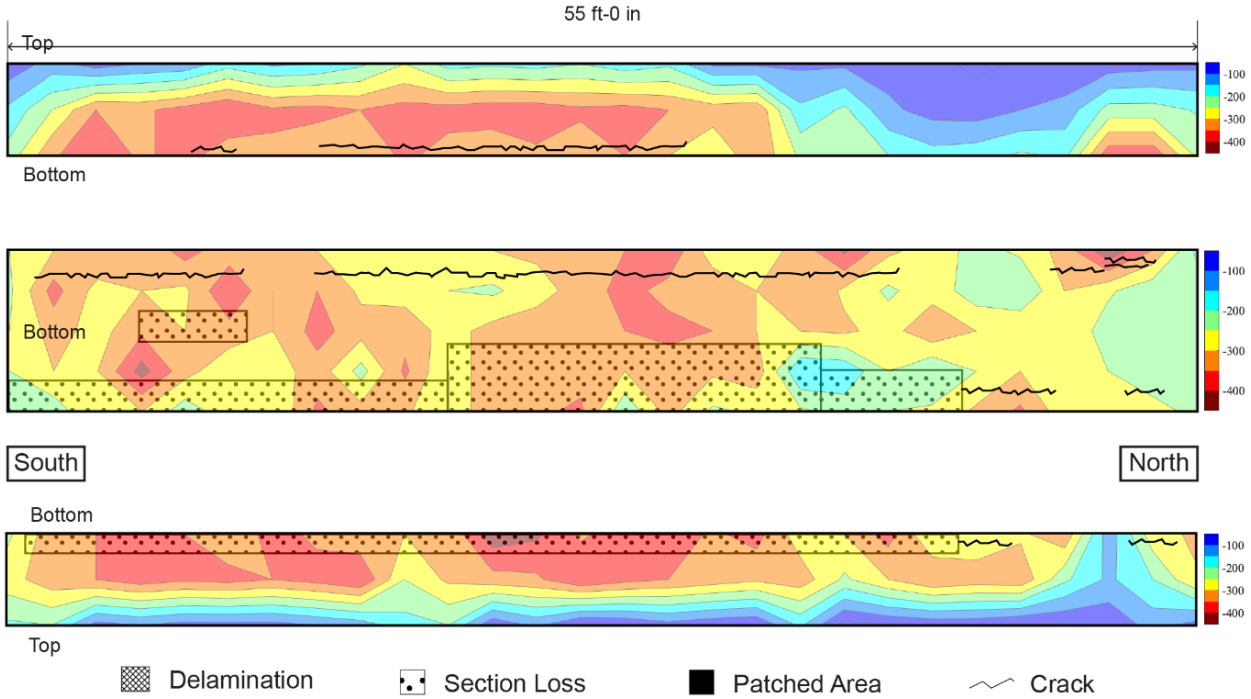

Figure 48. Contour Plot for Half-Cell - Box Beam 3 – Unrepaired – Tested in Shear

cracks and spalls. Similar plots comparing the half-cell potentials and the visible damage maps are presented in Al Rufaydah (2020), Moraes (2021), and Alfailakawi (2022). Table 12 shows the probability of corrosion for the eight beams, based on the number of readings in each category.

Table 12. Percentage of Half Cell Potential Readings with a Given Probability of Corrosion in the Beams

Beam	Side	Probability of Corrosion		
		<10%	Uncertain	>90%
I-Beam 1 – Repaired with External PT - Wax	Bay	28%	66%	6%
	Bottom	86%	13%	1%
	Inland	82%	17%	1%
I-Beam 5 – Repaired with External PT - Grout	Bay	44%	52%	4%
	Bottom	65%	34%	1%
	Inland	54%	43%	3%
I-Beam 4 – Repaired with CFRP	Bay	61%	35%	4%
	Bottom	80%	20%	0%
	Inland	87%	13%	0%
I-Beam 9 – Unrepaired	Bay	30%	66%	4%
	Bottom	81%	16%	3%
	Inland	77%	22%	1%
I-Beam 2 – Repaired with CFRP	Bay	56%	38%	6%
	Bottom	58%	42%	0%
	Inland	75%	18%	7%
Box Beam 3 – Unrepaired	East	46%	30%	24%
	Bottom	5%	78%	17%
	West	37%	38%	25%
Box Beam 5 – Repaired with CFRP	East	26%	47%	27%
	Bottom	29%	57%	14%
	West	18%	56%	26%
Box Beam 6 – Repaired with CFRP	East	76%	21%	3%
	Bottom	13%	82%	5%
	West	57%	28%	15%

Task 4: Implement Repair Techniques on Beams

Evaluation of Residual and Repaired Flexural Strength

The results of the calculations of undamaged strength, strength based on the currently observed level of damage, and strength based on an assumed amount of future corrosion damage are presented in Table 13. The calculated repaired strengths are also presented in the table. Figure 49 presents cross-sections of the four beams that were repaired to increase their flexural strength. Each cross-section presents the damage that was present within one development length on each side of the midspan of the beam.

Evaluation of Residual and Repaired Shear Strength

Table 14 shows the shear strength of the unrepaired beams calculated using the approaches presented in the Methods section. Figure 50 presents the damage for each end of each beam in the tested region. Table 15 and Table 16 present the calculated shear capacities for the beams before and after applying CFRP repair. The damage assumed at each end of each beam is presented in Figure 51.

Table 13. Calculated Flexural Capacity

Beam/Method	Undamaged Strength (k-ft)	Based on Assumed Damage over 20 years		Based on Current Observed Damage	
		Remaining Strength (k-ft)	Repaired Strength (k-ft)	Remaining Strength (k-ft)	Repaired Strength (k-ft)
I-Beam 1 - Repaired with EXT PT - Wax	1901	1398	2323	1752	2662
I-Beam 5 - Repaired with EXT PT - Grout	1901	1378	2318	1749	2656
I-Beam 4 - Repaired with CFRP	1901	1345	ACI: 1851 AASHTO: 2026	1718	ACI: 2272 AASHTO: 2349
Box Beam 5 - Repaired with CFRP	1452	1151	ACI: 1431 AASHTO: 1316	1243	ACI: 1579 AASHTO: 1519

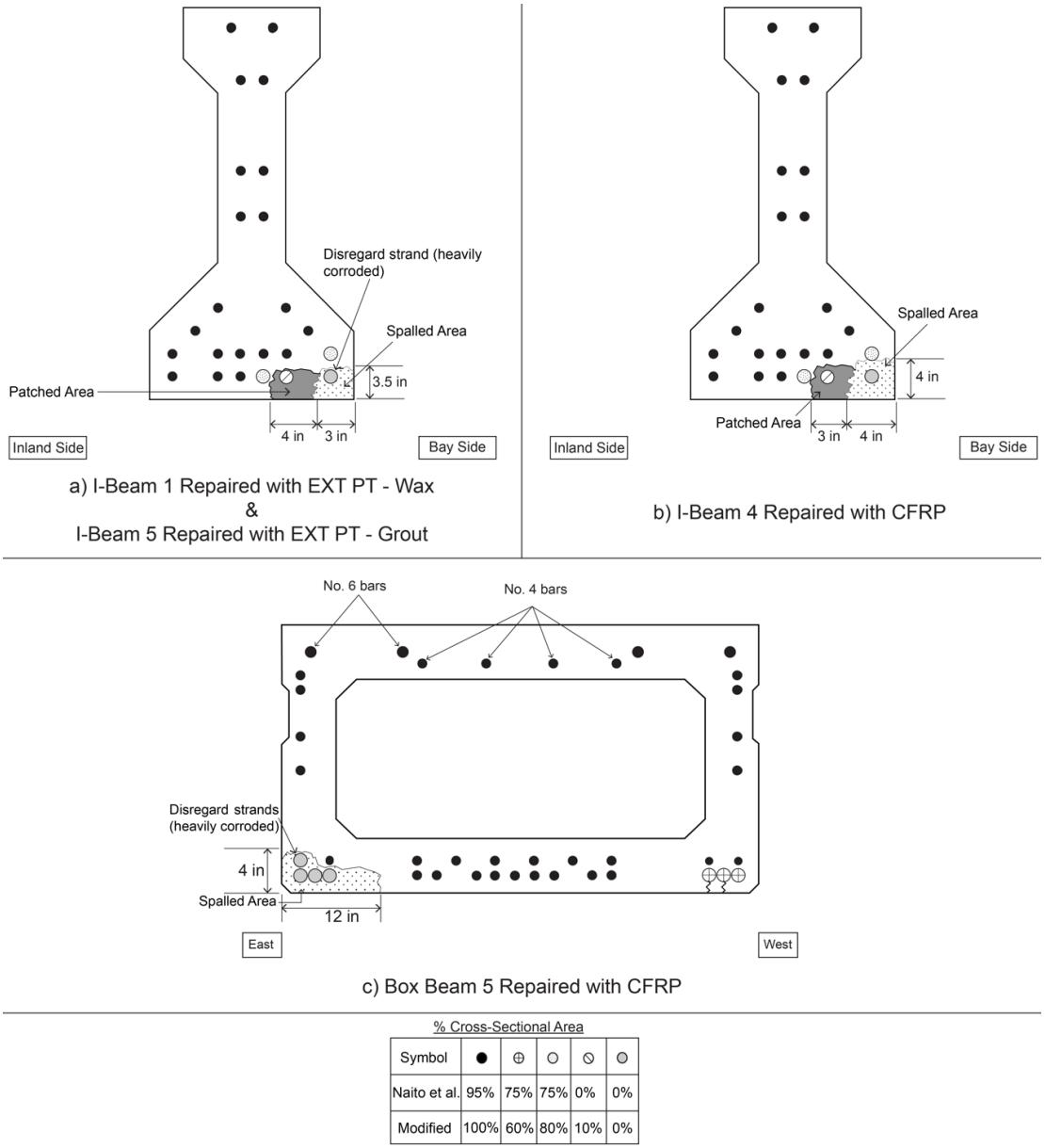

Figure 49. Assumed Damage Near Mid-Span for Beams Chosen for Flexural Tests

Table 14. Calculated Shear Capacity – Unrepaired Beams

Beam	Moment (k-ft)	ACI V_{ci}-V_{cw} (kips)		AASHTO (kips)		Strut and Tie Model (kips)
		V_c	V_n	V_c	V_n	
I-Beam 9 Unrepaired – 1st End	1812	108	225	47	228	306[1]
I-Beam 9 Unrepaired – 2nd End	1793	103	220	46	226	332[1]
Box Beam 3 Unrepaired – 1st End	1343	126	198	77	195	240[2]
Box Beam 3 Unrepaired – 2nd End	933.5	113	185	62	174	240[2]

[1] – Failure due to horizontal tension tie. [2] - Failure due to diagonal compression strut

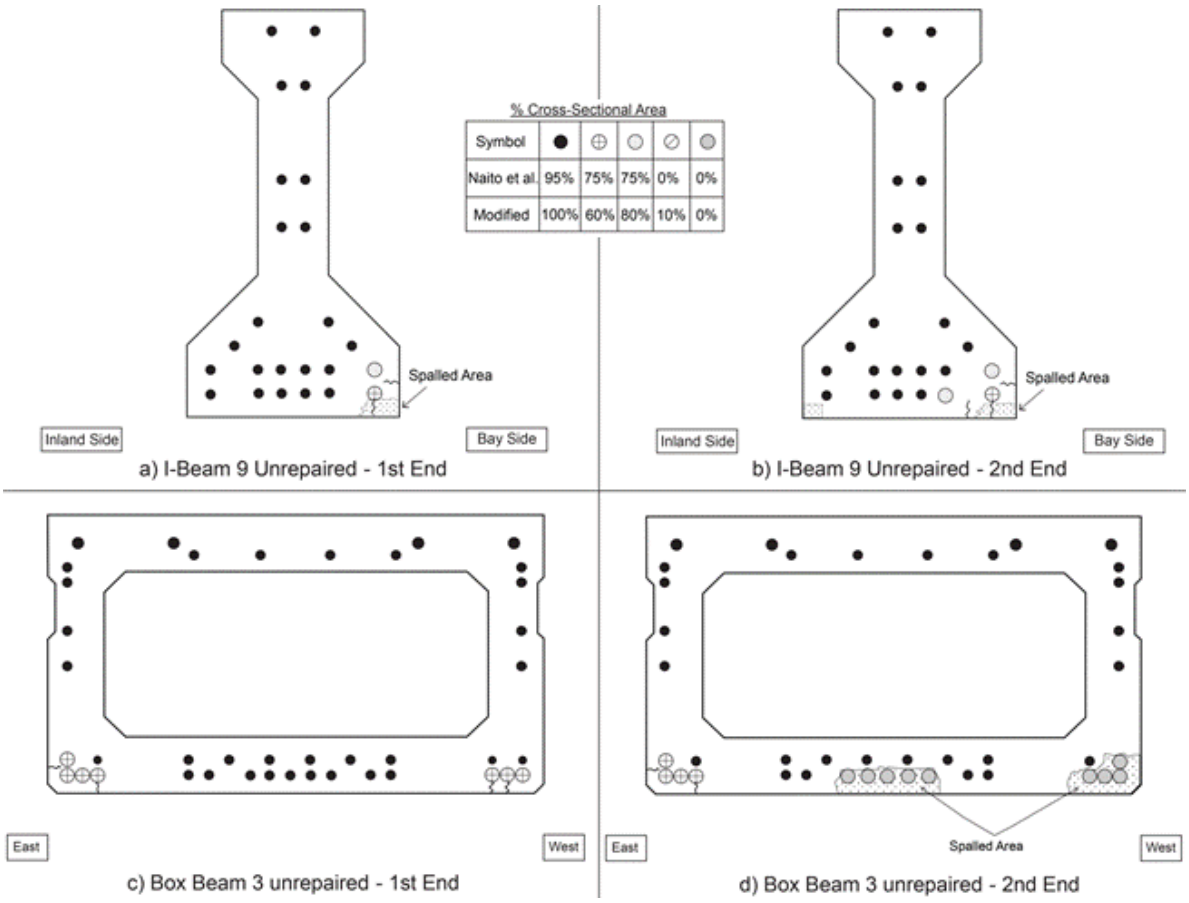

Figure 50. Assumed Damage at Each End of Beams Tested in Shear with No Repair

Table 15. Calculated Shear Capacity – Unrepaired Beams 2 and 6

Beam	Moment (k-ft)	ACI V_{ci} V_{cw} (kips)		AASHTO (kips)		Strut and Tie Model (kips)
		V_c	V_n	V_c	V_n	
I-Beam 2 Unrepaired – 1st End	1511	93	230	85	232	309[1]
I-Beam 2 Unrepaired – 2nd End	1245	93	230	80	232	276[1]
Box Beam 6 Unrepaired – 1st End	1328	108	180	87	200	240[2]
Box Beam 6 Unrepaired – 2nd End	1307	108	180	86	208	240[2]

[1] – Failure due to horizontal tension tie. [2] - Failure due to diagonal compression strut

Table 16. Calculated Shear Capacity –Beams 2 and 6 After CFRP Repair

Beam	Moment (k-ft)		ACI V_{ci} V_{cw} (kips)		AASHTO (kips)		Strut and Tie Model (kips)
	Concrete Crushing	Debonding	V_c	V_n	V_c	V_n	
I-Beam 2 Repaired with CFRP – 1st End	1892	1722	93	262	85	262	383[1]
I-Beam 2 Repaired with CFRP – 2nd End	1674	1445	93	262	80	262	383[1]
Box Beam 6 Repaired with CFRP – 1st End	1817	1663	108	180	87	200	240[1]
Box Beam 6 Repaired with CFRP – 2nd End	1798	1642	108	180	86	208	240[1]

. [1] - Failure due to diagonal compression strut

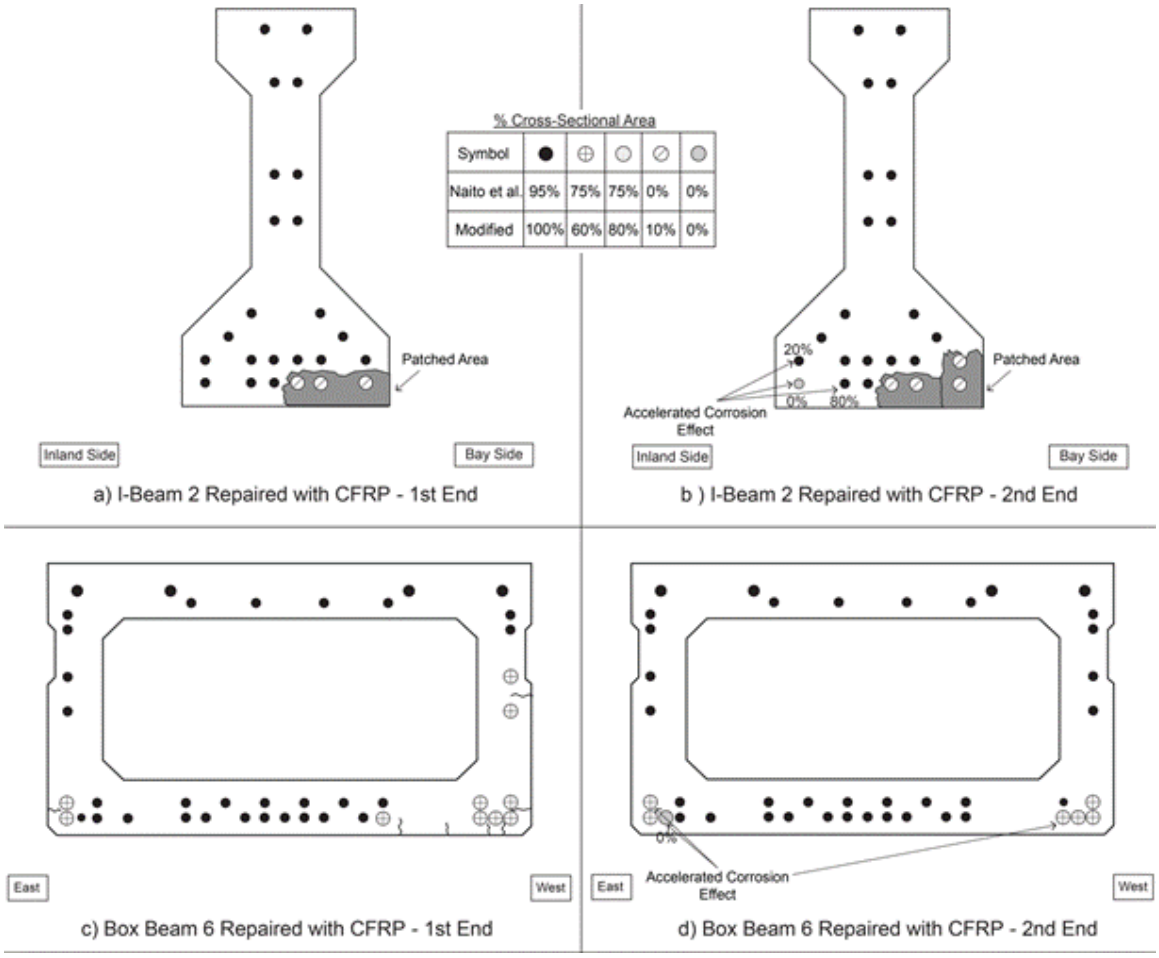

Figure 51. Damage Assumed in the Beams Repaired for Shear with CFRP

Task 5: Conduct Experimental Tests of Repaired Girders

I-Beam 1: Repaired with External Post-Tensioning – Flexible Filler – Flexural Test

For this test, the beam was loaded in increments of 10 kips until the load reached 250 kips, at which point a displacement control was employed. During the loading process, the concrete ahead of the anchor block on the inland side at the live end began to crack, with

shear cracks directed toward the load at 150 kips. At 160 kips, the first flexural crack formed, as indicated by the change in slope of the load-deflection plot (see Figure 52).

Continued loading resulted in further shear cracks in the web near the top side of each anchor block, oriented toward the support, as shown in Figure 53a. Flexural cracks originated at the bottom flange and propagated up to the mid-height of the web within the constant moment region at the midspan. By 250 kips, there were several concrete noises due to the formation of additional cracks, and one wire ruptured. The number of broken wires during the test is shown in Figure 53. After 260 kips of load, the graph began to flatten until the beam failed at 263 kips. The failure mechanism shown in Figure 53b is concrete crushing on the top of the beam that propagated to the bottom flange. It should be noted that there were no abnormal readings associated with the anchor blocks, confirming the effectiveness of the anchor block design.

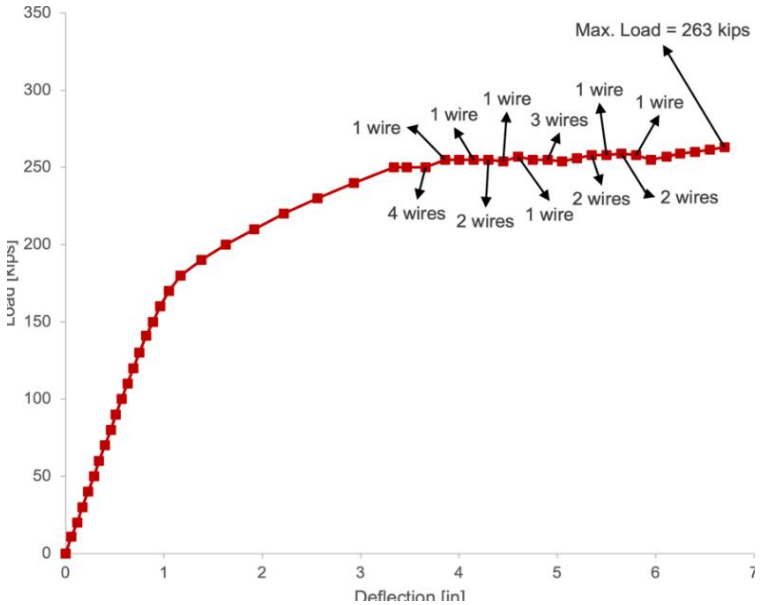

Figure 52. Load Versus Deflection - I-Beam 1 - Repaired with Eternal PT – Flexible Filler (notes in figure indicate when the sounds of wire breaks were heard during testing)



(a) **(b)**

Figure 53. Concrete Crushing at the Top of I-Beam 1 – Repaired with External PT – Flexible Filler

The failure of the beam was quite explosive because, although the bonded pretensioned strands had yielded, the external post-tensioned strands were still elastic. Upon crushing the concrete, the strands "snap back" to their original length and cause the explosive crushing of the entire cross-section.

In Table 13, the predicted flexural strength with the external PT repair was 2662 k-ft. The self-weight moment is 208 k-ft, so the applied moment was expected to be 2454 k-ft. With a distance from the supports to the load points of 20 ft, this equates to an applied load of 245 kips. The actual failure load of 263 kips indicates that the assumption that the stress in the external tendons is the effective prestress is somewhat conservative.

I-Beam 5: Repaired with External Post-Tensioning – Grout Filler – Flexural Test

The beam was loaded in 10-kip increments until the load reached 190 kips, and thereafter it was loaded in 5-kip increments. At a load of 100 kips, the first shear cracking occurred ahead of the anchor block on the bay side at the live end. By a load of 120 kips, a shear crack that had propagated ahead of each anchor block continued to propagate with each load step until the load reached 160 kips. At 160 kips, a shear crack developed behind the anchor block towards the live end. As evidenced by the change in slope of the load-deflection plot, the first flexural crack formed at load 170 kips (see Figure 54). With the increase in load, additional flexural cracks formed and propagated from the bottom flange to the top of the web.

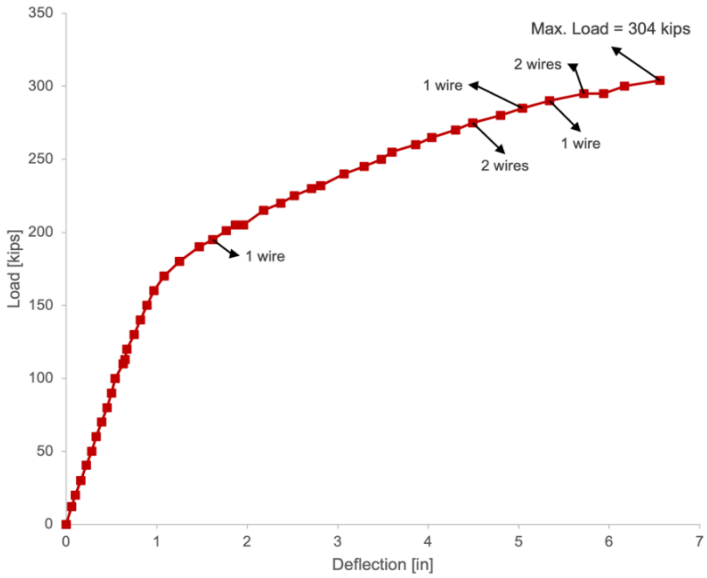

Figure 54. Load Versus Deflection - I-Beam 5 - Repaired with External PT – Grout (notes in figure indicate when the sounds of wire breaks were heard during testing)

Two wires from a deteriorated exposed strand ruptured at 195 kips (see Figure 55). Figure 54 shows the number of broken wires noted during the test. The cracks continued to grow, and the width of the existing cracks widened until the beam failed at 304 kips, with concrete crushing through the depth of the beam (see Figure 56). As with the other beam repaired with external PT, the failure was quite explosive. In Table 13, the predicted flexural strength with the external PT repair was 2656 k-ft. Based on the known self-weight moment and loading arrangement, this equates to an applied load of 245 kips to fail the beam. The actual failure load



Figure 55. Broken Wires During the Test of I-Beam 5



Figure 56. Concrete Crushing at the Top of the Beam – I-Beam 5 - Repaired with External PT – Grout

of 304 kips indicates that the assumption that the stress in the external tendons is the effective prestress was quite conservative.

The failure loads of the two beams repaired with external PT were 263 kips for the beam with wax filler in the ducts and 304 for the beam with grout in the ducts. However, the filler did not appear to influence the behavior up to a load of 250 kips. After this load, the beam with wax had many more sounds of wires breaking compared to the beam with grout. So, the difference in strength is attributable to the difference in initial condition, and not the filler material. The damage maps for both beams reveal similarities in the center of the beams, which is the section of interest for flexural analysis, and this is in accordance with the results obtained from the half-cell heat maps provided by Alfailakawi, (2022). However, based on the chloride content tests results listed by Alfailakawi, (2022) I-Beam 1 was considered to have a medium to high risk of corrosion, while I-Beam 5 had a negligible to medium risk of corrosion. These forensic investigations offered a general idea of the likelihood of corrosion in the beams, but they cannot be used as a quantification approach to be incorporated in the calculation to determine the residual flexural strength.

I-Beam 4: Repaired with Carbon Fiber Reinforced Polymer – Flexural Test

Throughout this test, the beam was loaded in 10-kip increments. At a load of 75 kips, the first flexural crack was detected near the midspan of the beam on the bay side. The load was increased to 170 kips, at which point the popping of CFRP stretching was audible. The load continued to increase until it reached 230 kips, at which point the beam was unloaded to 192 kips due to a technical issue. The beam was reloaded to 230 kips, when the CFRP failed and detached from the beam's soffit (see Figure 57)



Figure 57. CFRP Debonded

To determine the beam's capacity without the CFRP repair, the beam was unloaded to 130 kips, the CFRP was removed from the whole beam, and the beam was reloaded. After reaching 161 kips, the beam collapsed due to concrete crushing at the top, as shown in Figure 58. The load-deflection plot is presented in Figure 59.



Figure 58. Concrete Crushing Failure Mode and Cracking Pattern

In Table 13, the predicted flexural strength with the CFRP repair was 2272 k-ft (ACI method) or 2349 k-ft (AASHTO method). The known self-weight moment and loading conditions equate to an applied load of 206 kips and 215 kip, respectively. The actual failure load of 234 kips indicates that the method used to calculate the repaired strength was conservative. Also, note in Table 13 that the unrepaired strength was estimated to be 1718 k-ft, which equates to an applied load of 152 kips. The actual unrepaired strength was slightly higher at 161 kips.

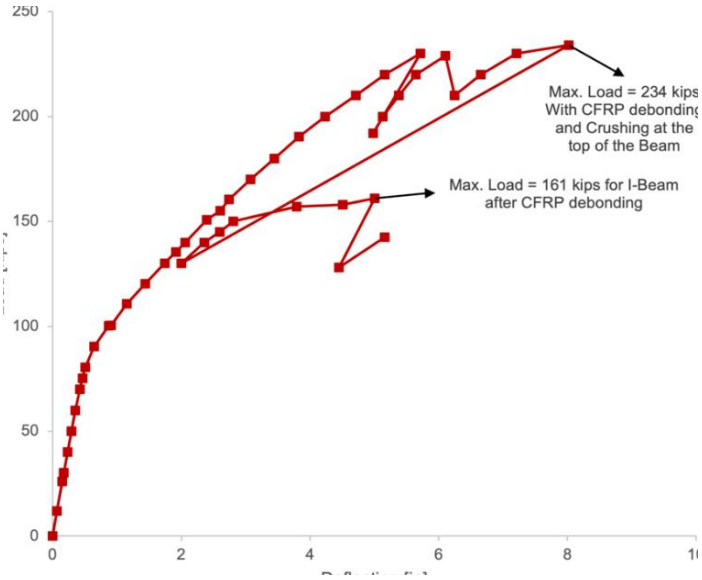

Figure 59. Load Versus Deflection – I-Beam 4 - Repaired with CFRP

Box Beam 5: Repaired with Carbon Fiber Reinforced Polymer – Flexural Test

The beam was loaded in increments of 10 kips until it reached 40 kips, at which point the load increment was reduced to 5 kips. At a load of 50 kips, the first flexural crack was seen, corresponding to the change in slope of the load-deflection plot illustrated in Figure 60. More cracking noises continued to be heard, mostly in the patched regions used to cosmetically repair the beam prior to repair with CFRP. At 50 kips, unexpected longitudinal cracks formed on both ends, which may be explained by a debonding between the concrete and the strands, rather than the CFRP. By 75 kips, CFRP debonding sounds were heard, but the location could not be determined. Additional sounds of concrete cracking and CFRP straining were heard, as well as the sound of a wire rupture at a load of 85 kips. The load was increased to 97 kips, at which point the test was interrupted due to technical issues.

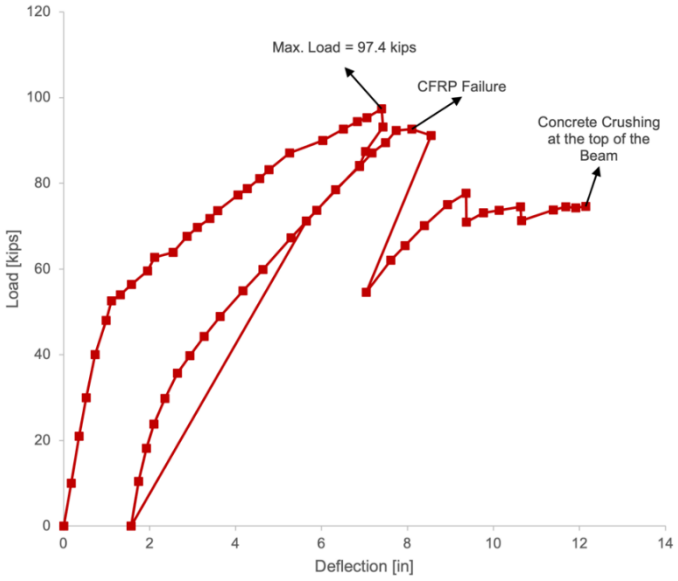

Figure 60. Load Versus Deflection - Box Beam 5 - Repaired with CFRP

The test proceeded with a 1.5 in residual deflection, and the load was increased until it reached 93 kips, at which point one of the three CFRP strips debonded and another ruptured (see Figure 61). When the load was reduced to 90 kips and then increased again, the whole CFRP debonded off the beam's soffit. The beam was then unloaded to 54 kips, and the CFRP strips were removed, allowing the beam to be retested without repair to obtain a load-deflection plot for the beam in its damaged condition. The loading was continued until it reached 77 kips. Two wires broke in the beam's center, resulting in a very big flexural crack. Finally, the beam collapsed due to concrete crushing at the top, with an ultimate load of 77 kips (see Figure 62).

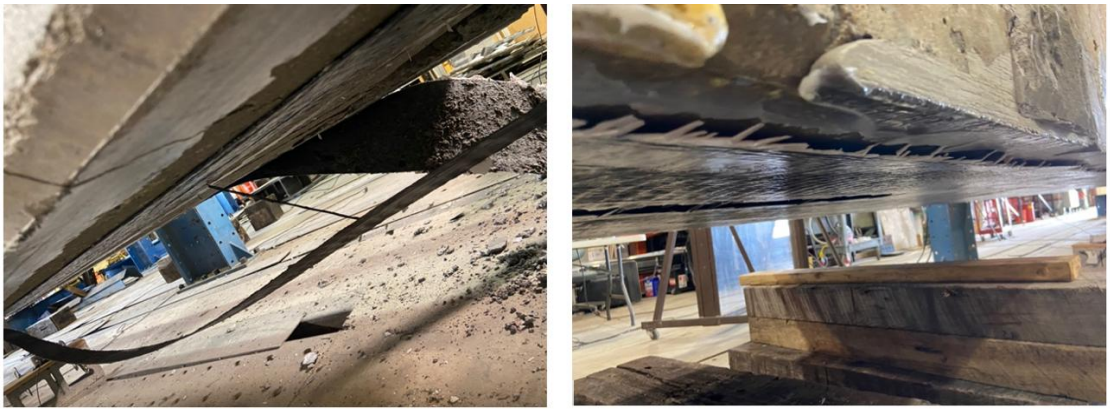

Figure 61. CFRP Debonded and Ruptured on Bottom of Box Beam 5



Figure 62. Concrete Crushing Failure Mode

In Table 13, the predicted flexural strength with the current level of corrosion damage and the CFRP repair was 1579 k-ft with the ACI method and 1519 k-ft with the AASHTO method. The self-weight moment is 253 k-ft. With a distance from the supports to the load points of 22.5 ft, this equates to an applied load of 117 kips and 113 kips, respectively. The actual failure load of 97 kips indicates that the method used to calculate the repaired strength was somewhat unconservative. Also, note in Table 13 that the unrepaired strength was estimated to be 1243 k-ft, which equates to an applied load of 88 kips. The actual unrepaired strength was slightly less at 77 kips. The post-test forensic examination revealed that the cardboard void formers in the box beam were moist, indicating that there was trapped water in the box beam.

This could have resulted in additional undetected corrosion of the prestressing. Previous tests have shown the reduction in cross-sectional area of the layer of strands next to the void is approximately 15% (Alfailakawi et al., 2020). Including the effect of water, the applied load calculated is 112 kips using AASHTO method and equal 104 kips using ACI method.

I-Beam 9: Unrepaired – Shear Test

First End Test

In this test, the load was applied in 5-kip increments throughout the test. The first shear crack was initiated at the middle of the beam's web at a load of 120 kips and located 46.5 in from the support, which was closer to the load point. This was very close to the critical section for shear, 48 in, per AASHTO LRFD (AASHTO, 2020). At the same time, the first flexural crack was observed on the bay side at a load of 141 kips. Cracking was confirmed by a change in the slope of the load-deflection plot shown in Figure 63. After that, several web-shear cracks and flexural cracks opened on both sides. Most of the cracks propagated upwards to the beam's top flange.

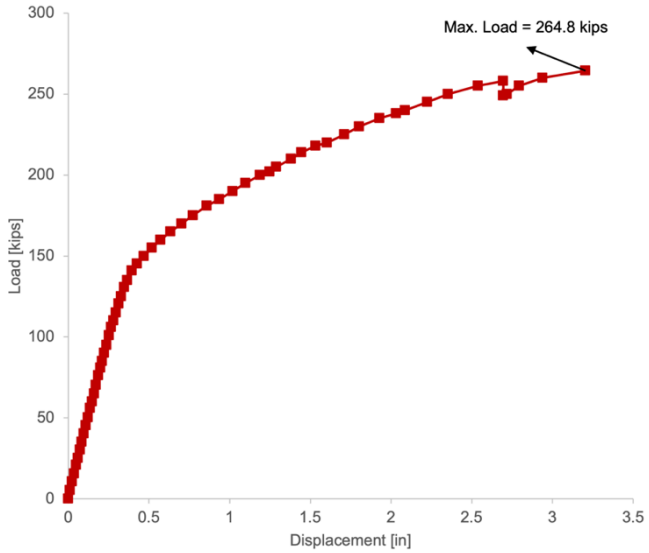

Figure 63. Load Versus Deflection Unrepaired I-Beam – First End Shear Test

At a load of 258 kips, chunks of concrete located at pre-existing damage fell off, and one strand ruptured on the bay side. This rupture was indicated by a small drop-off in the load-deflection plot in Figure 63. Post-testing investigation showed that one strand on the bay side had fractured (Figure 64c). Wide and shallow cracks formed near the strand rupture (Figure 64b). Not long after, the concrete deck crushed near the loading location at 264.8 kips of applied load, and the test was stopped. This load corresponds to a total shear of 236 kip at the critical section for shear. Figure 64a shows this beam end's failure mechanism.

Second End Test

The first web-shear crack was observed at a load of 136 kips on the inland side of the beam. This crack was located 43 in from the support that was closer to the load point. This location was 5 in away from the critical section for shear, or 48 in, per AASHTO. The first

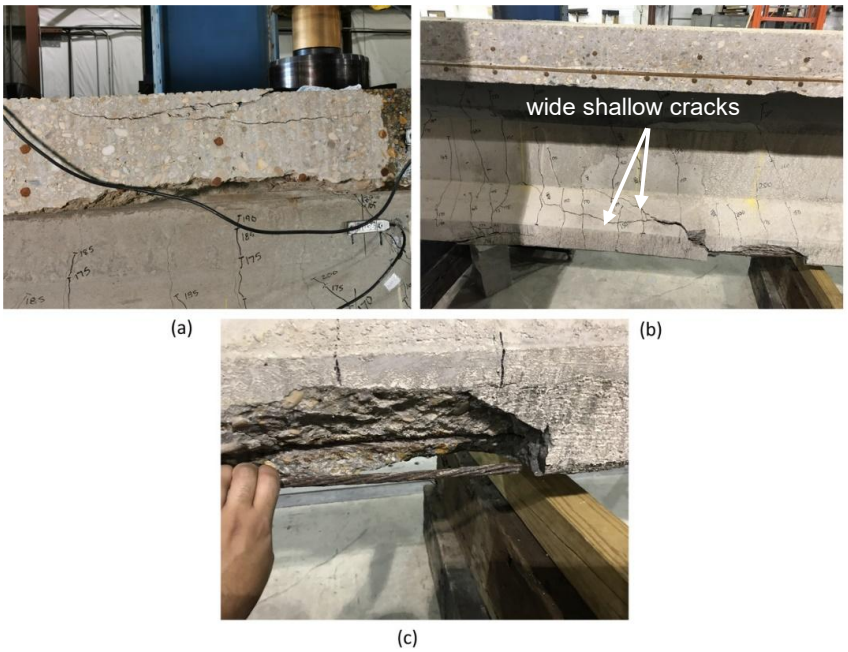

Figure 64. Failure Mechanism for Beam 9 – First End Shear Test. (a) Top Crushing, (b) Wide Cracking in the Bay Side where the Strand ruptured, (c) Strand Ruptured in the Bay Side

flexural crack was observed at a load of 206 kip and was located under the load point. After that, several web-shear cracks and flexural cracks opened on both sides. Figure 65 shows the cracking pattern for this test.



Figure 65. Cracking Pattern – I-Beam 9 - Second End Shear Test

After reaching 340 kips of applied load, many "popping" sounds were heard repeatedly. Because there was no major load drop in the load-deflection plot at 340 kips (Figure 66), these sounds were attributed to the opening of new cracks. In addition, the post-testing investigation showed that no strands appeared to be fractured during the test. The load was increased to 382 kips, at which point the web crushed in a very explosive and brittle manner. This load corresponds to a total shear of 318 kips at the critical section for shear. Figure 67 shows the failure mode of this beam end. Before the web crushed, cracks were inclined at about a 35-degree angle. However, the web crushed at a steep angle at failure, which took a short path from the point load to a nearby concrete spall instead of extending towards the support.

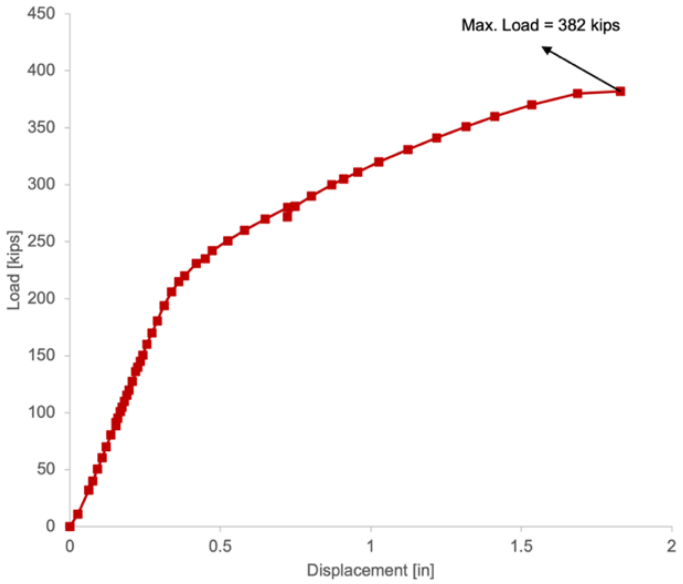

Figure 66. Load Versus Deflection – I-Beam 9 - Second End Shear Test

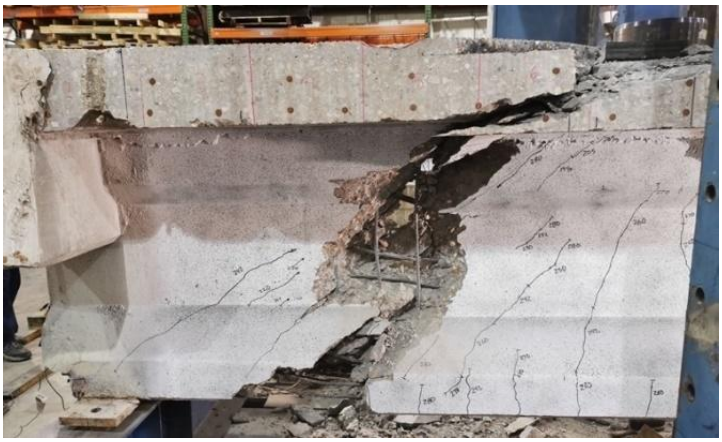

Figure 67. Web Crushing Failure Mode – I-Beam 9 – Second End Shear Test

I-Beam 2: Repaired with Carbon Fiber Reinforced Polymer – Shear Test

First End Test

In this test, although no cracks were visually detectable, the first cracking sounds were heard at a load of 193 kips. The first sounds from CFRP debonding were heard at 203 kips. The first shear cracks were visible on the beam at 223 kips. At 246 kips, louder noises were heard, and this is thought to have been from strands rupturing. Due to issues with the spreader beam, the beam had to be unloaded at 334 kips. Upon reloading, the final load before the failure was 329 kips at a deflection of 2.84 in. The expected failure mode of this specimen was concrete crushing at 330 kips calculated by strain compatibility, which was validated by the test results. It should be noted that the first Lesner Bridge beam shear test failed by concrete crushing at 264 kips, showing that the CFRP repair for this test increased the ultimate strength of the beam. The load-deflection plot for this beam is presented in Figure 68. Figure 69 shows the ruptured CFRP and the concrete crushing as a failure mode.

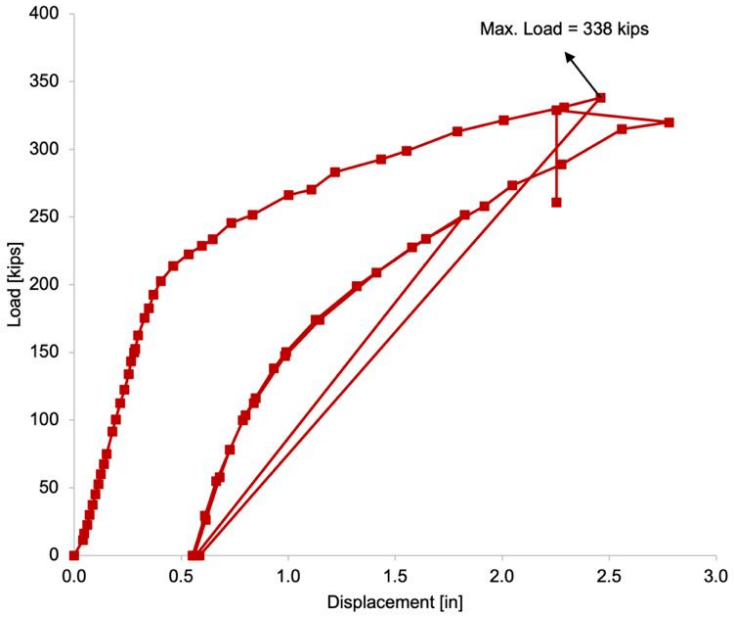

Figure 68. Load Versus Deflection - I-Beam 2 - Repaired with CFRP - First End Shear Test



Figure 69. CFRP Rupturing Failure Mode – I-Beam 2 - Repaired with CFRP - First End Shear Test

Second End Test

Sounds of CFRP stretching and glue cracking were first heard at a load of 213 kips. At this point, the first shear crack was noticed at the same location on both faces of the beam, and these cracks went from the point load toward the pin support. At a load of 313 kips, a crack directly under the point load went straight down between the CFRP sheets and became large enough to decrease the load on the beam to 295 kips. The CFRP ruptured at 302.5 kips, whereby the load dropped to 239 kips. Upon reloading, the beam failed at 255 kips by rupturing the strands. The estimated load to fail this specimen was 335 kips due to concrete crushing, but the beam failed because of strands rupturing. This failure mode indicates that the accelerated corrosion of the strands reduced the tensile strength of the prestress more than anticipated.

Figure 70 shows the load-deflection curve. At 166 kips, the slope changed, which indicated that value was the cracking load. Figure 71 shows the failure mode and the ruptured strands. Note that all longitudinal strands in the bottom flange and the web ruptured.

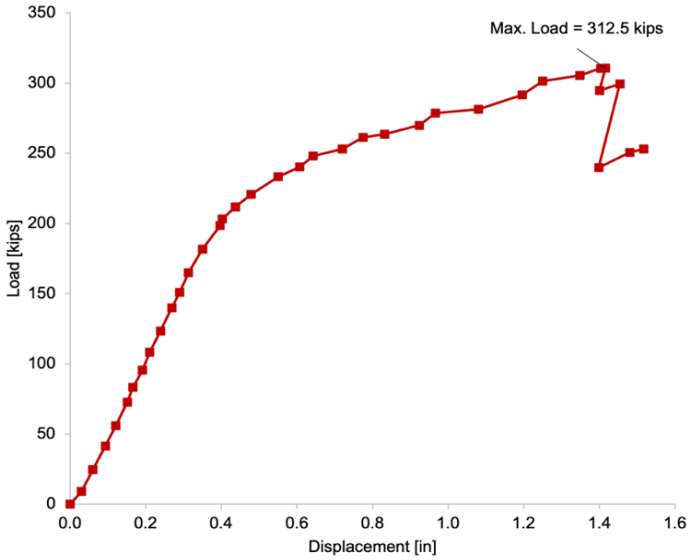

Figure 70. Load Versus Deflection - I-Beam 2 - Repaired with CFRP - Second End Shear Test



Figure 71. CFRP Rupturing Failure Mode- I-Beam 2 - Repaired with CFRP - Second End Shear Test

Box Beam 3: Unrepaired – Shear Test

First End Test

In this test, the load was initially applied in 10-kip increments until reaching close to the expected cracking load, at which point the load was applied in 5-kip increments until failure. The load-deflection plot for this test is shown in Figure 72. The first web-shear crack was observed at a load of 150 kips on the west side of the beam. This crack was located 46 in from the support closer to the load point.

The first flexural crack was observed on the west side of the beam at a load of 205 kips and was located under the load point. Generally, the flexural cracks did not propagate to the top of the beam, and the behavior was dominated mainly by shear deformations. Only a few parallel web-shear cracks formed on either side of the beam throughout the test. After reaching 250 kip of applied load, the critical web shear crack opened significantly, and the shear failure seemed imminent. The load was increased to 259 kips, at which point the beam separated into two

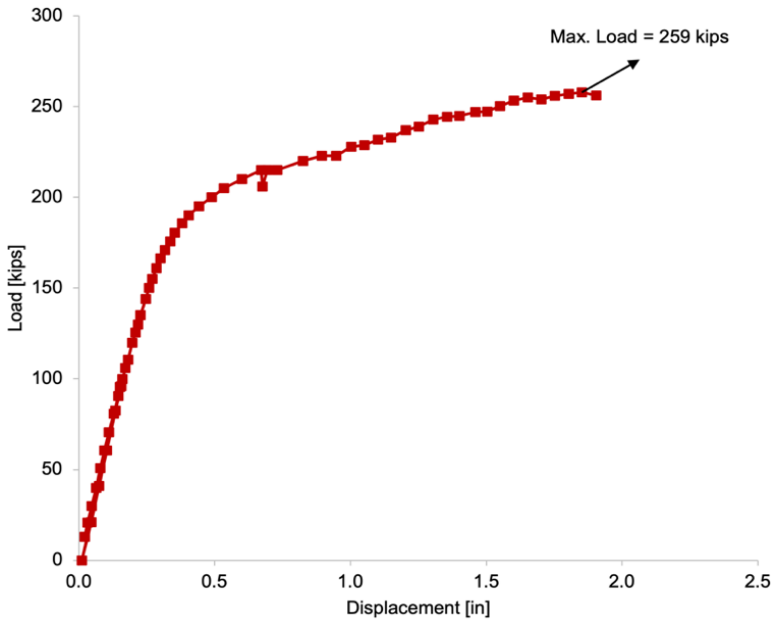

Figure 72. Load Versus Deflection – Box Beam 3 – Unrepaired – First End Shear Test

portions that slipped relative to each other, and the test was stopped. The failure mechanism of this beam is shown in Figure 73. This load corresponds to a total shear of 257 kip at the critical section for shear.



Figure 73. Diagonal Tension Failure Mode - Box Beam 3 – Unrepaired – First End Shear Test

Second End Test

In this test, the load was initially applied in 10-kip increments until reaching close to the expected cracking load; at which point, the load was applied in 5-kip increments until the protocol was changed to deflection control. The load-deflection plot for this test is shown in Figure 74. The first web-shear crack was observed at a load of 150 kips on the east side of the beam. This crack was located near the middle of the shear span, close to the critical section for shear, or 30.4 in, per AASHTO.

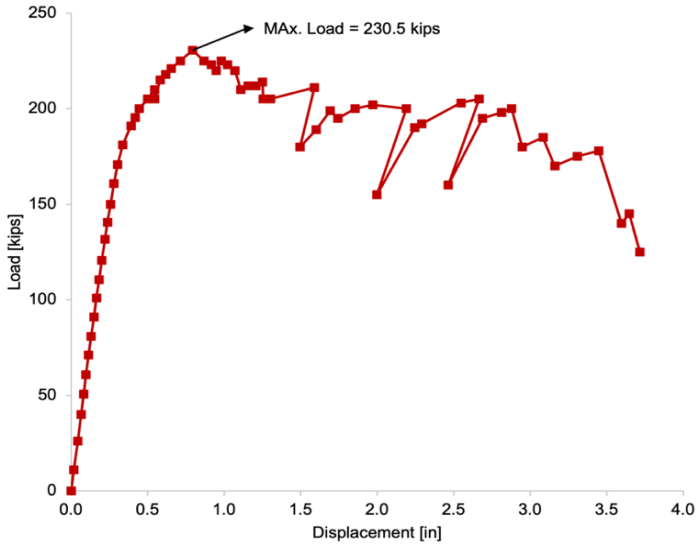

Figure 74. Load Versus Deflection – Box Beam 3 – Unrepaired - Second End Shear Test

The first flexural crack was observed on the west side of the beam at a load of 171 kips and was located under the load point. This low value of flexural cracking load can be attributed to the excessive pre-existing damage near the soffit of the beam where the bottom concrete cover was completely missing.

Similar to the first Aden Road Bridge test, only a few parallel web-shear cracks formed on either side of the beam throughout the test. At 190 kips of applied load, a shear crack propagated up, almost to the loading pad. When the applied load reached 225 kips, "popping" sounds were heard many times as the deflection increased. At each sound, a sudden drop in the load-deflection plot was noticed, as shown in Figure 74.

Meanwhile, severe flexural cracks propagated from a pre-existing spall on the bottom of the beam located about 4.5 ft from the point load towards the furthest end of the beam, as shown in Figure 75a. The "popping" sounds with the corresponding drops in the load-deflection plot were attributed to fracturing of strand wires. Ultimately, strand wires kept fracturing progressively, and the behavior of the beam became flexure-dominated as the curvature significantly increased at that location. Figure 75b shows the condition of strands after the test. The maximum recorded applied load was 230.5 kips. The test was terminated when the deflection at the point load location exceeded 3.5 in.

Box Beam 6: Repaired with Carbon Fiber Reinforced Polymer – Shear Test

First End Test

The first cracks were noticed in this test at a load of 170 kips. The first flexural crack was in a patched area, and the first shear crack was in the middle of the shear span. The shear crack was around 0.1 in wide at 250 kips. Due to the width of the crack, the beam started leaking water from both faces. This end of the beam failed similarly to the first test for the unrepaired box beam. This end was loaded up to 260 kips and failed in shear with a diagonal crack splitting the beam in two. The CFRP repair at the bottom of the beam did not debond or rupture, which



(a) (b)

Figure 75. Strands Rupturing Failure Mode - Box Beam 3 – Unrepaired - Second End Shear Test

indicates that the CFRP helped with the ultimate strength of the beam. The slope of the load-deflection plot, shown in Figure 76, changes at 150 kips, which indicates that the cracking moment was 555 k-ft. The calculated cracking moment for this end was 620 k-ft, suggesting that the accelerated corrosion reduced the number of effective strands more than anticipated.

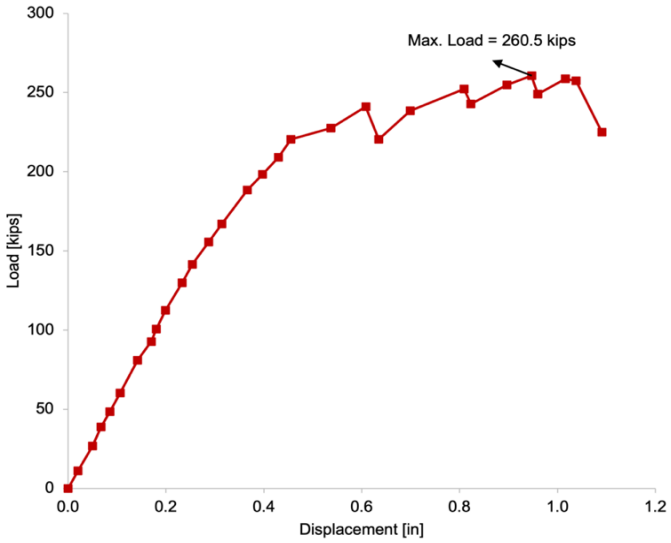

Figure 76. Load Versus Deflection – Box Beam 6 - Repaired with CFRP – First End Shear Test

Figure 77 shows the failure mode of the beam. One side had significantly more spalling of the concrete. This spalling could be due to the level of corrosion already present in the strands. There is also corrosion visible on the stirrups on this side. The other side had a large crack, but minimal spalling.

Second End Test

The first crack was noted in a patched area of the beam at a load of 120 kips. The first shear crack was seen at 130 kips. New shear cracks appeared and increased in size on the same side throughout the rest of the test, but no cracks were noted on the other side of the beam until 180 kips. This end failed at 230 kips in shear, as shown in Figure 78. The CFRP did not debond or rupture during the test.



Figure 77. Shear Failure Mode of Box Beam 6 - Repaired with CFRP – First End Shear Test



Figure 78. Shear Failure Mode of Box Beam 6 - CFRP Repair – Second End Shear Test

The load-deflection plot is shown in Figure 79. The load at which the slope changed was 150 kips, which indicates that the cracking moment was 543 k-ft. The calculated cracking moment for this setup was 592 k-ft, indicating that the accelerated corrosion changed the effective prestress enough to reduce the cracking moment.

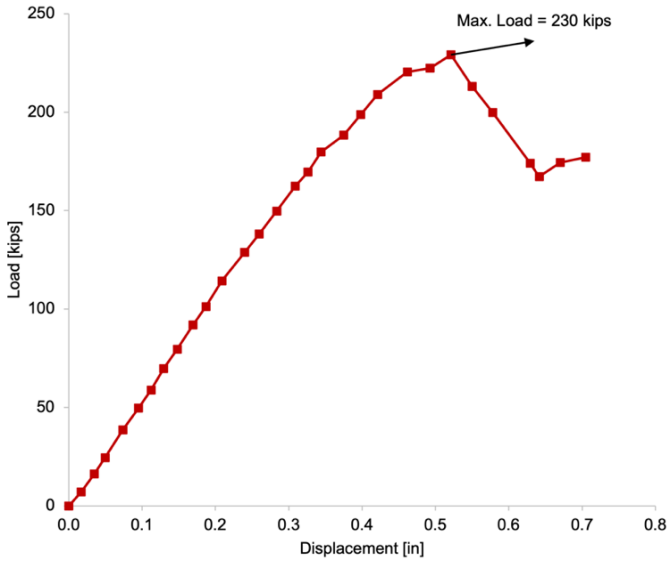

Figure 79. Load Versus Deflection of Box Beam 6 - CFRP Repair – Second Shear Test

Summary of Flexural Tests

Table 17 summarizes of all the flexural tests performed.

Table 17. Summary of Flexural Tests

Beam	Applied Load at Failure, kips	Moment			Failure Mode
		Total[1] Moment under Load at Failure, k-ft	Calculated Flexural Strength, k-ft	M_{test}/M_{calc}	
I-Beam 1 – Repaired with External PT - Wax	263	2832	2662	1.06	Concrete Crush
I-Beam 5 – Repaired with External PT - Grout	304	3242	2656	1.22	Concrete Crush
I-Beam 4 – Repaired with CFRP	234	2542	2349	1.08	CFRP - Debonding
Box Beam 5 – Repaired with CFRP	97.5	1350	1519	0.88	CFRP - Debonding
Box Beam 5 – Repaired with CFRP – Including Water Effect	97.5	1350	1425	0.95	CFRP - Debonding

[1] Total moment includes self-weight

Key findings from this table are:

- The AASHTO simplified method for flexural strength calculations for beams containing both bonded and unbonded tendons, combined with the recommended approach to account for corrosion damage in the strands, provided conservative estimates of flexural strength.

- For the I-beam, the AASHTO approach to calculating the flexural strength for beams strengthened with CFRP layups, gave conservative flexural strength estimations.

- Both the external PT repair and the CFRP repair increased flexural strength, but somewhat reduced ductility. An undamaged and unrepaired beam from the Lesner Bridge, which was tested in a previous phase of this project (Alfailakawi et al., 2020), failed at an applied load of 190 kips and an ultimate deflection of 9 in. The three repaired beams in this project had ultimate deflections between 6.8 and 8 in, so there was a slight loss of ductility.

Summary of Shear Tests

Table 18 presents a summary of all of the shear tests performed; the key findings are:

- The AASHTO LRFD shear strength calculations, combined with the recommended approach to account for corrosion damage in the strands, provided approximations of shear strength that were somewhat smaller than the shear strengths achieved in the tests, indicating the method is conservative.

- For the box beams, the addition of CFRP layups on the bottom flanges of the beams enhanced the flexural strength of the beams, so shear failures occurred prior to flexural

failure. However, the shear achieved in the tests was larger than that calculated with the AASHTO LRFD method.

Table 18. Summary of Shear Tests

Beam	Test No.	Applied Load at Failure, kips	Shear			Moment			Failure Mode
			Total[1] Shear at Half of Shear Span at Failure, kips	AASHTO Calculated Shear Strength, kips	V_{test}/V_{calc}	Total[1] Moment under Load at Failure, k-ft	Calculated Flexural Strength, k-ft	M_{test}/M_{calc}	
I-Beam 9 – Unrepaired	1	264.8	236	228	1.05	1887	1812	1.04	Flex.
	2	382.0	318	226	1.45	1929	1793	1.08	Shear
I-Beam 2 – CFRP Repair	1	329.0	305	262	1.16	1830	1722	1.06	Flex
	2	312.5	275	262	1.05	1652	1445	1.14	Flex
Box Beam 3 – Unrepaired	1	259.0	258	195	1.32	1030	1343	0.77	Shear
	2	230.5	224	174	1.29	899	934	0.96	Flex
Box Beam 6 – CFRP Repair	1	240.4	258	200	1.29	1032	1663	0.62	Shear
	2	208.1	222	208	1.07	887	1642	0.54	Shear

[1] Total moment and shear include self-weight

Task 6: Conduct a Forensic Analysis

Compression Test Results

Concrete cores were taken from the webs of the I-beams and from the top flanges of the box beams. In the I-beams, cores were also taken from the deck. For box beams, cores were taken from the top flange only. Table 19 shows the concrete compressive strength results.

Table 19. Compressive Strength for Concrete Cores

Beam / Sample	Average Factored Compressive Strength (psi)	
	Slab	Web
I-Beam 1 – Repaired with External PT - Wax	6030	7455
I-Beam 5 – Repaired with External PT - Grout	5660	5990
I-Beam 4 – Repaired with CFRP	6300	7320
I-Beam 9 – Unrepaired	4090	4960
I-Beam 2 – Repaired with CFRP	6240	6600
Box Beam 3 – Unrepaired	6080	
Box Beam 5 – Repaired with CFRP	6045	
Box Beam 6 – Repaired with CFRP	8050	

Table 20 and Table 21 present information about the strands retrieved from the I-beams and box beams. This information includes the beam identification, the condition of the concrete surface above the strand, a description of the damage, and a photograph.

Table 20. Description of Strands Samples 1-11

Sample #	Beam ID	Surface Damage	Description	Picture
1	I-Beam 1- wax	No Damage + Stain	Light corrosion with heavy pitting at the location of stain	
2	I-Beam 1- wax	No Damage + Stain	Light corrosion with heavy pitting at the location of stain	
3	I-Beam 1- wax	No Damage	No corrosion	
4	I-Beam 1- wax	No Damage	Light corrosion	
5	I-Beam 1- wax	No Damage + Stain	Light corrosion with pitting	
6	I-Beam 1- wax	No Damage	No corrosion	
7	I-Beam 1- wax	No Damage	Light corrosion with pitting (hammer drill)	
8	I-Beam 1- wax	No Damage	Light corrosion with pitting (hammer drill)	
9	I-Beam 1- wax	No Damage + Stain	Light corrosion	
10	I-Beam 1- wax	No Damage + Stain	Light corrosion	
11	I-Beam 5 -grout	No Damage	No corrosion	

Table 21. Description of Strand Samples 12-20

Sample #	Beam ID	Surface Damage	Description	Picture
12	I-Beam 5 -grout	No Damage	No corrosion with pitting (hammer drill)	
13	I-Beam 5 -grout	Longitudinal hairline crack	No corrosion with pitting (hammer drill)	
14	I-Beam 5 -grout	Patched Area	Fracture/Wire loss	
15	I-Beam 5 -grout	No Damage + Near Patched Area	Light corrosion	
16	I-Beam 5 -grout	No Damage + Near Patched Area	Light corrosion with pitting (hammer drill)	

Table 21 (continued). Description of Strand Samples 12-20

17	Box Beam 2 CFRP Flexural	Adjacent to a very wide crack	Heavy pitting and wire loss	
18	Box Beam 2 CFRP Flexural	Aligned with longitudinal wide crack / Concrete Spall	Heavy pitting and wire loss	
19	Box Beam 2 CFRP Flexural	Longitudinal wide crack / Concrete Spall	Heavy pitting and wire loss	
20	Box Beam 2 CFRP Flexural	Adjacent to a crack	Light corrosion	

Figure 80 presents stress-strain curves for selected extracted strands. Each curve is an example of a level of corrosion damage, namely no corrosion, light corrosion, light pitting, and heavy pitting. As can be seen, light corrosion does not significantly affect the stress-strain behavior, but pitting results in reductions of both ultimate strength and ultimate strain. Table 22 presents key information about each sample's stress-strain behavior.

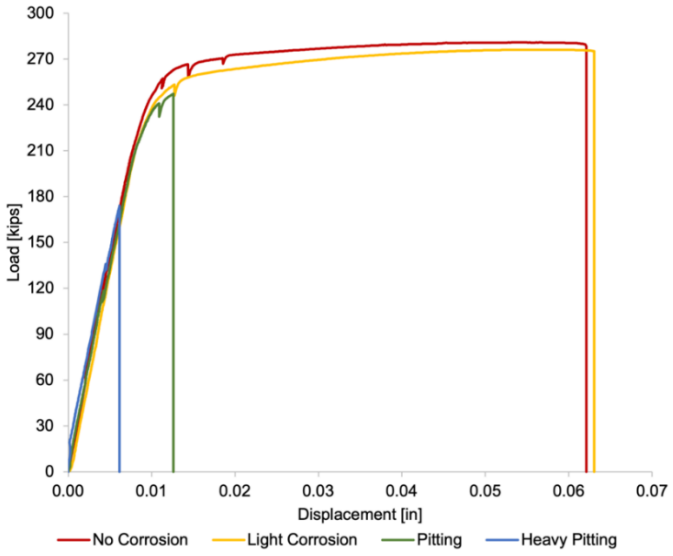

Figure 80. Stress-Strain Curves of Prestressing Strand with Various Levels of Damage

Chloride results

The threshold for corrosion risk due to chloride contents are given in Table 23. The chloride content testing results for I-Beams 4 and 9 are presented in Figure 81. The penetration depth of 1 in had a greater chloride content than the initial depth of 0.5 in for the inland side and bay sides. This may be explained by the fact that water or rain might have washed away chloride from the

Table 22. Description of Strands Extracted from Tested Beams

Sample #	Classification of Damage	Modulus of Elasticity, ksi	Yield Stress, ksi	Ultimate Stress, ksi	Ultimate Strain
1	Heavy pitting	28000	N.A.	174	0.0061
2	Heavy pitting	27500	N.A.	170	0.006
3	No damage	28000	251	275	0.033
4	Light corrosion	28000	241	272	0.043
5	Light pitting	28000	240	247	0.0126
6	Light corrosion	27500	246	276	0.063
7	Light pitting	28000	247	271	0.034
8	Light pitting	27500	243	277.5	0.0516
9	Light corrosion	27500	243	278.25	0.072
10	Light corrosion	28000	244	275	0.052
11	No damage	28000	253	280	0.064
12	No damage	28000	247	274	0.063
13	Light pitting	28000	247	279	0.063
14	Wire loss	N.A.	N.A.	88	0.0002
15	Light corrosion	28000	247	278	0.064
16	Light corrosion	28000	244	276	0.052
17	Heavy pitting and wire loss	28000	N.A.	158.5	0.008
18	Heavy pitting and wire loss	N.A.	N.A.	60.5	0.002
19	Heavy pitting and wire loss	N.A.	N.A.	47	N.A.
20	Light corrosion	29000	257	279	0.045

Table 23. Risk of Corrosion Compared to Chloride Content (Balakumaran, 2010)

% Chloride by mass of sample (concrete)	Risk	Chloride content per volume of concrete (lb/yd^3)
<0.03	Negligible	<1.17
0.03-0.06	Low	1.17-2.35
0.06-0.14	Medium	2.35-5.48
>0.14	High	>5.48

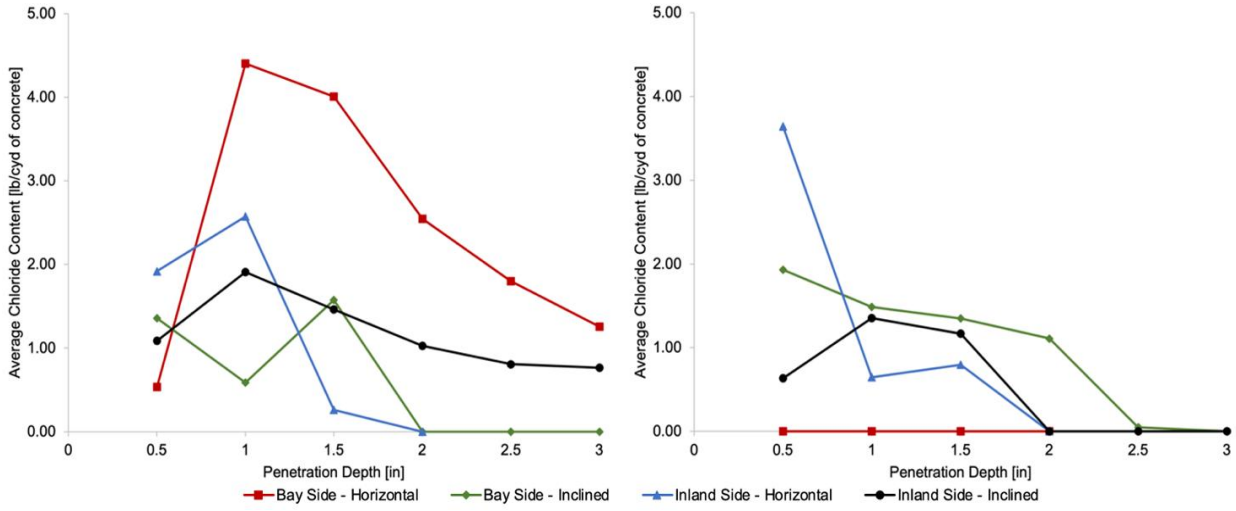

Figure 81. Results of Chloride Testing for I-Beam 4 (Left) and I-Beam 9 (Right)

surface of the concrete, resulting in a low value. In general, as the depth of the sample increased, the chloride content decreased on all sides. The only exception was the bay side – inclined on I-Beam 4, which had an increase in the chloride content from 1.0 in to 1.5 in. For I-beam 4, the chloride concentration on the bay side was much greater than on the inland side at each depth point, most likely due to the bay side being exposed to a harsher environment than the inland side. The two beams had similar concentration levels for a given side of the beam and pentration depth. Except for the horizontal bay side of I-Beam 4 and the horizontal inland side of I-Beam 9, both beams may be judged to have negligible to low-risk conditions.

The chloride concentrations in Box Beam 3 and Box Beam 5 are shown in Figure 82. As noted in the graph, the top section of the box beam had a low chloride level compared to the east and west sides. This outcome may be explained by the fact that the top of the box beam was covered with an asphalt overlay that served as a primary protector against chloride penetration. Additionally, cracks are known to form in the top surface and along the longitudinal joints between adjacent precast box beams. These longitudinal cracks allow chloride-laden water to flow directly to the side and bottom of the beams. As with the other I-beams, the chloride concentration decreased gradually as the sample depth increased. Both beams are classified as low to medium risk due to their chloride concentration of 2.62 lb/yd^3 and 2.57 lb/yd^3 for Box Beam 3 and 5, respectively. Also note that at the depth of the strand, 2 in from the surface, the chloride concentrations indicate low to negligible risk.

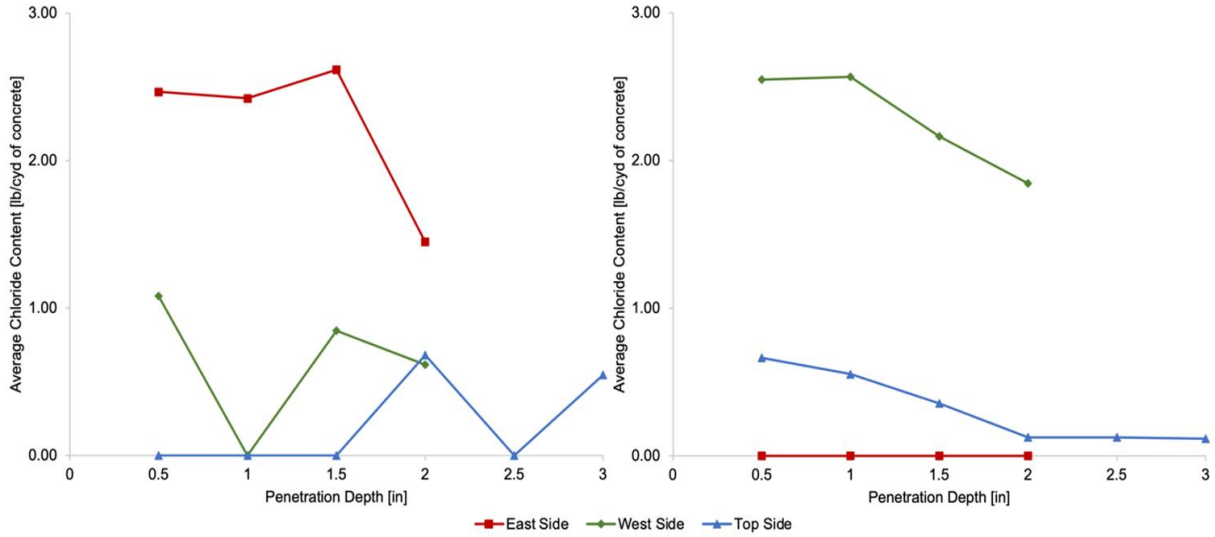

Figure 82. Results of Chloride Testing for Box Beam 3 (Left) and Box Beam 5 (Right)

Based on these samples, the chloride concentrations indicated low to negligible risk of corrosion at the level of the strand, but all four beams had significant corrosion damage. So, chloride concentration testing did not provide new information to assist in the quantification of the corrosion damage and estimation of residual flexural strength. However, it should be noted that chloride samples were not taken in close proximity to visible damage such as cracks and spalls. Samples were taken after testing, from relatively undamaged sections of the beams. Therefore, it is possible that chloride concentration testing could give more valuable information if samples are taken closer to locations of visible damage.

Task 7: Execute an Analytical Evaluation

Results for Beams Failed in Flexure

The analytically obtained load-carrying capacity of the prestressed beams with the I- and box-sections are summarized in Table 24. These beams were all tested in an unrepaired condition and were presented in Alfailakawi et al. (2020). Since the tested beams exhibited signs of corrosion damage, the analyses were performed to determine the flexural capacity of specimens with and without damage. This clarifies the impact of corrosion-induced damage on the flexural capacity. As Table 24 depicts, the beam model could accurately predict the flexural capacity of the I-beams. Given the flexural capacity of undamaged specimens, corrosion had a minor and severe impact on the flexural strength of I-Beam 3 and I-Beam 6, respectively. I-Beam 7 had no damage and served as a baseline for comparison to damaged beams.

The flexural capacities of box beam specimens were also accurately captured by the analytical model, as shown in Table 24. The analysis of undamaged specimens shows that the corrosion-induced damage had a moderate impact on the Box Beam 2 specimen, while severely affecting the flexural capacity of Box Beam 4.

The analytically obtained load-displacement curve and the experimental observation for the Box Beam 1 specimen are shown in Figure 83, where the analysis could accurately reproduce the experimental response, including peak flexural capacity, initial stiffness, and stiffness degradation. The drops in the experimental response are associated with the rupture of individual wires. The computation accounts for the wire rupturing effect by considering the results of the uniaxial tensile test on corroded specimens. Given the result for the undamaged specimen, corrosion had no impact on initial stiffness while significantly affecting the ultimate capacity.

Table 24. Load-Carrying Capacity of Flexure-Dominated Specimens (kips)

Method	Beam Type					
	I-Beam 3	I-Beam 6	I-Beam 7	Box Beam 1	Box Beam 2	Box Beam 4
Experiment	165.7	118.3	190.5	90.7	91.6	83.7
Analysis w/ damage	171.0	117.8	-	92.5	90.4	83.1
Analysis w/o damage	176.2	170.8	184.3	119.1	108.7	116.2

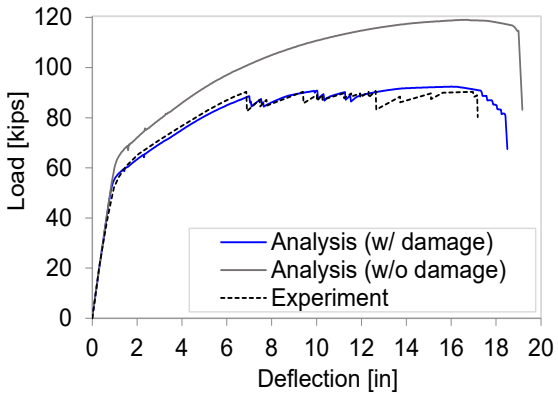

Figure 83. Analysis Results for Flexure-Dominated Box Beam 1 Specimen

Results for Beams Tested in Shear

The truss model could accurately capture the shear failure mode in the two unrepaired specimens that failed in shear, along with shear strengths. Table 25 summarizes the analysis results in conjunction with the experimentally observed response. Given the condition of the specimens, the truss modeling approach could reproduce the experimental test with a relative error of 1%.

Table 25. Load-Carrying Capacity of Shear-Dominated Specimens (kips)

Method	Beam Type	
	I-Beam 9	Box Beam 3
Experiment	382.0	258.0
Analysis w/ damage	-	260.6
Analysis w/o damage	377.2	261.6

The analytically obtained load-displacement response along with the experimental result for the shear-dominated specimen Box Beam 3 is shown in Figure 84. The analysis for the damaged specimen could closely retrace the experiment with an error in the initial stiffness. Additional analysis is performed to determine the impact of corrosion-induced damage on the shear strength of the beam. A comparison between the analysis of specimens with and without damage shows that corrosion had a trivial impact on the shear capacity. On the other hand, the damaged beam developed a larger deflection than the undamaged beam. It is not surprising that the corrosion-induced damage did not impact the shear strength as the stirrups were free from damage, and the damage zone that could reduce the shear strength was far from the web.

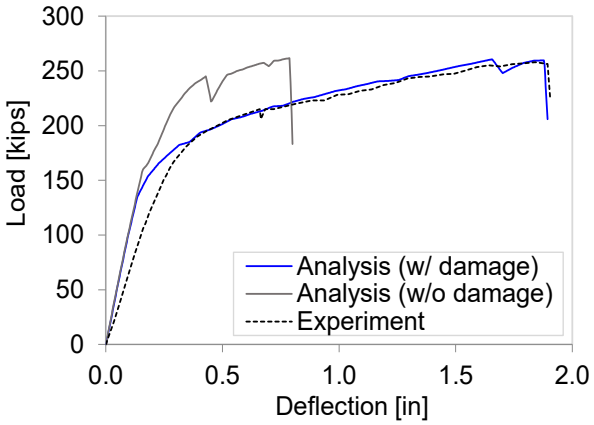

Figure 84. Analysis Results for Shear-Dominated Box Beam 3 Specimen

As discussed earlier, the truss modeling approach can capture the shear failure mode with a good degree of accuracy. Figure 85 shows the experimentally observed failure mode with its analysis counterpart. The computational simulation could determine the mode of failure where a wide diagonal crack started near the applied load and continued down to the support. The diagonal crack developed in the web is similar in both the analysis and experiment, corroborating the accuracy of the analysis.

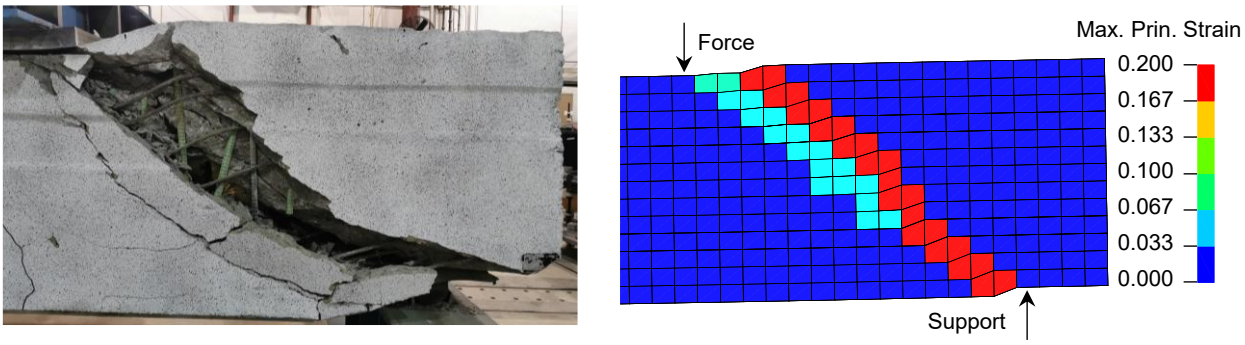

(a) Experimental observation (b) Computational simulation

Figure 85. Mode of Failure for Shear-Dominated Box Beam 3 Specimen

Task 8: Develop Guidelines for Repair of Corrosion-Damaged Beams

This section presents guidance for the evaluation and repair of corrosion-damaged prestressed concrete beams.

Evaluation of Corrosion Damage and Estimate of Residual Strength

A detailed damage map of the beam to be repaired must first be created. This damage map should detail the locations of longitudinal cracks, spalls, delaminations, and patches. Any exposed strands and their condition should also be recorded. For box beams, the recommendations of Naito et al. (2011) should be followed to assign a reduced cross-sectional area to strands in proximity to identified surface damage. For I-beams, the recommendations of Alfailakawi et al. (2020) should be used. Half-cell potential measurements and chloride concentrations can provide other qualitative information about the extent of possible corrosion damage, but the visible damage provides the best evidence to quantify the damage.

For the determination of flexural strength, using the reduced cross-sectional areas, a strain compatibility approach provides an excellent strength estimate. However, the AASHTO LRFD approximate method is also acceptable and provides more conservative results (Alfailakawi et al., 2020).

For the determination of flexural strength for corrosion damaged beams repaired with CFRP, ACI approach provides a more conservative estimation for I-beams than the AASHTO approach. However, both approaches give close estimation for box beams.

For the determination of shear strength, the AASHTO LRFD shear strength model provides a conservative strength estimate. The area of prestress used in calculating the concrete contribution to shear strength, V_c, should be reduced according to the strand area reduction recommendations also used for flexure. Furthermore, if there is significant corrosion damage near the end of a beam, AASHTO LRFD article 5.7.3.5 should be checked. This check ensures that the tensile strength of the prestressing crossing a critical shear crack near a simple support is adequate, even after accounting for damage and reduced capacity in the transfer length.

Selection of Repair Technique

The condition of the concrete cover is critical in determining the repair approach. Based on observations from the test of Box Beam 5, even if the CFRP adheres well to the soffit of the beam, a patched area that is added to provide a smooth surface to which to adhere the CFRP may debond at a lower load than that at which the CFRP debonds from the beam's soffit. With the external PT repair, these patches do not affect strength, but do help to mitigate additional corrosion in the long term. Unfortunately, with only one test exhibiting patch debonding, it is not possible to make a quantitative recommendation on the amount of soffit damage that would trigger a change from CFRP repair to external PT repair.

CFRP repairs should be used for adjacent box beams and I-beams with flexural damage that do not require strength increase of more than 20% to meet the strength demand at any section. This recommendation was based on a numerical investigation of typical I-beams repaired with three plies of CFRP (specifically, V-Wrap C400HM) across the bottom flange. In general, three plies is the maximum number for the repair of beams to result in a CFRP rupture or concrete crushing failure prior to debonding. Based on the ACI method (ACI440.2R-08), the three plies could return beams to their original strength if the loss of strength due to corrosion damage was no more than 20% (Alfailakawi, 2022).

To calculate the number and width of plies of CFRP required to return a beam to its required strength, the method found in the "AASHTO Guide Specifications for Design of Bonded FRP Systems for Repair and Strengthening of Concrete Bridge Elements" (AASHTO, 2012) can be used. However, for more detailed guidance, the "ACI Guide for the Design and Construction of Externally Bonded FRP Systems for Strengthening Concrete Structures" (ACI440.2R-17) is encouraged.

CFRP repairs should be used for adjacent box beams and I-beams with shear damage extensive enough so the calculated shear strength is less than the demand at any section. Corrosion damage to both the longitudinal prestressing and the shear reinforcing can cause reduction in shear strength, therefore, shear repairs should include both longitudinal CFRP on the bottom soffit and U-wraps around the bottom soffit and as high up on the web as possible. Since wraps are not possible on box beams, only bottom soffit layups can be implemented. The bottom soffit CFRP can result in increases in the concrete shear capacity (V_c) but the effect is small.

For I-beams requiring more than 20% increase in flexural strength, repair with external PT is recommended. The following additional guidance is suggested:

- The AASHTO simplified approach for estimating the flexural strength of beams containing bonded and unbonded tendons provides a conservative repair strength approximation. It can be used to determine the number and size of external strands required.

- The anchor blocks should be placed on the webs as close to the ends of the beams as is allowed by the construction and stressing process. The live-end anchor block may need to be placed farther from the end of the beam than the dead-end block to allow for access with the stressing ram.

- At the locations where anchor blocks and deviators are to be cast against the existing beam, the surface of the beam should be roughened to approximately ¼ in amplitude with a chipping hammer to improve the bond of the new concrete to the old.

- The anchor blocks should be designed for a force equal to the maximum jacking force times a load factor of 1.2. This is in accordance with the design of anchorage zones per the AASHTO LRFD Specifications.

- Anchor blocks should be designed as corbels, using conventional corbel design methods with shear friction or strut-and-tie methods.

- The main flexural and shear friction reinforcement should be passed through slightly oversized holes in the webs and developed in the anchor block on the opposite side of the web. The bars should be epoxied into the holes for better development and to reduce the possibility of the anchor blocks moving relative to the beam's web during stressing. Prior to drilling holes, web reinforcement should be located to prevent damage during the drilling process.

- The deviation points should be placed at the existing interior diaphragms. The diaphragm walls should be extended downward, so the deviation point of the new external tendons is as low as possible in the cross-section but not below the bottom of the bottom flange. The new lower part of the diaphragm should be widened to accommodate a deviation saddle.

- Grout or wax may be used to fill the duct in an external PT repair. However, wax is more likely to prevent corrosion initiation in the tendons in the long term.

CONCLUSIONS

- *The method presented in Naito et al. (2011) provides reasonable estimates for reducing the cross-sectional area of corrosion-damaged prestressing strands in concrete box beams, while the method presented in Alfailakawi et al. (2020) reasonably estimates the reduced cross-sectional area of corrosion-damaged prestressing strands in concrete I-beams.* Half-cell potential measurements and chloride concentrations can provide other qualitative information about the extent of possible corrosion damage, but the visible damage provides the best evidence to quantify the damage.

- *Using the reduced cross-sectional area of the strand, either a strain compatibility approach or the simplified method in AASHTO LRFD article 5.6.3.1.1 can be used to calculate flexural strength. The beam model analytical approach also gives very good estimates of the flexural capacity, along with deformability, mode of failure, and associated abrupt strength degradation.*

- *For beams repaired with unbonded tendons, the AASHTO simplified method for calculating flexural strength of beams that have a combination of bonded and unbonded tendons (AASHTO Article 5.6.3.1.3b) provides a conservative estimate of strength.*

- *For beams repaired with CFRP, the methods provided in ACI 440R (ACI 440, 2008) and the AASHTO Guide Specifications for Design of Bonded FRP Systems for Repair (AASHTO 2012) provide reasonable estimates of flexural strength.*

- *The AASHTO sectional method for the calculation of shear strength provides conservative estimates of strength. If a more detailed analysis is required, the proposed truss model approach gives excellent estimates of shear strength, deformability, and strength degradation. The mode of failure is also well captured by the truss model.* Any estimated corrosion damage to prestressing strands needs to be accounted for in calculating the concrete contribution to shear strength. Other failure modes must also be checked during the design of the repair.

RECOMMENDATIONS

1. *VDOT Structure and Bridge Division should revise the Structure and Bridge Load Rating User Manual to provide guidance in evaluating the extent of damage evident from telltale signs visible on the exterior surface of prestressed beams.* Inspectors should create a damage map identifying locations of cracks, spalls, delaminations, patches, and describe corrosion of any visible strands. If the beams are prestressed concrete box beams, the engineer should follow the recommendations from Naito et al. (2011) to determine the effective remaining strands and remaining cross-sectional area to be used for structural evaluation. If the beams are prestressed I-beams, the engineer should follow the recommendations from Alfailakawi et al. (2020) to determine the effective remaining strands and remaining cross-sectional area to be used for structural evaluation. Chloride concentration measurements can inform the engineer about the level of contamination of the cover concrete to determine how much should be removed before a patch is placed.

2. *VDOT's Structure and Bridge Division can calculate the flexural strength of corrosion-damaged prestressed concrete beams using either the strain compatibility approach or the AASHTO LRFD method.* If a more detailed analysis is desired, the engineer is advised to use the beam model approach to capture flexural response including ultimate capacity, deformability, and mode of failure.

3. *VDOT's Structure and Bridge Division can calculate the shear strength of corrosion-damaged prestressed concrete beams using the AASHTO LRFD approach with the reduced cross-section from Recommendation 1*. Spalling and loss of strand in this region need to be evaluated by the load rating engineer. The engineer should check the limitations of AASHTO LRFD article 5.7.3.5 if damage is evident near the bearing location. As an alternative, the truss model approach is highly recommended to capture shear capacity, deformability, and mode of failure.

4. *VDOT's Structure and Bridge Division can use CFRP or external PT as a repair method for the corrosion-damaged beam.* In the case where flexural strength controls the load capacity, CFRP is the recommended repair method for beams with strength loss that is less than 20% of the required flexural strength. If the reduction in flexural capacity is greater than 20% of what is required, then an external PT repair method should be used. In the case where shear strength at the beam ends controls the load capacity, then CFRP is the recommended repair method to restore the required strength that has been lost due to corrosion damage.

5. *VDOT Structure and Bridge Division should revise the Structure and Bridge Load Rating User Manual to provide the following guidance on evaluating the flexural or shear strength of repaired prestressed concrete girders:*
   - All calculations should incorporate the reduced cross-sectional area as well as the reduced strand capacity, as stated in Recommendation 1.
   - The flexural capacity of members repaired with external post-tensioned strands should follow the AASHTO Article 5.6.1.3b
   - The flexural capacity of members repaired with CFRP should be calculated using ACI 440R (ACI 440, 2008) or the AASHTO Guide Specifications for Design of Bonded FRP Systems for Repair (AASHTO 2012)
   - The shear capacity of members repaired with CFRP should be calculated using the AASHTO sectional method in section 5.7.3 of the LRFD Specifications.

IMPLEMENTATION AND BENEFITS

Researchers and the technical review panel (listed in the Acknowledgements) for the project collaborate to craft a plan to implement the study recommendations and to determine the benefits of doing so. This is to ensure that the implementation plan is developed and approved with the participation and support of those involved with VDOT operations. The implementation plan and the accompanying benefits are provided here.

Implementation

Regarding Recommendation 1, *VDOT inspectors already create detailed maps of damage, per the recommendations by the load rating engineer and per the National Bridge Inspection Standards.* Furthermore, VDOT already follows Naito et al. (2011) and Alfailakawi et al. (2020) for determining the remaining section of prestressing reinforcement in box beams and I-girders, respectively, as implemented after the research by Alfailakawi et al. Thus, no further action is needed to implement this recommendation.

Regarding Recommendations 2, 3, and 5, VDOT already follows AASHTO specifications for analysis of existing structures. Thus, no further action is necessary for implementing these three recommendations.

Regarding Recommendation 4, *VDOT's Structure and Bridge Division will incorporate the recommended practices for repair of corrosion-damaged prestressed concrete girders under a new dedicated heading,* 7.4 Repair of Corrosion-Damaged Prestressed Concrete Beams *of Structure and Bridge Division's new* Bridge Maintenance Manual *(formerly Chapter 32 of the* Manual of the Structure and Bridge Division*). This update will be implemented by June 30, 2027.*

Benefits

The results of this research provide VDOT with improved guidance on how to evaluate corrosion damage of prestressed concrete beams, and estimate the influence of the corrosion damage on capacity. The estimated corrosion damage can be based solely on visual evidence such as cracking and spalling. These recommendations should result in improved strength estimates to be used in load ratings and in decision making about repair or replacement of damaged beams.

The research also provides additional guidance on repairing beams using CFRP layups or external post-tensioning. The research verifies that current guidance in AASHTO publications is acceptable for the design of repairs but also provides additional recommendations. These recommendations should result in VDOT having greater confidence in the repair techniques that are implemented. Thus, the agency will have an enhanced ability to extend the service life of its existing inventory without the need to restrict travel across the Commonwealth.

ACKNOWLEDGMENTS

The authors gratefully acknowledge the guidance and assistance of Michael Sprinkel, Soundar Balakumaran, and Bernie Kassner of the Virginia Transportation Research Council. The assistance of David Mokarem, Brett Farmer, Dennis Huffman and Garrett Blankenship at the Murray Structural Engineering Laboratory at Virginia Tech is also gratefully acknowledged. The contributions of Abdullah Al Rufaydah and Alana Moares were instrumental to this project.

The Virginia Transportation Research Council would like to acknowledge the technical review panel members for their guidance on this project and for developing the implementation plan for this report: Adam D. Matteo, P.E., Assistant State Structure and Bridge Engineer for Maintenance and Bridge Management Systems; Gary A. Runco, P.E., P.S., District Structure and Bridge Engineer, Northern Virginia District; Mohamed Ali, P.E., District Structure and Bridge Engineer, Hampton Roads District; Andrew M. Zickler, P.E., Complex Bridge and ABC Support Program Manager, Central Office; Marc Stecker, P.E., Special Structures Manager, Central Office; and Stephen R. Sharp, Ph.D., P.E., Associate Principal Research Scientist, VTRC. The VTRC would also like to give thanks to Christopher R. Williams, P.E., Assistant Structure and Bridge Engineer for Inspections and Inventory; and Bryan J. Silvis, P.E., Maintenance Management Engineer, Central Office.

REFERENCES

Alfailakawi, A. *Experimental Investigations of Residual Strength and Repaired Strength of Corrosion Damaged Prestressed Bridge Beams.* Ph.D. Dissertation, Virginia Tech, Blacksburg, VA, 2022.

Alfailakawi, A., Roberts-Wollmann, C.L., Hebdon, M., and Koutromanos, I. *Experimental and Analytical Evaluation of Residual Capacity of Corrosion Damaged Prestressed Concrete Bridge Girders.* VTRC 21-R6. Virginia Transportation Research Council, Charlottesville, VA, 2020.

Aliasghar-Mamaghani M, Koutromanos I, Roberts-Wollmann C, Hebdon M. Analytical Evaluation of Corrosion-Induced Strength Degradation in Prestressed Bridge Girders. *Journal of Structural Engineering*. in press

Al Rufaydah, A. *Shear Strength Assessment of Corrosion Damaged Prestressed Concrete Girders*. Masters Thesis, Virginia Tech, Blacksburg, VA. 2020.

American Association of State Highway and Transportation Officials, *LRFD Bridge Design Specifications*. AASHTO, Washington, D.C., 2020.

American Association of State Highway and Transportation Officials. *Guide Specifications for Design of Bonded FRP Systems for Repair and Strengthening of Concrete Bridge Elements*. AASHTO, Washington, D.C., 2012.

American Concrete Institute Committee 440. *Guide for the Design and Construction of Externally Bonded FRP Systems for Strengthening Concrete Structures*. ACI PRC 440.2R-17, American Concrete Institute, Farmington Hills, MI, 2017.

ASTM. *Standard Test Methods for Testing Multi-Wire Steel Prestressing Strand.* ASTM A1061, West Conshohocken, PA, 2009.

ASTM. *Standard Test Method for Acid-Soluble Chloride in Mortar and Concrete*. ASTM C1152, West Conshohocken, PA, 2012.

ASTM. *Standard Test Method for Compressive Strength of Cylindrical Concrete Specimens*. ASTM C39, West Conshohocken, PA, 2005.

ASTM. *Standard Test Method for Obtaining and Testing Drilled Cores and Sawed Beams of Concrete*. ASTM C42, West Conshohocken, PA, 2016.

ASTM. *Standard Test Method for Half-Cell Potentials of Uncoated Reinforcing Steel in Concrete.* ASTM C876, West Conshohocken, PA, 2015.

Balakumaran, S. S. G. *Influence of Bridge Deck Concrete Parameters on the Reinforcing Steel Corrosion*. Virginia Tech, 2010.

Balasubramaniam, V., Raghunath, P. N., and Suguna, K. Performance of Corrosion-Damaged HSC Beams Strengthened with GFRP Laminates. *International Journal of Computer Science Engineering & Technology*, *1*(11).

Bennitz, A., J.W. Schmidt, J. Nilimaa, B. Täljsten, P. Goltermann, and D. Ravn. Reinforced Concrete T-beams Externally Prestressed with Unbonded Carbon Fiber-Reinforced Polymer Tendons. *ACI Structural Journal*, Vol. 100, No. 4, April 2012, pp. 521-530.

Dong, J., Wang, Q., and Guan, Z. Structural Behaviour of RC Beams with External Flexural and Flexural–Shear Strengthening by FRP Sheets. *Composites Part B: Engineering*, 44(1), 2013, pp. 604-612.

Duthinh, D., and Starnes, M. Strength and Ductility of Concrete Beams Reinforced with Carbon Fiber-Reinforced Polymer Plates and Steel. *Journal of Composites for Construction*, 8(1), 2004, pp. 59-69.

Harries, K.A. (2009). Structural Testing of Prestressed Concrete Girders from Lake View Drive Bridge. *ASCE Journal of Bridge Engineering,* Vol. 14, No. 2, March/April 2009, pp.78-91.

Klaiber, F. W., Wipf, T. J., and Kempers, B. J. Repair of Damaged Prestressed Concrete Bridges using CFRP. *Proceedings of the 2003 mid-continental transportation research symposium, Ames, Iowa*. 2003.

Koutromanos I. *Fundamentals of Finite Element Analysis: Linear Finite Element Analysis*. John Wiley and Sons, Inc., New York, 2018.

Lee, H. S., Tomosawa, F., Masuda, Y., and Kage, T. Effect of CFRP Sheets on Flexural Strengthening of RC Beams Damaged by Corrosion of Tension Rebar. *Proceedings of 3rd International Symposium on Non Metallic (FRP) Reinforcement for Concrete Structures,* Oct. 1997, pp. 23-23.

Lee, S.H., K.J. Shin, and H.D. Lee. Post-Tensioning Steel Rod System for Flexural Strengthening in Damaged Reinforced Concrete (RC) Beams. *Applied Sciences*, 8, 1763, 2018.

Leicht, L., Roberts-Wollmann, C.L., Koutromanos, I., Hebdon, M.H., and Mosig, O. Experimental and Analytical Investigation of a 64-Year Old Prestressed Beam Retrofitted with External Post-Tensioning“, *ASCE Journal of Bridge Engineering*, Vol. 27, No. 4, April 2022.

Moraes, A.A. Shear Strength Assessment of Corrosion-Damaged Prestressed Concrete Girders Repaired with CFRP. Masters Thesis, Virginia Tech, Blacksburg, VA. 2021.

Naito, C., Jones, L., and Hodgson, I. Development of Flexural Strength Rating Procedures for Adjacent Prestressed Concrete Box Girder Bridges. *ASCE Journal of Bridge Engineering*, Vol. 61, No. 5, Sept/Oct 2011, pp. 662-670.

Rose, A. L., Suguna, K., and Ragunath, P. N. Strengthening of Corrosion-Damaged Reinforced Concrete Beams with Glass Fiber Reinforced Polymer Laminates. *Journal of Computer Science*, 5(6), 2009, pp. 435-445.

Sayed-Ahmed, E.Y., A.H. Riad, and N.G. Shrive. Flexural Strengthening of Precast Reinforced Concrete Bridge Girders Using Bonded Carbon Fiber Reinforced Polymer Strips or External Post-Tensioning. *Canadian Journal of Civil Engineering.* 31, 2004, pp. 499-512.

Soudki, K. A. FRP Repair of Corrosion-Damaged Concrete Beams—Waterloo Experience. *Advances in Engineering Structures, Mechanics & Construction*, 2006, pp. 165-173. Springer.

Zhang, X., L. Shuang, W. Zhang, O. Ikechukwu, L. Dai, and L. Wang. Second Remediation of Long-Term Deflection and Cracking of PT Box-Girder Bridge Using External Post-Tensioning. *Journal of the Performance of Constructed Facilities.* Vol. 34, No. 5, May 2020.